Universidad de Valladolid

Escuela de Doctorado Universidad de Valladolid

PROGRAMA DE DOCTORADO EN

INVESTIGACIÓN BIOMÉDICA

TESIS DOCTORAL

Remodeling of G protein-coupled receptor signaling pathways in essential hypertension

Presentada por NURIA DAGHBOUCHE RUBIO para optar al grado de Doctora por la Universidad de Valladolid

Dirigida por:

Dra. Mª Teresa Pérez García

Dr. José Ramón López López

"Science is not only a disciple of reason but, also, one of romance and passion"

Stephen Hawking

"No human is limited"

Eliud Kipchoge

Acknowledgements

Embarking on the arduous and fulfilling journey of completing this thesis may be like finishing a marathon. Discipline, endurance, and resilience are needed to achieve it. However, one will also need the support and contributions of many people to complete this race. Thank God, I was lucky to meet them in the right time and place to cope with this academic marathon.

First, I would like to extend my deepest appreciation to my thesis advisors, Tere, Joserra, and Pili. They gave me the opportunity to do a PhD in the lab, with them as supervisors and references in life. Their guidance and unwavering support were crucial during this academic marathon. Their expertise, patience, and encouragement provided the necessary fuel to keep me moving forward, even when the road ahead seemed daunting. They trained us not only to be specialists, but also thinkers. Therefore, I truly believe that I have become a greater scientist and person, thanks to them. Moreover, a special appreciation goes to my dedicated and adorable C2 labmates, Espe, Sara, Marycarmen, Irina, Lucía, Jorge, and Diego. Their camaraderie and collaborative spirit provided the laboratory with a space for inspiration and motivation. They became my fellow marathoners, running by my side, and we encouraged each other to persevere. They were also key during the process of becoming a better scientist and person.

Second, I would like to express my heartfelt thanks to my lovely friends from the C1 lab, Elisa, Aida (and Javi), Sara, Paloma, Carol, Ángel, Juan, and Álex. They were a source of encouragement and understanding during the highs and lows of the academic marathon. Your friendship added a lot of joy and laughs, which provided the necessary support, especially for the last PhD year. I would also like to appreciate past and present IBGM members that were also relevant to my path: Lauri, Alba, Nagore, Patri, Julia, Patry, Karla, Miriam Corraliza, Laura, Lara (and Toni), Clara, Virginia, Beatriz Durán, Tania, Vero, Dino, Sergio, Miguel, Alberto and Sendoa. A special mention of Lauri and Patri, since they were a source of calm and always ready to listen to me. Moreover, thank professors Lola and Diego for their willingness to be helpful and caring during the path. I would also always remember the funny and lovely coworkers from Vicente Bodí lab in Valencia, César, and José. I started this academic marathon with them and each day was packed with laughter and joy. In addition, thank you to the professors Susana, Carlos and Vicente to help me and encourage me doing a PhD and then ending up in Valladolid.

Third, I am also grateful to the Madeline and Manuel lab in Davis, together with their members Abby, Yumna, Lily, Tori, Miguel, Víctor, June, Eric, Jose, Navid, and Raghu. They provided invaluable insights, constructive feedback, and the latest novel technologies, which significantly contributed to the refinement of

this work. They offered collective kind and passionate expertise, feeling that I was at home, even being a thousand miles away during my research stay there. Also related to that city, I am grateful and happy to know my second family in California, Debie, Jane, Genene, Kimo, Antonio and Paco. They also contributed to the feeling of being at home, thanks to their kindness, care, and love during these months.

Fourth, I also acknowledge the encouragement and understanding of the rest of my friends from high school, college, the scouts group, the running club, and the gym. Lau, Andrea, Clau, Ester, Cris Cárcel, Isa, Mayde, María Asins, Lidia, Cris, Cynthia, Raquel, Luismi, Jorge, Pepe, Pedro, Juan Carlos, Sidi, David, Luís, Ramón, Javi and Adri. In addition, thank you Chris for conducting funny and out of the ordinary English classes and providing moments of disconnection in this last year of PhD. I also do not want to forget my neighbors in the building, Carmen, Dori and Frutus. They always looked after me and treated me like their daughter. In this regard, all of them stood by me during the ups and downs of the academic journey. Your moral support provided the necessary motivation to navigate the challenges of researching and writing this thesis. A special mention to Adri, for representing a role model of perseverance, even when life hits hard.

As I reach the finish line of this academic marathon, I am overwhelmed with gratitude and love for the unwavering support and encouragement provided by my family, grandparents, parents, aunts and uncles. Mensi, Bego, Martita, Sarita, Yasmina, Fátima, Carmen, Soumia, María José, Yolanda, Hamoudi, Pepe, Abdessalem, Antonio, and José. Marathon runners rely on a support system to provide them with water and motivation, and my family has been both an intellectual and emotional nourishment. Your trust in my capabilities has been the fuel that kept me going, especially during moments of fatigue and self-doubt. Thank you for your sacrifice, guidance and boundless love. Last, but not least, a special mention to Ana, who become a source of peace and calm and gave me tools to change my mindset.

With love and thank you all.

To my parents, Mensi and Hamoudi
To my aunt and uncle, Bego and José
To my supervisors, Tere and Joserra

Funding

This work was carried out as part of the following research projects:

Los canales iónicos del músculo liso como marcadores, dianas y efectores en el remodelado vascular (BFU2016-75360-R).

- Funding entity: Ministerio de Ciencia e Innovación.
- Duration: 2016 – 2020.
- Principal researchers: María Teresa Pérez García and José Ramón López López.

Nuevas terapias farmacológicas y génicas para la prevención y tratamiento de enfermedades vasculares oclusivas (VA114P17).

- Funding entity: Junta de Castilla y León (JCyL), Consejería de Educación
- Duration: 2017 – 2019.
- Principal researchers: María Teresa Pérez García.

Los canales Kv1.3 como nuevas dianas terapéuticas para la prevención de las complicaciones macrovasculares en diabetes: Un abordaje multidisciplinar (VA172P20).

- Funding entity: Junta de Castilla y León (JCyL), Consejería de Educación.
- Duration: 2020 – 2023.
- Principal researchers: María Teresa Pérez García.

Canales iónicos y Fisiopatología Vascular: Historia de dos canales. (PID2020-118517RB-I00).

- Funding entity: Ministerio de Ciencia e Innovación.
- Duration: 2021 – 2024.
- Principal researchers: María Teresa Pérez García and José Ramón López López.

In addition, this work was carried out with the following financial support:

FPI Predoctoral Contracts 2017

- Duration: 2018 - 2022. Reference: BES-2017-081938.
- Project title: Los canales iónicos del músculo liso como marcadores, dianas y efectores en el remodelado vascular.

Mobility of Doctoral Students FPI

- Mobility of doctoral students. Economic support for short stays for the development of doctoral theses. Call 2021. Reference: BES-2017-081938.
- Duration: August 2021 – March 2022.
- Location: Davis, California, United States.
- **This research collaboration was also supplemented by grants from UC Davis University.**

Mobility of Doctoral Students UVa

- Mobility of doctoral students. Economic support for attendance in international conferences in the development of doctoral theses. Call 2023.
- Conference: European Society for Microcirculation.
- Duración: April 2023.
- Lugar: Aarhus, Denmark.

Articles published

2021:

Title: Ischemia-reperfusion injury to coronary arteries: comprehensive microscopic study after reperfused myocardial infarction. Cesar Rios-Navarro; **Nuria Daghbouche-Rubio**; Jose Gavara; Elena de Dios; Nerea Perez-Sole; Jose M Vila; Francisco J Chorro; Amparo Ruiz-Sauri, Vicente Bodi. Ann Anat. 2021. PMID: 34144157. doi: 10.1016/j.aanat.2021.151785.

2022:

Title: Vascular smooth muscle ion channels in essential hypertension. **Nuria Daghbouche-Rubio**, José Ramón López-López, María Teresa Pérez-García, Pilar Cidad. Review Front Physiol. 2022. PMID: 36213221. doi: 10.3389/fphys.2022.1016175.

Participation in conferences

INTERNATIONAL

2023:

1. Title: *"P2Y6 purinergic receptor as a molecular switch of essential hypertension".*

Type of communication: Poster.

Authors: **Nuria Daghbouche-Rubio**, Inés Álvarez-Miguel, Jorge Rojo-Mencía, Esperanza Alonso, Pilar Cidad, M. Teresa Pérez-García and José R. López-López.

Congress: European Society for Microcirculation, ESM Congress.

Location and date: from 24th April to 27th April in Aarhus, Denmark.

2022:

2. Title: UC Davis Cardiovascular Symposium.
Type of communication: Only attendance.
Authors: **Nuria Daghbouche-Rubio**.
Congress: International. Cardiovascular Research Symposium at UC Davis.
Location and date: from 24th to 26th March in Davis, California, US.

2021:

3. Title: *"Signaling pathways activated by G protein coupled receptors in essential hypertension: differential contribution of Gq11 and G12-13 proteins".*
Type of communication: Poster.
Authors: **Nuria Daghbouche-Rubio**, Pilar Cidad, Esperanza Alonso, Virginia Revuelto Fernández, M Teresa Pérez-García and José R. López-López.
Congress: The Physiological Society. Physiology 2021.
Location and date: from 12th July to 16th July. Online event.

2019:

4. Title: *"Histopathological damages in the epicardial coronary artery after ischemia and reperfusion injury in swine".*
Type of communication: Poster.
Authors: C. Rios Navarro, A. Ruiz-Sauri , **N. Daghbouche-Rubio** , J. Gavara , V. Marcos- Garces , G. Minana , FJ. Chorro , V. Bodi.
Congress: World Congress of Cardiology, ESC Congress Paris.
Location and date: from 31th August to 4th September in Paris, France.

NATIONAL

2022:

1. Title: *"Functional implication of P2Y6 and AT1 heterodimers in the pathogenesis of essential hypertension".*

Type of communication: Poster.

Authors: **Nuria Daghbouche-Rubio**, Inés Álvarez-Miguel, Jorge Rojo-Mencía, Pilar Cidad, M Teresa Pérez-García and José R. López-López.

Congress: National. Spanish Network of Ionic Channels Congress. VIII Reci Congress.

Location and date: from 24th May to 27th May in Alicante, Spain.

2019:

2. Title: *"Regulation of vascular tone in a mice model of essential hypertension: role of calcium-dependent chloride channels".*

Type of communication: Poster.

Authors: **Nuria Daghbouche-Rubio**, Inés Álvarez-Miguel, Pilar Cidad, Esperanza Alonso, M Teresa Pérez-García and José R. López-López.

Congress: National. Spanish Network of Ionic Channels Congress. VII Reci Congress.

Location and date: from 15th to 17th May in Cáceres, Spain.

3. Title: *"Characterization of the microscopic damage in the epicardial artery after an acute myocardial infarction in a porcine model".*

Type of communication: Poster.

Authors: Rios Navarro C., Ruiz-Sauri A., **Daghbouche-Rubio N**., Gavara J., Marcos- Garces V., Bonanad C., Miñana G., Díaz A., Chorro FJ., Bodi V.

Congress: National. Congress of Cardiovascular Diseases of the Valencian Society of Cardiology.

Location and date: from 23th to 24th May in Alicante, Spain.

Research dissemination

- "Three-Minute Thesis" competition, 2019 edition. University of Valladolid.
- "Three-Minute Thesis" competition, 2022 edition. University of Valladolid.
- "Training and Competition in Science Communication" competition, 2023 edition. SGroup Universities in Europe.

Index

Abstract

Introduction

Hypertension (HT) is the most common modifiable risk factor for cardiovascular disease, Strategies to control HT have a limited success, so there is an unmet need for identification of more efficient treatments for HT. A better understanding of the mechanisms regulating blood pressure, using genetic, molecular and physiological approaches, could identify novel pathways that can be potential drug targets, so that we can treat HT with a mechanistic-driven approach.

Materials and methods

We have use a mice model of essential HT (BPN, blood pressure normal, and BPH, blood pressure high) to explore the changes in the contractile responses of mesenteric arteries to agonists acting through G protein-coupled receptors (GPCR).

Results

Microarrays of vascular smooth muscle cells (VSMCs) from BPN and BPH mice provided differential expression of several elements in GPCR signaling pathways, and some of the most significant changes were functionally investigated. We found an increased expression of the purinergic receptor P2Y6 the, which correlates with augmented UTP-induced contractions in BPH arteries. Moreover, we described here that the upregulation of P2Y6R affects the contractile responses to angiotensin II (AgII), favoring the formation of heterodimers with the AgII receptors ATR1. ATR1 desensitization in the P2Y6R-ATR1 complexes is decreased, and this can contribute to the increased contractile responses to AgII in HT arteries. In spite of this increased response, we found reduced circulating AgII levels and less hypotensive effect in response to treatment with the ATR1 blocker losartan, indicating that overstimulation of the renin-angiotensin aldosterone system (RAAS) does not contribute to HT in BPH. Our data suggest that P2Y6R levels may represent a molecular switch to induce HT, so that this receptor may become a promising target for the treatment of HT.

We also characterize the variations in α-adrenergic signaling pathways in HT. The α1-adrenergic agonist Phenylephrine (Phe) elicited larger contractions in BPH vessels, so we investigated the potential mechanisms involved in this enhanced response. We explored the contribution of Ca^{2+} release from intracellular stores or the activation of L-type Ca^{2+} channels (LTCC), Ca^{2+} activated Cl^- channels and the transient receptor potential cation channels (TRPC3/6). Although some of these elements show changes in the BPH vessels, none of them recapitulates the increased contractile response. The contribution of phospholipase C (PLCβ) or rho-associated protein kinase (ROCK) to Phe-induced contraction was also decreased in BPH vessels, suggesting the presence of an additional mechanism activated by Phe and distinct from PLCβ or ROCK signaling pathways in BPH.

Conclusions

Overall, we found that the increased contractile responses to GPCRs agonist in HT is the result of a complex dysregulation of multiple molecular components rather than caused by changes in single elements. This pattern is in clear agreement with the multifactorial nature of the disease. Another important conclusion derived from the complex nature of this disease is the need to explore the effect of every molecular element in the proper context, considering the likely concomitant changes of its partners in the pathway.

Abbreviations

$\alpha\beta$-MeATP: α,β-methylene adenosine 5'-trisphosphate trisodium salt.

AC: Adenylate cyclase.
ACE: Angiotensin-converting enzyme.
Ach: Acetylcholine.
Ag I: Angiotensin I.
AgII: Angiotensin II.
AR: Adrenergic receptor.
ATR1: Angiotensin II type 1 receptor.

BK_{Ca}: Large conductance Ca^{2+}-dependent potassium channels.
BP: Blood pressure.
BPH: Blood pressure high.
BPN: Blood pressure normal.
BR2: Bradykinin type 2 receptor.

$Ca_v1.2$: L-type voltage gated Ca^{2+} channel subtype 1.2.
CaCCs: Calcium-activated Cl^- channels.
CFTR: Cystic fibrosis transmembrane conductance regulator.
CGRP: Calcitonin-gene-related-peptide.
CICR: Ca^{2+}-induce-Ca^{2+} release.
CLCs: Voltage-gated Cl^- channels.
CO: Cardiac output.
Ct: Threshold cycle.
CVD: Cardiovascular diseases.

DAG: Diacylglycerol.
DBP: Diastolic blood pressure.
DTT: Dithiothreitol.

E_{Cl^-}: Chloride equilibrium potential.
EDHF: Endothelium-derived hyperpolarizing factor.
EDTA: Ethylenediaminetetraacetic acid.
EGTA: Ethylene glycol tetraacetic acid.
eNOS: Endothelial nitric oxide synthase.
ET-1: Endothelin-1.

GAPDH: Glyceraldehyde-3P-dehydrogenase.
GDP: Guanosine diphosphate.
GPCR: G-protein coupled receptor.

GRK: G protein-coupled receptor kinase.

HEPES: 4-(2-hydroxyethyl)-1-piperazineethanesulfonic acid.
HT: Systemic arterial hypertension.
HW/BW: ratio between heart weight and body weight.
HW: Heart weight.

IC100: Vessel internal circumference at which 100 mmHg transmural pressure of passive conditions.
IC1: Vessel internal circumference at which active responses are maximal.
IC: Internal circumference.
IP_3: Inositol triphosphate.
IP_3R: Inositol 1triphosphate receptor.

JG: Renal juxtaglomerular cell.

K_{ATP}: ATP-dependent potassium channels.
K_{Ca}: Ca^{2+}-dependent potassium channels.
K_{IR}: Inward rectifier potassium channels.
K_v: Voltage-dependent potassium channels.

LTCCs: Voltage-gated calcium channels L-type.

MBP: Mean blood pressure.
MgPSS: Magnesium physiological solution.
MHC: Myosin heavy chain.
MII: Myosin II-type.
MLCK: Myosin light chain kinase.
MLCP: Myosin light chain phosphatase.
MT: Myogenic tone.

NA: Noradrenaline.
NCX: Na^+ - Ca^{2+} exchangers.
Nif: Nifedipine.
NP: Natriuretic peptide.

OD: Optical density.
Orai1: Ca^{2+}-release-activated Ca^{2+}-channel protein 1.

P2Y6R: Purinergic receptor P2Y6.
Phe: Phenylephrine.
PIP_2: Phosphatidylinositol 4,5-bisphosphate.
PKA: Protein Kinase A.
PKC: Protein Kinase C.

PKG: Protein Kinase G.
PLA: Protein ligation assay.
PLCβ: Phospholipase C β.
PM: Plasma membrane.
PMCA: Plasma membrane Ca^{2+}- atpase pump.
PSS: Physiological saline solution.
Pyr10: Pyrazole 10 compound.

RAAS: Rennin-angiotensin-aldosterone system.
RCA: Rolling circle amplification.
RGS: Regulators of G-protein signaling.
RhoA: Rho family of GTPases member A.
RhoGEFs: Nucleotide exchange factors.
ROCK: Rho-associated protein kinase.
ROCs: Receptor operated channels.
RP18S: Ribosomal protein 18s.
RT-qPCR: Real time quantitative polymerase chain reaction.
RT: Room temperature.
RyR: Ryanodine receptor.

SACs: Stretch-activated channels.
SBP: Systolic blood pressure.
SDS-PAGE: Sodium dodecyl sulfate polyacrylamide gel electrophoresis.
SEM: Standard error of the mean.
SERCA: Sarcoplasmic reticulum Ca^{2+}-ATPase pump.
sGC: Nitric oxide-sensitive guanylate cyclase.
SHR: Spontaneously hypertensive rats.
SMDS: Smooth muscle dissociation solution.
SNP: Sodium nitroprusside.
SNS: Sympathetic nervous system.
SOCs: Store operated channels.
SR: Sarcoplasmic reticulum.
STIM1: Stromal interaction molecule 1.
STOCs: Spontaneous transient outward currents.

TIRF: Total internal reflection fluorescence.
TLDA: TaqMan low density array.
TMEM16: Anoctamin family of Ca^{2+} activated Cl^{-} channels.
TPR: Total peripheral resistance.
TRP: Transient receptor potential channels.
TRPC: Transient receptor potential canonical family of channels.
TRPM: Transient receptor potential melastatin family of channels.
TXA_2: Thromboxane A2.

UDP: Uridine diphosphate.
UTP: Uridine triphosphate.

V_M: Membrane potential.
VDCCs: Voltage-dependent calcium channels.
VPR: Volume pressure recording.
VSMCs: Vascular smooth muscle cells.

1 Introduction

1.1 Essential Hypertension

1.1.1 Definition, etiology and treatment of hypertension

Systemic arterial hypertension (HT) is considered a highly modifiable risk factor and is associated with the development of numerous cardiovascular diseases (CVD), including renal, cerebral, and cardiac events. HT has a prevalence of 30% in the adult population of developed countries. In fact, HT is experiencing a steady increase and affects both sexes and all age groups. Overall, CVD causes more than 7 million deaths annually. Successful prevention and treatment of HT is key to reducing the burden of this disease (Mills *et al.* 2020).

HT is defined as persistently elevated arterial blood pressure (BP). Based on the new BP guidelines, different categories have been defined according to the criteria shown in **Figure I.1**. Importantly, systolic BP (SBP) and diastolic BP (DBP) measurements are obtained from the average of two or more data points recorded on two separate occasions. In this context, human BP is measured in the brachial artery using a non-invasive method, the sphygmomanometer. In drug-naïve individuals, antihypertensive treatment is initiated when > is 20/10 mmHg above the target value (Flack, Adekola 2020).

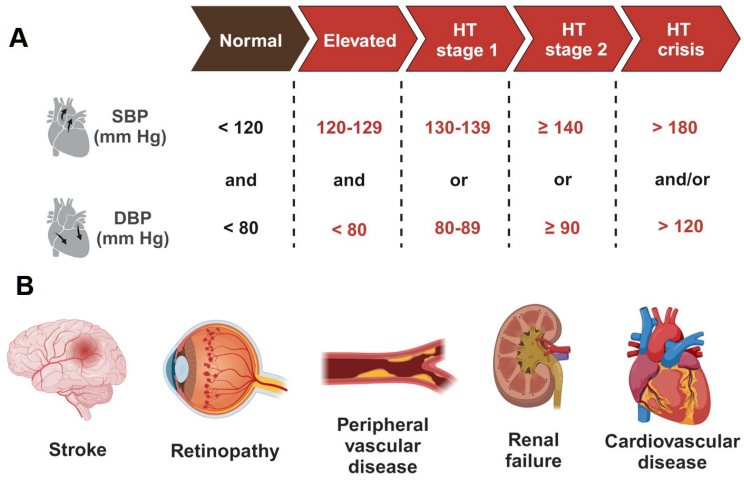

Figure I.1: *In A), Categories of HT and in B), Vascular disease associated with high BP disorder.*

Antihypertensive treatments are administered either as monotherapy or in combination. BP is not controlled with monotherapy in many patients, especially those with severe HT. Therefore, combinations of antihypertensive medications are required. Available drugs include 1) angiotensin II converting en-

zyme (ACE) inhibitors, 2) angiotensin II receptor inhibitors, 3) dihydropyridine calcium channel inhibitors, 4) thiazide diuretics, and 5) β-adrenoreceptor inhibitors. In addition, factors such as ethnicity influence response to antihypertensive treatments (Oparil *et al.* 2018). For example, calcium channel blockers and diuretics are usually the first choice for drug treatment in black individuals. Non-pharmacological interventions may have additional effects in lowering BP levels. Weight loss, physical activity, moderate alcohol consumption, dietary changes, and smoking cessation are usually recommended (Messerli *et al.* 2007).

Regarding etiology, most patients ($90 - 95\%$) had a heterogeneous primary, essential, or idiopathic form of HT. A complex interaction of genetic and environmental factors is involved in the pathology. Regarding genetics, a positive family history is common in HT patients and most studies show a heritability of $\sim$30 - 50% (Messerli *et al.* 2007). In some cases, HT is caused by a single genetic mutation that fully explains the cause of the disease. For example, PDE3A mutations (encoding the cGMP-inhibited 3′, 5′-cyclic phosphodiesterase A) lead to a decrease in cAMP levels and impaired vasodilation (Oparil *et al.* 2018). Regarding environmental influences, several components play a role in HT pathophysiology, such as high sodium intake, excessive alcohol consumption, psychological stress, poor sleep quality, or obesity-metabolism syndromes. The remaining $5 - 10\%$ of diagnosed cases are due to a secondary HT occurring because of an underlying medical condition. In particular, hyperaldosteronism, preeclampsia, and certain medications may be involved (Herring and Paterson 2018).

Several hypotheses have been proposed to explain the HT pathophysiology. Increased sympathetic nervous system (SNS) activity along with overstimulation of the renin-angiotensin-aldosterone system (RAAS). In particular, changes in the function and/or expression of ion channels in VSMC have been associated with HT, but controversial results have been found. The vascular bed and the experimental HT animal model used are crucial when examining the results in the literature. Of note, electrical remodeling involving different ion channels was identified as a characteristic feature of HT in our laboratory (Daghbouche-rubio *et al.* 2022). In terms of functionality, decreased activity of K^+ channels together with increased activity of $Ca_v1.2$ channels have been proposed as key factors in HT (Cox, Lozinskaya, *et al.* 2001; Pratt *et al.* 2002).

1.1.2 Animal models of hypertension

The study of essential HT as multifactorial disease is usually conducted by deconstructing the system into isolated components. The individual molecular and cellular changes are assessed with animal models genetically modified. The ultimate goal is to understand comprehensively these elements and reconstruct

a network for targeted therapeutic interventions. However, these approaches might not reflect the pathophysiological conditions during high BP development (Jama *et al.* 2022).

Alternatively, the researchers have widely characterized the molecular basis of HT using genetic and/or induced animal models (**Figure I.2**). Each of them present some advantages and disadvantages. Induced animal models, as AgII infusion or salt dietary treatment, allow researchers to induce HT in a controlled manner and focusing on the study of specific mechanisms. However, these models may not replicate the multifactorial nature of human essential HT, which can represent a potential limitation. Moreover, the induction process might cause varied responses, as well as, secondary effects unrelated to essential HT, adding complexity to the isolation of the primary causes of HT. Conversely, genetic models such as spontaneously hypertensive rats (SHR) or the Schlager BPHmice, reproduce the slow onset and polygenic nature of essential HT seen in humans, providing a more relevant context for study. Of note, genetic animal models are relatively low cost and widely available for research. In addition, these tools allow exploring the natural history of high BP development, partly due because they show a consistent hypertensive phenotype. However, genetic models may have a complex genetic background, making it challenging to characterize the factors responsible for HT. Moreover, these models might not fully account for the environmental factors that also contribute to human HT (Jama *et al.* 2022).

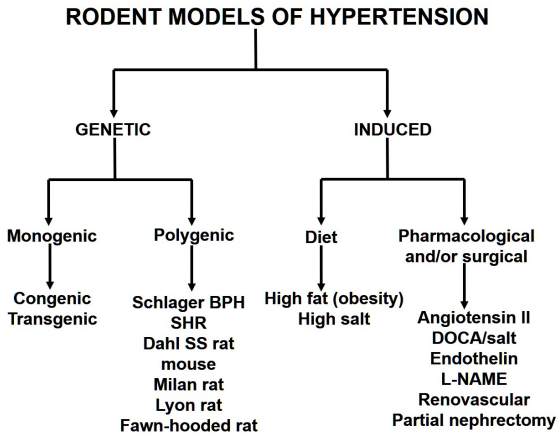

Figure I.2: *Summary of the most commonly used models of essential HT.*

In conclusion, choosing between genetic and induced models is dependent on the question to be answered in the research projects. In the present study, we have selected the Schlager BPH mice because we have detected a paucity in understanding the pathophysiology of HT in this model, as discussed in the next section.

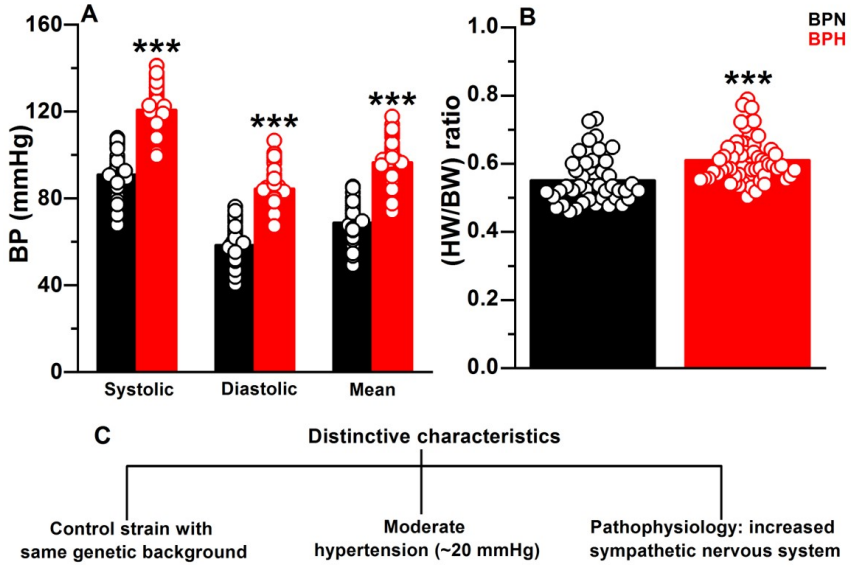

Figure I.3: *In A), BP measurements (expressed in mmHg) estimated in each group using the tail-cuff technique. Data represents the mean±SEM, where BPN=24 and BPH=16 animals. In B), Cardiac remodelling calculated by heart weight relative to body weight in BPN=41 and BPH=57 animals, respectively. The ratio was significantly higher in the BPH mice. Student's t-test was applied for unpaired parametric data, while Wilcoxon test for unpaired non-parametric data, where p-value ***< 0.001. In both cases for the data collection, the age of the animals was comprised between 4-6 months. In C), The schematic shows the distinctive feautures that make BPH a suitable model for studying HT pathophyiology.*

1.1.3 Schlager mouse model of essential hypertension

Experimental models of HT have developed over years and have fulfilled some gaps of knowledge. However, selecting the appropriate animal model is key for a better understanding of the disease. In the present study, adult male hypertensive mice, BPH/2J, and their corresponding normotensive control mice, BPN/3J were used (Schlager 1974).

These mice were obtained by crossbreeding with eight different strains selecting natural variants with high BP. This approach established three inbred lines sharing a genetic background of low (BPL/1J), normal (BPN/3J), and high BP (BPH/2J) (Schlager 1974). The BPN and BPH phenotypes were confirmed in our laboratory, as shown in the **Figure I.3**. BPH mice showed mildly elevated BP from 6 weeks of age, with maximal divergence at 21 weeks. This offer complementary information to investigate the HT progression and to examine novel drug targets. Importantly that, this model shares many features with human

HT, and with other genetic models such as, SHR detected (K. L. Jackson, Head, *et al.* 2019).

Moreover, BPH mice show an increased heart rate, a lower body weight, and a reduced lifespan compared to BPN mice. Global metabolic abnormalities, enhanced oxidative stress, and alterations in elements of the mitochondrial electron transport chain, which could be relevant to metabolism and ROS production were also detected (K. L. Jackson, Head, *et al.* 2019). In terms of HT pathophysiology, several lines of evidence point to a predominantly neurogenic mechanism, with increased activity of the SNS. Recently, novel insights were provided. In particular, endothelial dysfunctions and diminished NO-mediated vasodilator responses in BPH mesenteric arteries (Jelinic *et al.* 2023).

Overall, the presence of a control strain with a similar genetic background (BPN mice) enhances the suitability of the BPH model for study essential HT (Daghbouche-rubio *et al.* 2022). However, over past years there was a paucity of research studying the mechanisms underlying vascular pathophysiology in BPH. Although several studies have characterized the major changes in the resistance vasculature and its involvement in the progression of HT, further research is needed, to create an integrated model to understand the pathophysiology of essential HT.

1.2 Vascular system overview

1.2.1 Functional classes of vessels

Blood vessels can be classified by size, function, or cell composition as elastic, conduit, resistance, and exchange vessels which is shown in **Figure I.4** (Herring, Paterson 2018).

1. **Elastic arteries.** These large arteries represent temporary blood reservoirs that store mechanical energy. Their extracellular matrix is mainly composed of elastin. The aorta, iliac and pulmonary arteries are included in these categories.

2. **Conduit and feed muscular arteries.** Medium-sized feed arteries are responsible for flow conduction from elastic arteries to smaller arteries. These vessels actively control their diameter, because of their increased muscular layer. The brachial, radial, femoral, cerebral, and coronary arteries belong to this classification.

3. **Resistance arteries.** These vessels dominate the net resistance of the blood flow. In fact, they can be considered as taps of circulation because

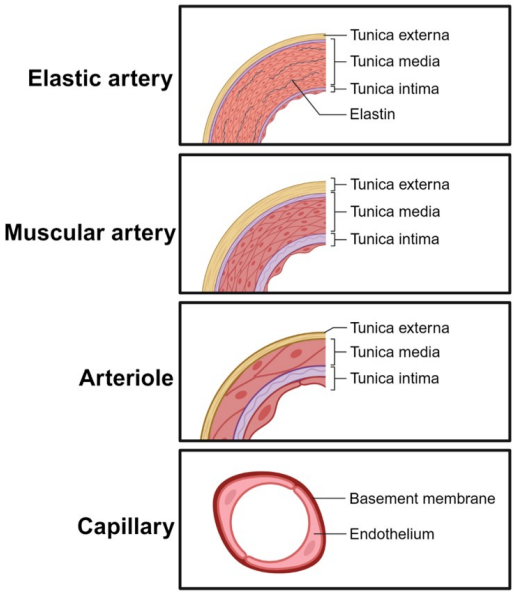

Figure I.4: *Illustration of the conceptual differences related to the diversity of vascular beds present in the organism.*

local blood flow can be switched or not, depending on the local cell demand. The proximal resistance vessels (terminal arteries) are richly innervated by sympathetic nerve fibers, and the muscular wall is thick relative to the lumen, while distal resistance vessels (terminal arterioles) are poorly

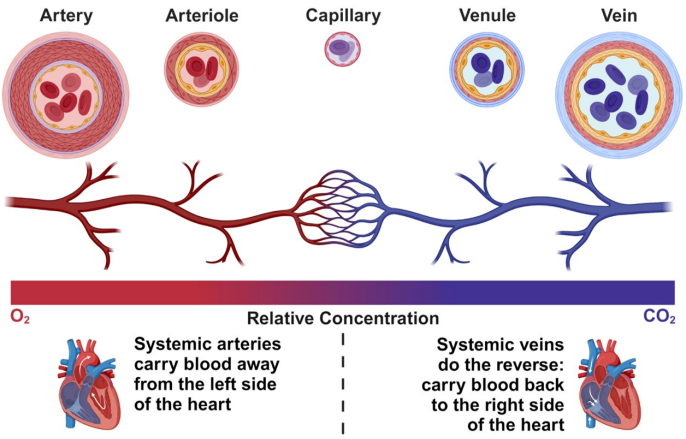

Figure I.5: *Overview of the cardiovascular system and the vascular arterial tree involved.*

innervated.

4. **Exchange arteries.** Capillaries are responsible for providing and interchanging O_2, CO_2, metabolites, and fluids between the blood and tissue. The structure of the capillary wall comprises a single layer of endothelial cells with no media or adventitia. The large cross-sectional area of the capillary bed slows the blood velocity, allowing correct gas exchange form blood to tissues.

The pressure gradient is the most important factor driving the blood flow along the bloodstream. Ventricular ejection increases the aortic pressure to approximately 100 mmHg. The BP alternates between SBP (around 120 mmHg) and DBP (80 mmHg) due to pulsatile hearth pumping (**Figure I.5**). As blood flows through the systemic circulation, pressure gradually decreases to finally dissipate at the entrance into the right atrium (Aaronson *et al.* 2004).

1.2.2 The vascular wall

Blood vessels wall is composed of a three-layered structure, except in capillaries, consisting of the tunica intima, tunica media, and tunica adventitia with different histological and functional properties (**Figure I.6**).

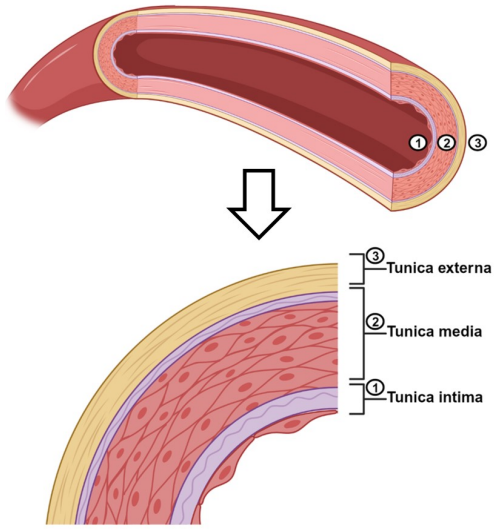

Figure I.6: *Three differentiated layers in a resistance vessel.*

The tunica intima

The intimal layer consists of a sheet of flattened endothelial cells that rest on a thin layer of connective tissue. Tight junctions connect endothelial cells lining the vascular lumen of the vessels. The basement membrane is adjacent to the endothelium. Endothelial cells have several physiological functions such as vascular permeability, local vascular control, angiogenesis, and regulation of homeostasis. Endothelial dysfunction can lead to various pathological disorders, including HT, atherosclerosis, stroke, or inflammatory syndromes (Aird 2007).

The tunica media

The tunica media consists of spindle-shaped VSMCs arranged in a spiral and embedded in a matrix of elastin and collagen fibers. Two elastin layers, the inner and outer elastic laminae, mark the boundaries of the media. Their main function is to provide mechanical strength and contractile force. Intimal endothelial cells are in close contact through myoendothelial connections to allow the transmission of signals from the intima to the media. VSMC are arranged in multiple layers in large-caliber resistance vessels. However, in arterioles, a single layer of smooth muscle (SM) cells forms tunica media (Levick 2003).

The tunica adventitia

The tunica adventitia is a connective tissue sheath with no clear outer boundary. The outer elastic lamina separated the tunica media from the tunica adventitia. Its main function is to connect the vessel to the surrounding tissue. In addition, most vessels contain sympathetic fiber terminals. Each terminal, in turn, has numerous bead-like thickenings (also called varicosities) that release vasoconstrictors. For example, norepinephrine and other neurotransmitters are produced to regulate local contractility, and thus, resistance and blood flow. The adventitia in large arteries and veins also contain small blood vessels called *vasa vasorum* that nourish vessel wall (Aaronson *et al.* 2004).

1.3 Biology of the vascular smooth muscle cell

1.3.1 Vascular smooth muscle cell structure

VSMCs are mononuclear and typically have a spindle-shaped or irregularly elongated cylinder whose diameter gradually decreases toward the end. These cells had a diameter of 5-10 μm and a length of 50–200 μm. The elongated shape of

VSMCs allows them to spiral around the vessel and changes in their tone will contract or dilate the vessel (Levick 2003).

Two cytoplasmic proteins form the contractile machinery of VSMCs, with an actin:myosin ratio of 10:1 (Gabella 1984). Actin filaments lack troponin, which is responsible for regulating Ca^{2+} sensitivity in skeletal and striated muscles. Instead, VSMC possess another regulatory protein, calmodulin. Myosin filaments bind to actin and exhibit enzymatic ATPase. Actin filaments are rooted in dense bands on the inner cell membrane and dense bodies in the cytoplasm, which function like Z-lines in cardiac muscle cells. A third kind of filament, intermediate filaments links dense bodies and dense bands, so that the entire cell contract as a single unit. Gap junctions electrically connect VSMCs such as in cardiac muscle cells. These low-resistance intercellular connections allow the propagation of responses along the length of the blood vessels (Aaronson *et al.* 2004).

The VSMC also form gap junctions with the endothelial cells, referred as heterocellular or myoendothelial gap junctions. Although, their role is controversial, they might transmit hyperpolarizing signals from the endothelium to the tunica media (Wit *et al.* 2008). The membrane surface of VSMCs contains numerous small invaginations called caveolae. It increases the surface area of the cells by up to 75% (Makarewich *et al.* 2012). The sarcoplasmic reticulum (SR) is the major releasable Ca^{2+} source in cells, with a storage capacity of 10-100 μm. The SR of VSMC is relatively underdeveloped, especially in resistance vessels, where it occupies only 2-6% of the cell volume. SR is equipped with two types of Ca^{2+} release channels, inositol 1,4,5-trisphosphate receptors (IP_3Rs) and ryanodine receptors (RyRs). The nucleus is located in the central part of the cell, and organelles, such as the Golgi complex or the mitochondria, are mainly located in the perinuclear region (Woll, Van Petegem 2022).

1.4 Vascular smooth muscle function

1.4.1 Crossbridge cycle

VSMC contraction depends on crossbridge formation between thick myosin filaments and thin actin filaments, regulated by cytosolic $[Ca^{2+}]_i$. Ca^{2+} increase can result from either Ca^{2+} entry trough different PM ion channels or Ca^{2+} release from internal stores (**Section 1.4.3**). Ca^{2+} elevation allows the formation of the Ca^{2+}-calmodulin complex, which in turn activates myosin light chain kinase (MLCK). MLCK phosphorylates the myosin light chain (MLC), enabling actin and myosin interactions to form crossbridges (Z. Liu, Khalil 2018). This process is represented in the **Figure I.7**.

Vascular relaxation occurs via myosin light chain phosphatase (MLCP),

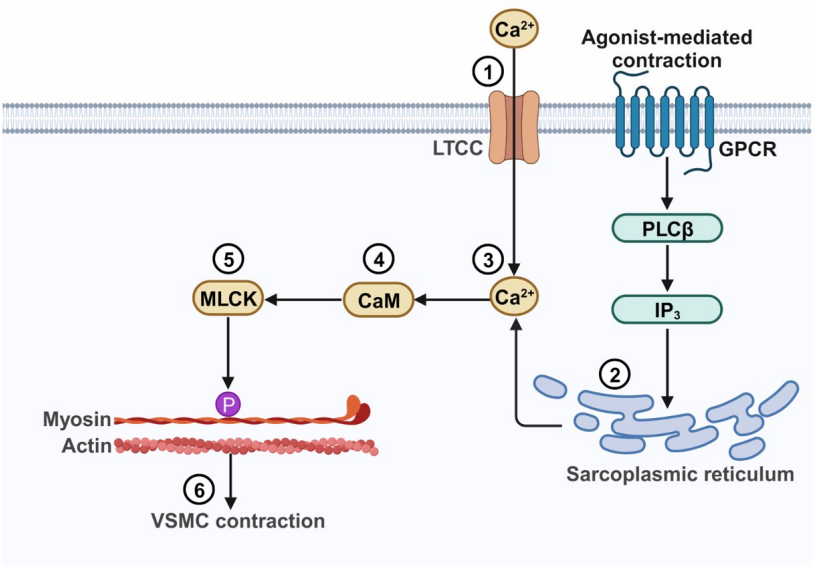

Figure I.7: *After GPCR agonist stimulation, both extracellular* Ca^{2+} *entry (1), mainly through LTCCs, and* Ca^{2+} *release from SR (2) induce an intracellular* Ca^{2+} *elevation (3). This leads to* Ca^{2+}*-calmodulin complex formation (4) and MLCK activation (5). This ultimately triggers the phosphorylation of the MLC and VSMC contraction (6).*

which turns off the myosin-actin apparatus. When cytosolic Ca^{2+} concentrations declines, MLCK activity decreases and MLCP activity increases. MLCP removes the phosphate group of the myosin chain and avoid crossbridge formation. Thus, the degree of contraction is the net balance between MLCK and MLCP enzymes (Silverthorn 2018). Of note, VSMC contraction is modulated by a plehtora of stimuli (see **Section 1.4.3**), including changes in resting membrane potential (V_M) and natural ligands acting on PM receptors. In particular, after agonist-receptor interactions, two components are recognized in the contractile responses, as is indicated in **Figure I.8**. Tipically, an initial rising phase is promoted due to the Ca^{2+} release from SR, followed by a tonic sustained phase due to extracellular Ca^{2+} influx and Ca^{2+} sensitization mechanisms (Herring, Paterson 2018).

In contrast to skeletal muscle, VSMCs are capable of maintaining longer contractions, altough at a slower pace and with a reduced energy expenditure. Under certain conditions, SM can enter a state known as the “latch state”, where actin and myosin remain bound, allowing sustained tension without ongoing ATP energy consumption. Additionally, the relatively low rate of ATP consumption in VSMCs contributes to prolonged tension (Murphy, Rembold 2005).

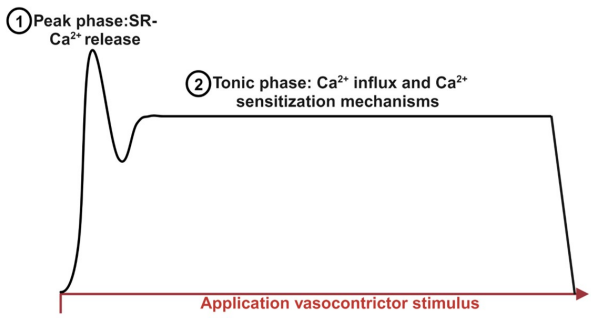

Figure I.8: *Two components are distinguished in agonist-mediated contractions. In 1) an initial rise phase due to the release of* Ca^{2+} *from internal stores. In 2) a sustained tonic phase follows due to* Ca^{2+} *influx from the extracellular medium and* Ca^{2+} *sensitization mechanisms.*

1.4.2 Intracellular calcium homeostasis

Vascular tone is controlled by the degree of contraction of VSMCs, which in turn is determined by $[Ca^{2+}]_i$. Upon receptor stimulation, Ca^{2+} concentration depends mainly on three mechanisms: Ca^{2+} influx from extracelullar media, Ca^{2+} release from internal stores, and Ca^{2+} extrusion pumps (Gorlach *et al.* 2006).

Calcium influx from extracelullar media

This Ca^{2+} entry can take place through voltage-dependent and voltage- independent Ca^{2+} channels (Sanders 2001).

1. **Voltage-dependent calcium channels (VDCCs)**, such as L- and T-type Ca^{2+} channels which are activated by depolarization (Nelson *et al.* 1990).

2. **Voltage-independent calcium channels.** These include (1) receptor-operated channels (ROCs), (2) store-operated channels (SOCs), and (3) mechanosensitive-activated channels (SACs).

(1) ROCs are regulated by agonist-receptor interactions, independently of V_M changes. After receptor stimulation, downstream molecular effectors are activated and channel opening is promoted (Brozovich *et al.* 2016). (2) SOCs are activated by SR depletion of intracellular Ca^{2+} ions. This initiates Ca^{2+} refilling of internal stores. Direct or indirect interactions have been observed between TRPC channels, stromal interaction molecule 1 (STIM1), and Ca^{2+} release-activated Ca^{2+} channel protein 1 (Orai1). Specifically, STIM1, a protein

located in the SR, translocates to the PM and associates with TRPC1. However, the molecular constituents belonging these cascades are not fully established. In addition, the role of these pathways in VSMC contraction remains unclear (Sanders 2001). (3) SACs are mechanosensitive channels induced by stretching of the vessel wall, thereby contributing to the myogenic tone (MT) responses. Various TRP channels have been associated, including TRPC6 (Welsh *et al.* 2002).

Calcium release from internal stores

The release of Ca^{2+} from internal stores is an agonist and inositol triphosphate (IP_3) dependent process. PLCβ activation hydrolyzes phosphatidylinositol bisphosphate (PIP_2) to activate the second messenger IP_3. Soluble IP_3 rapidly diffuses to the nearby SR to activate large-conductance IP_3R channels. Large local Ca^{2+} signals are generated in the cytosol with a small number of IP_3Rs. Furthermore, a biphasic response to $[Ca^{2+}]_i$ is exhibited, referred to as bell-shaped Ca^{2+}. Low concentrations cause activation, while high concentrations lead to inhibition of channel opening. RyRs are also present in the SR; however, their functional role in VSMC Ca^{2+} signaling is still not fully understood Woll, Van Petegem 2022).

Calcium extrusion pumps

Different pumps tightly regulate Ca^{2+} concentration in VSMC. The SR Ca^{2+} -ATPase (SERCA) is responsible for Ca^{2+} reuptake into the internal stores. PM Ca^{2+}-ATPase (PMCA) accomplishes Ca^{2+} extrusion. Other key components in Ca^{2+} homeostasis are the Na^{2+}-Ca^{2+} exchangers (NCX). Notably, a limited but continuous Ca^{2+} influx occurs under resting conditions, mainly via LTCCs. Therefore, Ca^{2+} PM pumps are actively involved in Ca^{2+} clearance to maintain the vascular homeostasis. In HT, the balance between Ca^{2+} mobilizing and Ca^{2+} removal mechanisms might be disrupted, overall leading to an increased $[Ca^{2+}]_i$ and prolonged vasoconstriction (Herring, Paterson 2018).

1.4.3 Excitation-contraction coupling

SM contraction can be induced by a variety of stimuli. When V_M is the main stimulus the process of excitation-contraction is defined as “electromechanical coupling”, whereas the term “pharmacomechanical coupling” is used if the contractile response is elicited by chemical agents (**Figure I.9**).

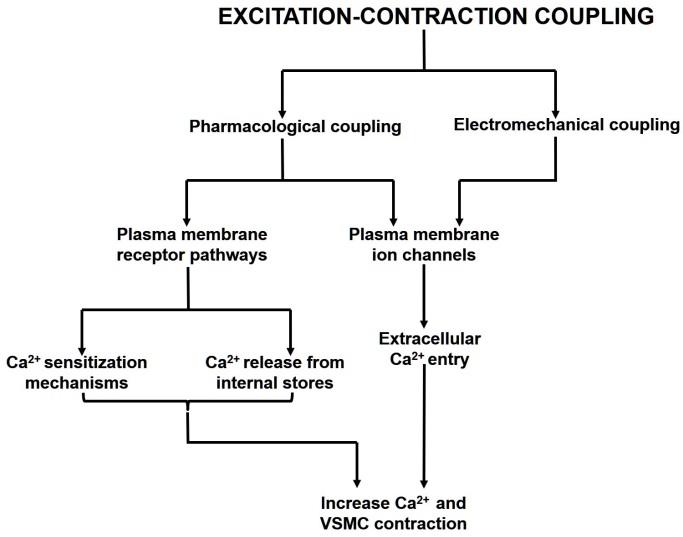

Figure I.9: *In electromechanical coupling, changes in the V_M are the driving forces in the SM responses. However, in pharmacomechanical coupling, downstream signaling pathways are inductors of SM responses. In particular, receptor-ligand interactions modulate the activation of intracellular cascades.*

Electromechanical coupling

Under physiological resting conditions, VSMCs present V_M values ranging from -40 to -60 mV. Variations in V_M finely modulate the contractile state of VSMCs. Cell depolarization increases the opening probability of LTCC channels, causing $[Ca^{2+}]_i$ elevation and contraction. Conversely, cell hyperpolarization decreases the opening probability of LTCC channels, decreasing Ca^{2+} entry and inducing relaxation. In this scenario, the balance between hyperpolarizing and depolarizing influences determine the net contractile state of VSMC and therefore, BP. This balance is mainly controlled by the activity of K^+ and Ca^{2+} channels (Nelson *et al.* 1990).

Pharmacomechanical coupling

Pharmacomechanical coupling is driven by receptor-ligand interactions (**Figure I.10**). This leads to the activation of downstream signaling pathways and contraction can be achieved via V_M-independent mechanisms. In fact, in many cases changes V_M are secondary to the activation of these pathways. The most relevant pathways that regulate the vascular tone depend of the activation of GPCR. After receptor stimulation, different subtypes of heterotrimeric

G-proteins bind to the receptor. In the inactive state, G_α, G_β, and G_γ subunits are bound forming a trimeric complex. Upon activation, G_α dissociates from the G_β and G_γ subunits. As a result, vasoconstrictor or vasodilator responses are initiated, depending on the activated G protein subtype (Brozovich *et al.* 2016).

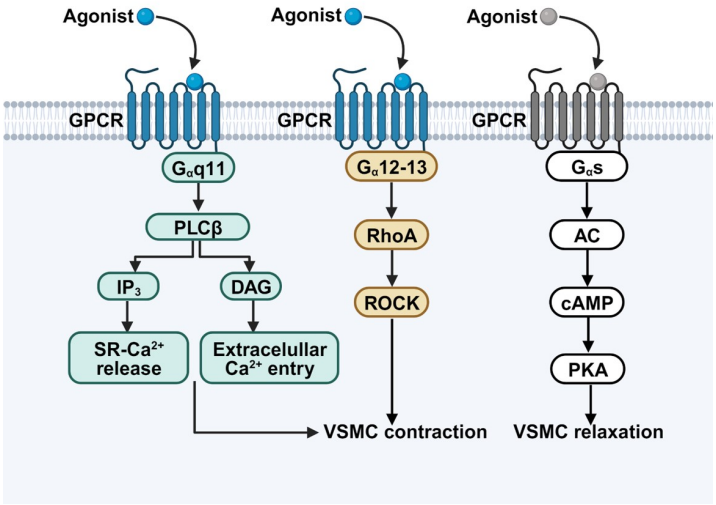

Figure I.10: *Diagram of the correlation between the response specificity and the activated G protein subtype. Adrenergic, purinergic, and AgII systems are coupled to at least one of these G proteins to mediate either vasoconstrictor or vasodilator responses.*

Vasodilator mechanisms: They are exemplified by some adrenergic receptors (ARs). β_2-AR are coupled to adenylyl cyclase (AC) through the activation of G_αs proteins. The membrane-bound AC catalyzes the conversion of ATP to cyclic adenosine monophosphate (cAMP). cAMP in turn activates protein kinase A (PKA), which triggers VSMC relaxation through phosphorylation of multiple targets. This ultimately leads to a decrease in $[Ca^{2+}]_i$ and VSMC dilatation Morgado *et al.* 2012).

Vasoconstrictor mechanisms: A large number of GPCR agonists induce G_αq11 and G_α12-13 signaling pathways, for instance the mimetic α_1-AR agonist phenylephrine (**Figure I.11**). Global increase in $[Ca^{2+}]_i$ triggered VSMC contraction. Ca^{2+} release from the SR and Ca^{2+} influx from the extracellular space are the main related sources. However, Ca^{2+}-independent mechanisms are also involved in SM contractile responses (Brozovich *et al.* 2016).

Following G_αq11 activation, downstream molecular effectors are activated. PLCβ, is a membrane-bound enzyme responsible for cleaving PIP_2, resulting in the generation of IP_3 and DAG. IP_3 and DAG regulate two parallel pathways, increasing $[Ca^{2+}]_i$ and finally promoting MLC phosphorylation. IP_3 regulates

Ca^{2+} release from SR into the cytosol, causing a rapid and transient increase in $[Ca^{2+}]_i$. Following the $[Ca^{2+}]_i$ peak, there is a sustained elevation of Ca^{2+} above basal levels due to receptor-operated channels on the plasma membrane, which facilitates Ca^{2+} entry from the extracellular space (Z. Liu, Khalil 2018).

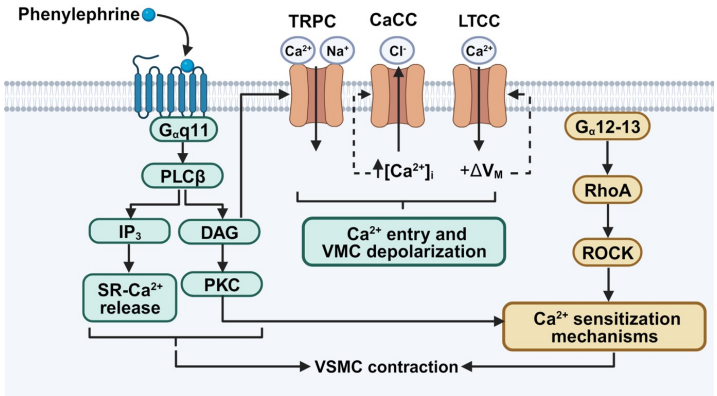

Figure I.11: *After receptor stimulation, $G_\alpha q11$ and $G_\alpha 12$-13 are induced, representing the two major pathways of VMSC contraction.*

DAG mediates VSMC contraction via activation of protein kinase C (PKC). PKC is a serine/threonine kinase, and three isoforms have been described in VSMC. PKCα and PKCβ are dependent on DAG activation and $[Ca^{2+}]_i$, while, PKCε is only dependent on DAG. Overall, PKC modulated VSMC contraction by phosphorylating MLCK, Rho-kinase (ROCK) and various ion channels and transporters (Z. Liu, Khalil 2018).

G_α12-13 activates the RhoA/ROCK signaling pathway. ROCK blocks MLCP, preventing MLC dephosphorylation and then, sustaining contraction independently of Ca^{2+} levels (Ca^{2+}-sensitization). RhoA is a small monomeric G-protein activated by GTP binding. This process is triggered by nucleotide exchange factors (RhoGEFs) that catalyze the exchange of GDP for GTP. The RhoA-GTP complex stimulates ROCK, a serine/threonine kinase that phosphorylates several target proteins including the myosin phosphatase target subunit 1 (MYPT1). This leads to MLCP inhibition, preventing MLC dephosphorylation.

Altogether, the G_α12-13-RhoA-ROCK signaling pathways maintain VSMC contraction in the absence of significant changes in $[Ca^{2+}]_i$ (Gohla *et al.* 2000).

In addition to the regulatory effects of ROCK, CPI-17 is another protein whose phosphorylation leads to inactivation of MLCP. CPI-17 phosphorylation occurs in Ca^{2+}-dependent and-independent manners. PKC is involved in Ca^{2+}-dependent mechanisms and rapidly regulates CPI-17 phosphorylation. In Ca^{2+}-independent mechanisms, either PKC or ROCK is involved in CPI-17 phospho-

rylation in the later phases (Woodsome *et al.* 2006).

In HT, some of the molecules involved in the GPCR dependent pathways might be altered. In particular, ROCK may be crucial in HT pathogenesis. This has been suggested in different experimental HT models, either genetically or pharmacologically induced (Z. Liu, Khalil 2018). A higher of RhoA/ROCK activity was detected in VSMC from conduit arteries (aorta), suggesting a common mechanism in the progression of the disease in four rat HT experimental models. *In vivo* administration of ROCK inhibitors lowered BP levels (Seko *et al.* 2003). In the same line, an increased RhoA/ROCK activity substantially contributed to cerebral artery tone *in vivo* in two different HT rat models (Chrissobolis, Sobey 2001). However, no studies were reported in resistance vessels (mesenteric arteries). Altogether, further research is needed to elucidate the changes in vascular contractility and its involvement in HT.

1.5 Vascular tone regulation

The vascular tone regulates the diameter of vessels and thus blood flow and BP. In fact, the contractile activity of the VSMCs in small arteries walls is the main determinant of the resistance in the vascular circulation (Herring, Paterson 2018). Blood flow (Q) depends of the pressure drop from arteries to veins (ΔPa) and the resistance of the vessels (R):

$$Q = \frac{\Delta P\mathrm{a}}{R} \qquad (Darcy's\ Law) \qquad \text{(Eq. 1.1)}$$

Jean Leonard Marie Poiseuille elucidated the factors governing tube resistance. He found that resistance was directly proportional to fluid viscosity (η) and tube length (L) and inversely proportional to the tube radius (r) raised to the fourth power:

$$R = 8\eta \cdot L/\pi r^4 \qquad \text{(Eq. 1.2)}$$

Combining this equation with Darcy's Law and rearranging terms:

$$\Delta P_a = Q\, 8\eta\, L/\pi r^4 \qquad \text{(Eq. 1.3)}$$

From this equation, it is evident that small changes in radius result in big effects on mean arterial pressure, constituting an extremely powerful mechanism by which blood vessels regulate both local blood flow and mean arterial pressure (Aaronson *et al.* 2004). Since the vascular tone defines the vessel radius, VSMCs finely control both $\overline{P_a}$ and blood flow.

In terms of vascular tone regulation, VSMCs are influenced by both intrinsic and extrinsic factors. In this sense, the resistance vessels are exposed to a complex interplay of vasoconstrictor and vasodilator stimuli, which ultimately determines the net contractile state of the SM (Levick 2003).

In HT, during the early stages, an increase in CO may be observed, with a normal or slight elevation of TPR. However, during the stable stage, CO tends to return to normal levels, whereas TPR is high because due to the increased vascular tone in the small arteries. Compensatory mechanisms might be activated to normalize the left ventricular function and arterial wall tension, thereby maintaining CO normal (Mayet, Hughes 2003).

1.5.1 Intrinsic mechanisms

The myogenic response (MT)

The MT is an autoregulatory mechanism elicited in VSMCs upon BP changes, which was first described by Sir William Bayliss in 1902 (W. M. Bayliss 1902). When BP increases, the stretch in the vessel wall is transduced to a contractile response. Conversely, when BP drops, the decrease in stretch leads to relaxation (**Figure I.12**). This is a crucial mechanism to maintain blood flow despite variations in BP, ensuring a continuous supply of O_2 and nutrients to the tissues (Schubert, Mulvany 1999).

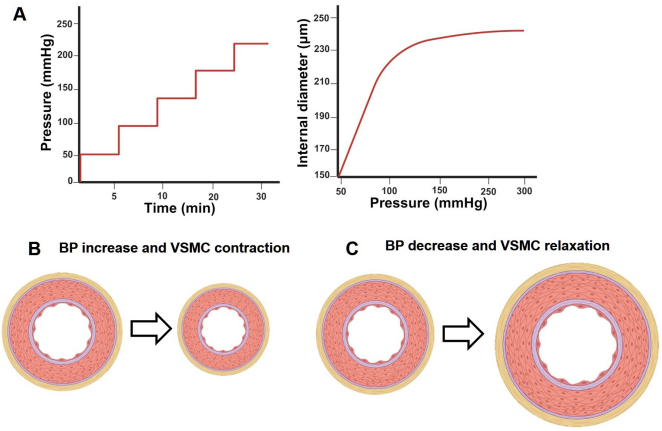

Figure I.12: *In A), Is depicted an experimental protocol, where an increasing gradual rise of BP is applied to the mesenteric arteries mounted in the pressure myograph over time. Then, a pressure-diameter curve is constructed, highlighting that in BPH mice a higher MT was described compared to BPN (data not shown). In B) and C), Are indicated the conceptual differences regarding the two possible scenarios of the MT and the link between BP and VMSC responses.*

The MT response is initiated by activation of SAC channels. Although, their molecular identity is not fully understood, TRPC6 and the epithelial Na^{2+} channels are among the candidates (Kim *et al.* 2013; Welsh *et al.* 2002). Their activation leads to cell depolarization, which in turn triggers LTCCs channels opening to further increase $[Ca^{+2}]_i$ and initiate VSMC contraction (Brayden, Nelson 1992; Knot, Nelson 1998). GPCRs coupled to $G_\alpha q11$ and $G_\alpha 12\text{-}13$ signaling pathways may also contribute to MT (Gudi *et al.* 1998; Narayanan *et al.* 1994).

Endothelial mediators

Endothelial vasoactive substances play a key role in vascular tone and BP regulation. Nitric oxide (NO) as vasodilator and endothelin (ET-1) as vasoconstrictor are particularly relevant (Versari *et al.* 2009).

NO is produced by shear stress, inflammatory mediators or certain agonists (**Figure I.13**). All these stimuli increase $[Ca^{2+}]_i$, activating the endothelial NO synthase (eNOS). NO rapidly spread out into the SM layer, where interacts with the soluble guanylyl cyclase (sGC), producing cyclic guanosine monophosphate (cGMP) and activating the protein kinase G (PKG1). Phosphorylation of PKG1 targets lead to a decrease in $[Ca^{+2}]_i$ and SM relaxation (Kraehling, Sessa 2017). The classical dogma establishes that HT is characterized by an attenuation of the

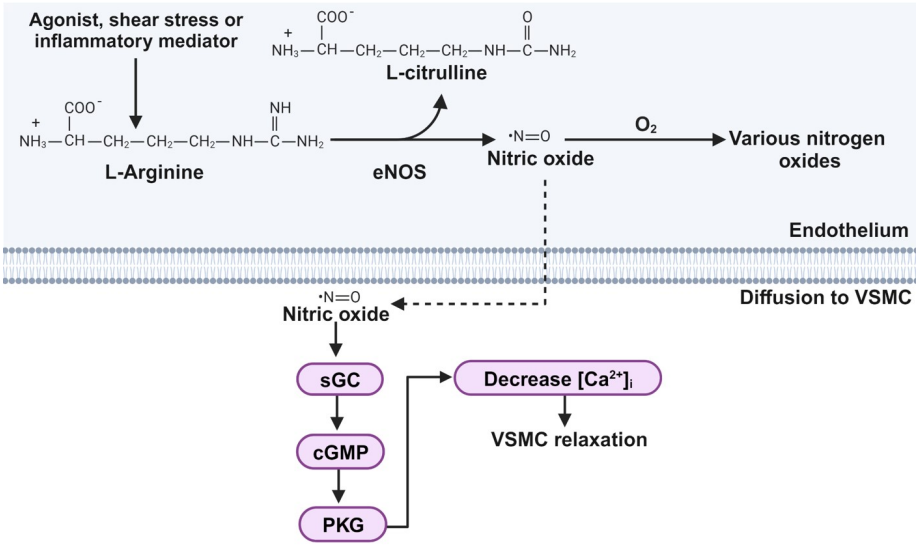

Figure I.13: *Overview of the endothelial nitric oxide synthesis and the VSMC relaxation pathway activated.*

vasodilator responses. The molecular components of the signaling cascade NO-sGC-cGMP-PKG have been studied with knockout (KO) mice. In particular, PKG1 KO mice, showed a significantly impaired VSMC dilatation (Pfeifer *et al.* 1998). However, further studies are needed to elucidate the NO signaling pathways changes in VSMC and its involvement in HT.

ET-1 is a potent endothelial vasoconstrictor and various isoforms have been described. In VSMCs, ET-A is the predominant receptor that mediates VSMC contractile responses via the $G_{\alpha}q11$ and $G_{\alpha}12$-13 signaling pathways (Compeer *et al.* 2013; Wirth *et al.* 2008).

Other local vasoactive agents

Other local vasoactive chemicals, released by neighbor cells such as circulating neutrophils or platelets can have a significant effect on VSMC responses. These include thromboxane A2 ($TXA_2$2), which is produced by platelets during hemostasis. Additional factors could be involved, as inflammation. $TXA_2$2 is coupled to GPCRs, activating $G_{\alpha}q11$-PLCβ pathway. In VSMC, $TXA_2$2 released by platelets is responsible of the potent local vasoconstriction to limit blood loss and to facilitate platelet aggregation. In HT, some studies have suggested the role of $TXA_2$2 in BP and vascular tone regulation, with controversial results in the literature (Sellers, Stallone 2008).

Nerve endings, leukocytes, platelets, SM and endothelial cells are also able to release nucleotides to the extracellular space. Among them, uridine triphosphate (UTP) and uridine diphosphate (UDP) are relevant to VMSC, where they bind to several types of P2Y metabotropic receptors (Burnstock 2017), such as P2Y2R, P2Y4R and P2Y6R. UTP is a natural agonist of P2Y2R and P2Y4R, while UDP selectively activates P2Y6R. However, because UTP is rapidly degraded to UDP, the study of receptor subtypes involved in UTP-mediated effects in VSMCs becomes even more complex (Lazarowski, Boucher 2001). In addition, molecular characterization is limited by the lack of specific agonists and antagonists (Müller, Namasivayam 2021). Nevertheless, several studies have undoubtedly pointed to P2Y6R as a relevant player in vascular tone and BP regulation. In physiological conditions, UTP and UDP-induced contractile responses in mouse mesenteric arteries with similar potency, likely through P2Y6R (Vial, Evans 2002). The purinergic signalling in the cardiovascular system is widely studied, although some questions remain to be solved in HT.

1.5.2 Extrinsic mechanisms

Sympathetic nervous system

The SNS plays a crucial role in vascular tone and BP regulation. The majority of the resistance arteries are highly innervated with sympathetic nerves present in the tunica adventitia. NA is released together with ATP. ATP stimulates P2X ionotropic purinergic receptors and NA binds to α_1-ARs. Overall, this mediates VSMC contractions (Herring, Paterson 2018).

Sympathetic fibers are tonically active. This contributes significantly to the setting of the vascular tone at rest. In general terms, an increase of SNS activity leads to vasoconstriction, while, a decrease of SNS activity causes a vasodilatation. In alterations such as hypovolemia, a larger sympathetic outflow allows to keep BP and CO constant. This effect is obtained by reducing peripheral blood flow, displacing blood from the peripheral to central veins, promoting interstitial fluid absorption, and increasing TPR.

Renin-angiotensin aldosterone system

Angiotensin II (AgII) is a potent vasoconstrictor produced under hypovolemia and hypotension, as represented in **Figure I.14**. AgII secretion is modulated by renin, a proteolytic enzyme produced by the renal juxtaglomerular cells (JG), via β_1 -AR stimulation. Renin cleaves off the hepatic angiotensinogen to generate the angiotensin I (Ag I). This low-activity compound is hydrolyzed by ACE on the surface of endothelial cells, primarily in the lungs. ACE produces the active octapeptide AgII. The concentration of circulating AgII depends on the rate of renin production by the JG cells. Renin exocytosis is activated by several factors including hypotension, increased sympathetic activity, and decreased Na^{2+} or Cl^{-} concentrations. Conversely, AgII inhibited renin secretion in a negative feedback loop (Su *et al.* 2021). AgII is the major vasoactive peptide of the vascular system and a myriad of effects have been reported. Vasoconstrictor-mediated effects increase vessel resistance and BP levels.

AgII also promotes sympathetic nervous activity. In addition, AgII acts on the hypothalamus to stimulate thirst sensation, leading to fluid intake directed to restore plasma volume. AgII induces aldosterone secretion in the adrenal cortex, leading to increased Na^{2+} reabsorption rate in the distal renal tubules, associated to water reabsorction via osmosis. Overall, these actions maintain constant plasma volume and intraluminal arterial pressure (Mehta, Griendling 2007). In HT, RAAS system dysfunction has been reported (Ma *et al.* 2023).

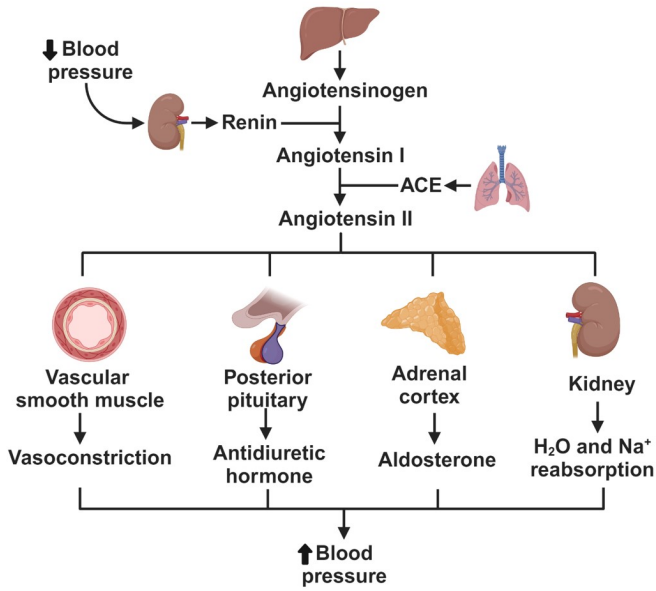

Figure I.14: *Overview of the AgII synthesis pathway.*

Other vasoactive hormones

Other vasoactive hormones could be involved in the regulation of vascular tone and BP.

Adrenaline is released by the adrenal medulla in response to SNS. In contrast to NA, adrenaline has a mixed effect on TPR and BP. NA released from sympathetic nerve endings causes widespread constriction, which greatly increases TPR and arterial BP. In contrast, adrenaline activates β_2-ARs, leading to vasodilation, particularly in skeletal muscle. The vasodilator effect of adrenaline on β_2-ARs in skeletal muscle outweighs the vasoconstrictor effect on α_1-ARs in other tissues. As a result, the net effect of adrenaline is a reduction in TPR, while still increasing CO, leading to a slight or little change in BP (Herring, Paterson 2018). In pathological conditions, elevated plasma levels of adrenaline have been observed in experimental animal models of HT SHR (Jablonskis, Howe 1994).

Natriuretic peptide (NP) is a vasodilator peptide hormone secreted by the heart, particularly the atria, in response to increased cardiac stretching and volume overload. Atrial natriuretic peptide (ANP) is the major circulating isoform. NP receptors are present on VSMCs, the endothelium, and tubule epithelium. NP mediates vasodilation via cGMP signaling pathways. In addition, NP induces renal salt and water excretion (Lorigo *et al.* 2022).

1.6 Vascular smooth muscle ion channels

VSMCs exhibit a large variety of ion channels in their PM, involved in the regulation of contractility and vascular tone (W. F. Jackson 2000). Ion channels present in VSMCs can be classified in the following groups:

1. **Potassium channels**, including voltage-dependent K^+ (K_v) channels, inward rectifying K^+ channels (K_{ir} and K_{ATP}) and large-conductance Ca^{2+}-activated channels (BK_{Ca}).

2. **Voltage-gated calcium channels**, including L-type (LTCCs) and T-type.

3. **Transient receptor canonical family of channels (TRPC)**, which belong to the three subcategories of ROCs, SACs and SOCs channels, as described previously.

4. **Chloride channels** (Cl^- channels), such as Ca^{2+}-activated Cl^- channels (CaCCs), bestrophins, voltage-gated Cl^- channels (CLCs) and cystic fibrosis transmembrane conductance regulator (CFTR).

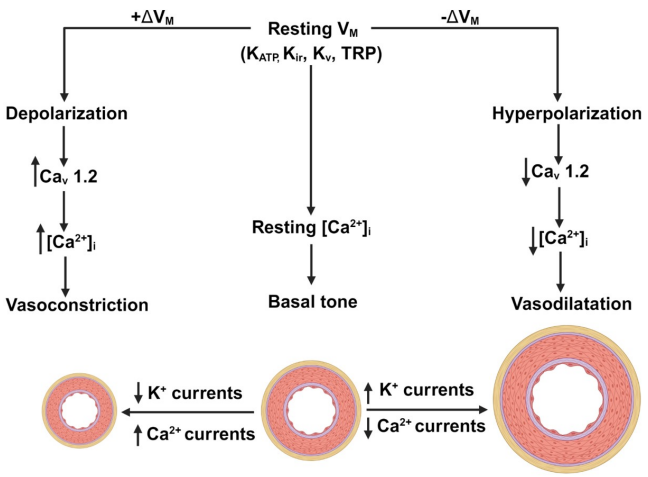

Figure I.15: *Ion channels modulate V_M $[Ca^{2+}]_i$ and vascular tone. Resting V_M is very dependent on K^+ channels activity. Vascular tone depends on $[Ca^{2+}]_i$ which is mainly determined by the V_M dependent activity of $Ca_v1.2$. Depolarization activates $Ca_v1.2$, increases Ca^{2+} influx and $[Ca^{2+}]_i$ leading to vasoconstriction. On the contrary hyperpolarization leads to closure of $Ca_v1.2$ channels and ultimately to vasodilation. Adapted from (Daghbouche-rubio* et al. *2022).*

1.6.1 Potassium channels

K^+ channels play a key role in setting up the resting V_M. Under physiological conditions, the activation of K^+ channels leads to hyperpolarization of VSMCs, reducing the opening probability of LTCCs and promoting vasodilation. In contrast, closure of K^+ channels leads to the depolarization of VSMCs, increasing the opening probability of LTCCs, boosting Ca^{2+} influx and vasoconstriction (see **Figure I.15**).

1. **Voltage-gated K^+ channels (K_v channels)** are activated by membrane depolarization in the range of resting V_M values (approximately -35 to -45 mV) and provide negative feedback to depolarization. Reduced functional expression of K_v1, K_v2, and K_v7 are among the most common alterations in HT (W. F. Jackson 2018). In BPH, expression and function studies have shown that specific members of the K_v1 and K_v2 subfamilies are major contributors to K_v currents. Notably, both K_v1 and K_v2 currents modulate the resting V_M in VSMCs, but no differences in their contributions were found between BPN and BPH, suggesting that alterations in K_v channels do not explain the depolarization of mesenteric VSMCs in BPH (Moreno-Domínguez *et al.* 2009).

2. **Inward-rectifying K^+ channels (K_{IR} and K_{ATP})** exhibit higher conductance for inward K^+ currents than for outward currents and are active at more negative voltages than K_v channels. In addition to V_M, external K^+ concentration modulates K_{IR} activity and K_{ATP} channels are inhibited by intracellular ATP. Several studies have suggested the decreased expression and function of K_{IR} and K_{ATP} channels in HT (Sobey 2001). In BPH, mRNA expression of the most abundant K_{IR} ($K_{IR}2.1$, $K_{IR}4.1$) and K_{ATP} ($K_{IR}6.1$ and Sur2) channels was decreased. The amplitudes of K_{IR} and K_{ATP} currents also decreased significantly. However, only the changes in K_{ATP} levels were relevant for explaining the vascular tone differences in HT (Tajada, Cidad, Moreno-Domínguez, *et al.* 2012).

3. **Large-conductance Ca^{2+}-activated channels (BKCa)** exhibit a large unitary conductance, which is activated by increases in $[Ca^{2+}]_i$ and/or V_M. Local Ca^{2+} transients elicited by Ca^{2+} release from the RyR stimulate BKCa channel opening and K^+ efflux, which limits vasoconstriction (Wellman, Nelson 2003). Contradictory changes related to the expression and function of BKCa in HT have been reported. Enhanced BKCa currents have been found in arteries of hypertensive rats as a protective mechanism to limit vasoconstriction (Cox, Rusch 2002). However, reduced BKCa currents with lower Ca^{2+} sensitivity have also been reported

(Moreno-Domínguez *et al.* 2009), thus that impaired negative feedback by BKCa channels could contribute to the hypertensive phenotype.

1.6.2 Voltage-gated calcium ion channels

VDCCs play a central role in regulating the vascular tone. Depolarization causes channel opening and vasoconstriction, whereas hyperpolarization causes channel closure and vasodilation (Nelson *et al.* 1990). Two components of voltage-activated Ca^{2+} currents have been identified. A long-lasting L-type current (LTCC), which is activated by relatively large depolarizations and inactivated relatively slowly, and a transient T-type current, which is activated by relatively small depolarizations and inactivated relatively rapidly. Both LTCC and TTCC are blocked by cadmium, cobalt, and lanthanum, but the LTCC is selectively blocked by dihydropyridines (as nifedipine) and enhanced by Bay-K8644 (Zhang *et al.* 2007). In the resistance vasculature, LTCCs are highly expressed, particularly the $Ca_v1.2$ isoform (W. F. Jackson 2000). $Ca_v1.2$ currents have high single-channel conductance, and slow voltage-dependent (Tykocki *et al.* 2017).

Upregulation of $Ca_v1.2$ is a characteristic feature of HT in several animal models of arteries after increased BP and/or VSMC depolarization (Pesic *et al.* 2004;Pratt *et al.* 2002). However, in BPH mesenteric arteries there was a marked decrease in whole-cell $Ca_v1.2$ currents and mRNA and protein expression of the pore-forming α_1-subunit (Tajada, Cidad, Colinas, *et al.* 2013). The influx of Ca^{2+} through single or clustered $Ca_v1.2$ channels can be detected as "Ca^{2+} sparklets" (Santana *et al.* 2008). They exhibited a higher frequency and density in BPH VSMCs. Although the currents are smaller overall, the differences in "Ca^{2+} sparklets" suggest more efficient clustering of $Ca_v1.2$ channels in BPH, which can be explained in part by the different compositions of $Ca_v1.2$ auxiliary subunits (Dixon, Navedo, *et al.* 2022; Tajada, Cidad, Colinas, *et al.* 2013).

1.6.3 Transient receptor non-selective cationic channels

TRP were first discovered in mutant photoreceptors that exhibit light-mediated transient depolarization. Twenty-eight nonselective cation channels have been described and classified into seven subfamilies. Among them, TRPCs have been identified as important players in the regulation of vascular tone, either by controlling V_M and/or providing a Ca^{2+} entry pathway independent of LTCCs activation (Earley, Brayden 2015). Upon stimulation by a GPCR ligand, PLC leads to the production of DAG, which directly activates TRPC3/6/7 channels, and thus, cell depolarization.

Numerous observations have linked altered expression of TRPC3 and TRPC6 channels to HT in animal models (Daghbouche-rubio *et al.* 2022). Several studies

have reported that increased expression of TRPC3 (D. Liu *et al.* 2009; Noorani *et al.* 2011) or TRPC6 channels (Linde *et al.* 2012; Zulian *et al.* 2010) correlates with increased agonist-induced Ca^{2+} influx and contraction. Unexpectedly, TRPC6 KO mice were hypertensive due to a compensatory upregulation of TRPC3 channels (Dietrich *et al.* 2005).

A larger expression of TRPC3 channels was found in BPH VSMCs. The higher expression of TRPC3 in BPH resulted in differences in the TRPC3/C6 ratio and composition, which promoted cell depolarization in HT. Increased TRPC3 expression leads to increased cation permeability at rest, which contributes to membrane depolarization in BPH cells (Álvarez-Miguel *et al.* 2017). Altogether, the entire electrical remodelling involving different on channels in BPH mice is described in **Figure I.16**.

1.6.4 Chloride ion channels

Chloride concentration ($[Cl^-]_i$) in VSMCs is higher than in other cell types, ranging from ∼30 to ∼50 mM. The estimated equilibrium potential for Cl^- (E_{Cl^-}) is between ∼-30 and ∼-20 mV. As the resting V_M is between ∼-60 mV and ∼-40 mV in VSMCs, Cl^- channel activation results in Cl^- efflux, membrane depolarization, increase in $[Ca^{2+}]_i$, and SM contraction (Bulley, Jaggar 2014).

Expression and functional studies have highlighted the physiological significance of Cl^- channels in VSMCs (see **Figure I.17**). In particular, calcium-activated Cl^- channels (CaCCs) in VSMC are relevant for vascular tone and BP: regulation (Goto, Kitazono 2022). However, their molecular identity is not fully understood. In addition, the lack of selective inhibitors is an added difficulty in CaCC molecular characterization (Boedtkjer *et al.* 2015). Alternative genetic tools to perform knockdown (with siRNAs) or knockout studies with mice were used (Scudieri *et al.* 2012). Recently, a small molecule inhibitor of TMEM16A has emerged, the acylaminocycloalkylthiophene, TMinh-23 (Cil *et al.* 2021). In terms of functionality, CaCCs currents are described in conduit and resistance vessels from multiple species (Goto, Kitazono 2022). In fact, in 2008, three research groups independently found that TMEM16, in particular TMEM16A, was the molecular correlate of CaCCs (Caputo *et al.* 2008; Schroeder *et al.* 2008; Y. D. Yang *et al.* 2008).

In physiological conditions, siRNA against TMEM16A in mesenteric arteries suggested that TMEM16A involvement in BP and vascular tone might be more complex, as they can regulate other PM ion channels, as LTCCs (Jensen *et al.* 2018). Indeed with this line, using a TMEM16A KO mice a marked increase of force development was pointed out in several resitance vessels, as saphenous and tail arteries. These findings contrasts with the traditional hy-

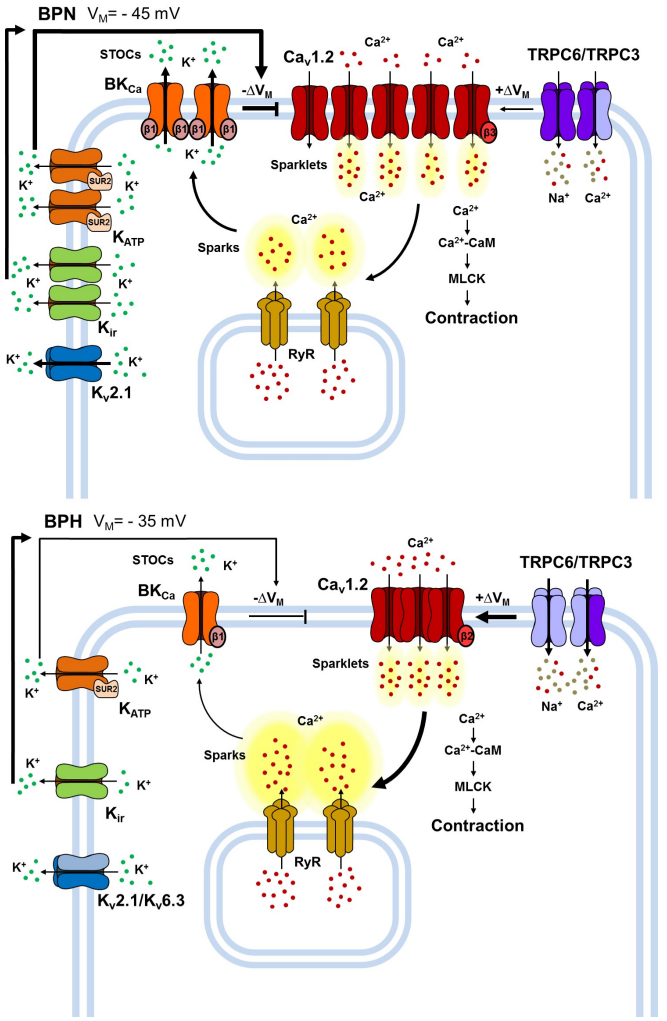

Figure I.16: *Ion channels differences between mesenteric BPN and BPH VSMCs. Smaller K^+ currents in BPH cells lead to a depolarized resting V_M. $K_v2.1$ currents are smaller because of the "de novo" expression of the $K_v6.3$ subunit. K_{IR}, K_{ATP} and BKCa channels functional expression is smaller, and BKCa have a decreased sensitivity to Ca^{2+} due to the decreased expression of the BKCa β_1 subunit. BPH VSMCs also have a higher expression of TRPC3 and a different composition of the TRPC3/TRPC6 heterotetramers. Larger TRPC currents contribute to the depolarized resting V_M. Surprisingly, $Ca_v1.2$ expression and total Ca^{2+} currents are smaller in BPH, but the different expression of β subunits generate clusters of channels that produce higher Ca^{2+} sparklets and induce larger RyR Ca^{2+} sparks. However, these larger sparks do not induce larger STOCs, due to the reduced Ca^{2+} sensitivity of BKCa channels, jeopardizing the "Ca^{2+} break". Ca^{2+} (red dots), K^+ (green dots) and Na^+ (grey dots) ions. Adapted from (Daghbouche-rubio* et al. *2022).*

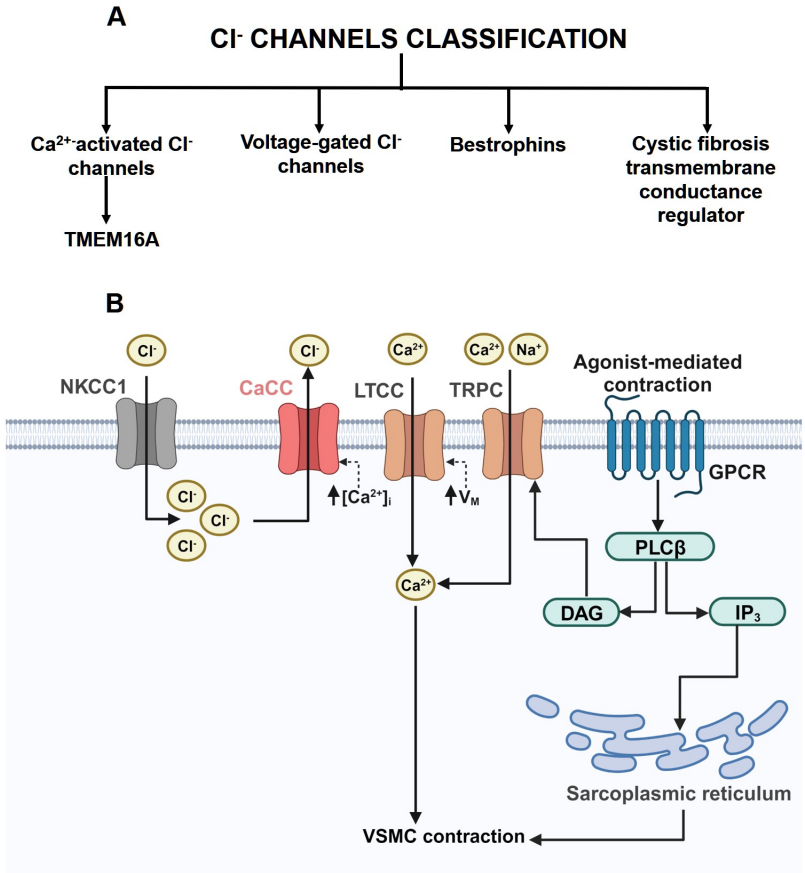

Figure I.17: *A), Classification of Cl^- channels and B), The functional relevance of CaCCs in VSMC. Four distinctive hallmarks of CaCCs have been described in VSMC. First, the molecular identity of CaCCs was related to TMEM16A. Second, a high $[Cl^-]_i$ was found in VSMC leading to a E_{Cl^-} positive values than resting V_M. Third, after agonist-mediated responses, the increase of $[Ca^{2+}]_i$ lead to Cl^- efflux and participation in depolarization and thus contraction. Finally, TMEM16A studies are complex because the lack of selective inhibitors.*

pothesis raised, suggesting additional roles of TMEM16A in agonist-mediated contractions (Matchkov *et al.* 2020).

Under pathological conditions, increased functional expression of TMEM16A was detected in several vascular beds, including mesenteric arteries, and described in the genetically SHR rat model. In this context, TMEM16A contributes to the enhanced vascular contractility and elevated BP in HT. Using different experimental approaches, either by genetic or pharmacological tools, a decrease in BP levels together with lesser VSMC contractile responses were demonstrated

by different groups (Goto, Kitazono 2022). TMEM16A expression was upregulated in resistance arteries from SHR rats and both genetic and pharmacological inhibition prevent HT development (Wang *et al.* 2015). Recently, a novel small molecule inhibitor of TMEM16A was developed and raised as a promising drug target for antihypertensive treatments. This blocker prevented vasoconstriction in different isolated vascular beds, as mesenteric arteries, and reduced BP in a long-term manner in SHR (Cil *et al.* 2021).

1.7 G protein coupled receptors signaling pathways

Several systems are involved in BP and vascular tone regulation via GPCR signaling pathways. Either vasoconstrictor or vasodilator responses can be elicited.

1.7.1 Adrenergic mediated signalling pathways

The ARs play a central role in regulating vascular tone and BP. Three types of receptors (α_1, α_2, and β) have been identified in the vasculature. They are all metabotropic GPCRs, being α_1-ARs and β-ARs the most abundant in VSMCs. Expression and/or functional changes in these ARs are linked to the pathogenesis of HT (Johns *et al.* 2000).

Vasodilator mechanisms

cAMP is one of the main secondary messengers linked to VSMCs relaxation, along with cGMP (**Section 1.4**). After β_2-AR stimulation, $G_\alpha s$ mediates AC activity to increase cAMP levels. cAMP activates PKA, which phosphorylates numerous targets involved in increased Ca^{2+} reuptake into SR, decreased SR-Ca^{2+} release, increased in the opening probability of K^+ channels, decrease in the opening probability of LTCCs channels and/or MLCP inhibition to prevent the crossbridge formation (Morgado *et al.* 2012). Overall, $[Ca^{2+}]_i$ decrease, cell hyperpolarization, and smooth relaxation is achieved (see **Figure I.18**). Recently, β_1-AR was also functionally relevant in small mesenteric arteries from rats, which was typically attributed in the cardiac tissue (Søndergaard *et al.* 2019).

In HT, expression and/or functional changes in downstream molecular mediators of β_2-AR have been described. For instance, decreased gene expression of β_2-ARs receptors was found in HT patients (Mhatre V. Ho *et al.* 2008). Furthermore, an overexpression of PDE3A, which degrades cAMP levels, was associated with high BP by using genetically modified mice (Ercu *et al.* 2020).

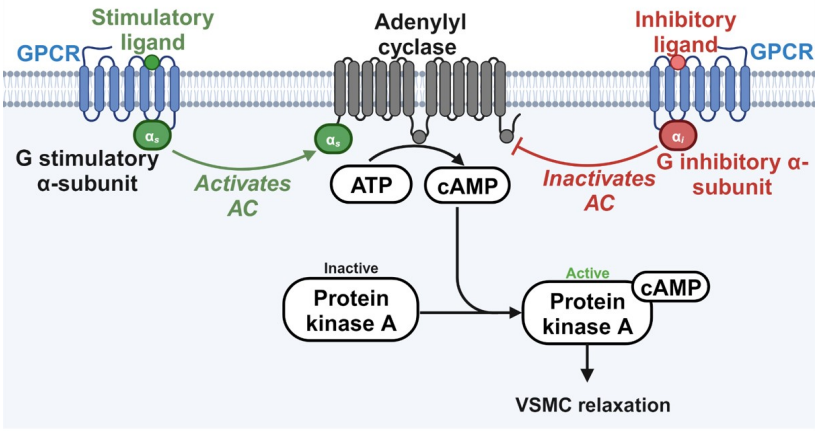

Figure I.18: *Vasodilator pathway regulated by the cAMP effector. After agonist stimulation, $G_\alpha s$ protein is activated to increase cAMP levels through transmembrane AC. On the other hand, this intracellular cascade is inhibited by $G_\alpha i$ protein coupled pathways.*

Vasoconstrictor mechanisms

In VSMCs, α_1-ARs are highly expressed and are strongly involved in SNS-mediated effects (A. P. Somlyo, A. V. Somlyo 2003). Three α_1-ARs subtypes (A, B and D), are described, whose relative contribution varies depending on vessel size (T. Kitazawa, K. Kitazawa 2012). In the resistance vasculature, some works support the involvement of α_1A-ARs, while others works provide α_1B-ARs as the key modulator in VSMC adrenergic constrictions (Z. J. Chen, Minneman 2005).

After receptor stimulation, either Ca^{2+} mobilization (G_αq11) or Ca^{2+} sensitization mechanisms (G_α12-13) pathways are activated (Perez 2021). Surprisingly, using KO mice for all three subtypes of IP_3Rs, and hence removing the major source of Ca^{2+} mobilization from internal stores, Phe- induced contraction in mesenteric arteries was not dramatically affected (Lin *et al.* 2016).

In HT, there is a limited information regarding the main changes occurring in adrenergic signaling pathways. In HT human patients, an augmented SNS activity and an enhanced adrenergic contraction was described (Supiano *et al.* 1999). In experimental HT animal models, an enhancement of efficiency and activation of GPCR signaling pathways have been proposed. The relative contribution of either Ca^{2+} mobilization or Ca^{2+} sensitization processes might be altered. In particular, a larger ROCK-mediated Ca^{2+} sensitization mechanisms in adrener-

Purinergic receptor	Agonist	VSMC function	Ion channel/GPCR
P2X1	ATP, Up_4A, αβ-MeATP	Contraction	Ion channel
P2Y1	ATP, ADP	Relaxation	Gαq11
P2Y2	ATP, UTP	Contraction	Gαq11
P2Y4	ATP, UTP	Contraction	Gαq11
P2Y6	UDP	Contraction	Gαq11
P2Y11	ATP, UTP	Contraction	Gαq11 and Gαs

Table I.1: *Summary of the different purinergic receptors expressed in VSMCs. Created with power point and modified from (Martin-Aragon Baudel* et al. *2020).*

gic contraction was described in mesenteric arteries from HT rats with high salt diet (Crestani *et al.* 2017). Although the role of adrenergic system in CV system has been widely studied, its involvement in HT requires further research.

1.7.2 Purinergic mediated signalling pathways

Two different families of purinergic receptors have been identified and classified according to their primary agonist. P1 family interacts with the natural ligand adenosine and P2 family, which bind purine and pyrimidine nucleotides (ATP, UTP, ADP, or UDP). Further pharmacological and structural studies provided two P2 subdivisions. Ligand-gated ionotropic P2X and P2Y metabotropic GPCR (Burnstock 2012). Seven subtypes of P2X ionotropic receptors (P2X1-7) and eight subtypes of P2Y metabotropic receptors (P2Y1, P2Y2, P2Y4, P2Y6, P2Y11, P2Y12, P2Y13, and P2Y14) have been identified to date (Ralevic 2021). **Table I.1** summarizes the expression and functionality of different purinergic receptors in VSMCs.

P2X receptors are cation-permeable ligand-gated ion channels. Under physiological conditions, ATP mediates rapid responses via the entry of Ca^{2+} and Na^{2+}. Consequently, VSMC depolarization, Ca^{2+} influx via LTCCs, and SM contraction are evoked. P2X receptors are involved in vascular tone and BP regulation, particularly trough P2X1. In P2X1-KO mice, ATP and the selective P2X1 agonist α,β-methylene ATP ($\alpha\beta$-MeATP) failed to evoke contractile responses in wide range of vascular beds (Lamont *et al.* 2006; Vial, Evans 2002). In HT, the elevated vascular tone increases the ATP component of sympathetic neurogenic vasoconstriction (Burnstock 2017).

P2YR subtypes in VSMCs (P2Y1, P2Y2, P2Y4, P2Y6 and P2Y11) are GPCR activating $G_\alpha q11$. Pharmacological tools have been used characterized their function in BP and vascular tone regulation. P2Y6R are of particular importance in VSMC, but there are opposing effects (contraction/relaxation) based

on the vascular bed examined (Haanes *et al.* 2016).

In pathological contexts, P2Y6R upregulation has been proposed as a "molecular switch" in certain diseases, including HT (Sunggip *et al.* 2017). For instance, P2Y6R overexpression has been detected in endothelial cells and is linked to inflammatory vascular responses (Riegel *et al.* 2011). In cardiomyocytes, P2Y6R overexpression is related to pressure overload and cardiac fibrosis (Nishida *et al.* 2008). In conduit arteries (aorta) from mice, increased P2Y6R expression associated with aging has been described, and it has been involved in HT-induced by AgII, although the causes of P2Y6R upregulation are unknown (Nishimura, Sunggip, Tozaki-saitoh, *et al.* 2016). These authors found that KO P2Y6R mice showed resistance to develop HT-induced by AgII, providing a potential role of these purinergic components in the pathogenesis of CVD (Nishimura, Sunggip, Oda, *et al.* 2017). Nevertheless, their characterization is challenging due to the lack of specific pharmacological tools (Sunggip *et al.* 2017).

1.7.3 Angiotensin II mediated signalling pathways

The RAAS system is key to vascular tone and BP levels regulation, as detailed in Section 1.5. AgII is recognized by ATR1 and ATR2, which are both GPCRs. ATR1 is expressed in most tissues, including VSMCs. Two isoforms with 95% sequence identity (ATR1A and ATR1B) have been identified, although they are functionally and pharmacologically indistinguishable. Nevertheless, *in vivo* experiments suggested that the ATR1A isoform is the most relevant in BP and vascular tone regulation (X. Chen *et al.* 1997; Gasc *et al.* 1994). ATR1 activates $G_\alpha q11$ and $G_\alpha 12\text{-}13$ signaling pathways. ATR2 may antagonize some ATR1 mediated functions, although its physiological relevance remains controversial (Wirth *et al.* 2008).

Changes in the expression and/or function of RAAS system components may be associated with HT. Variations in downstream signaling pathways as well as in circulating AgII levels have been described. Concretely, an enhanced effect of AgII on ATR1 receptors in VSMC has been found in HT (Okuno *et al.* 2023). Differential contributions of molecular constituents belonging to the $G_\alpha q11$ and $G_\alpha 12\text{-}13$ cascades were found in experimental models (Cat, Touyz 2011). In particular, downstream mediators activated within the $G_\alpha 12\text{-}13$ pathway were identified as key factors in AgII contractility and HT progression. Arhgef1, a subtype of RhoGEFs, is specifically responsible for AgII-induced activation of RhoA signaling in VSMCs and is central to the development of AgII-dependent HT (Guilluy *et al.* 2010). Similarly, another RhoGEF subtype, the LARG protein, was also found to be key in AgII contractility via the enhancement of $G_\alpha 12\text{-}13$ pathways and was linked to salt-induced HT (Wirth *et al.* 2008). In both cases, *in vivo* blockade of different subtypes of RhoGEFs prevented HT de-

velopment, but did not alter BP levels under basal conditions. Therefore, these RhoGEFs were proposed as novel targets in HT. However, notably, these *in vitro* studies were performed in conduit arteries (aorta).

Furthermore, increased renin release (Born *et al.* 2007), enhanced ACE activity (Goetz, Holtz 1999), and increased AgII levels (Catt *et al.* 1971) have been described in several HT models, leading to augmented ATR1 stimulation and VSMC contraction. Moreover, recently compelling evidences indicate that the crosstalk of ATR1 with other GPCR might be a key factor in the development of HT (Nishimura, Sunggip, Tozaki-saitoh, *et al.* 2016; Quitterer *et al.* 2019). This could potentially provide novel antihypertensive drugs, since there has been a paucity of HT therapeutic development over years.

1.8 Modulators of GPCR dependent mechanisms

1.8.1 Receptor desensitization

Two sequential steps turn off the GPCR signaling pathways: receptor phosphorylation and β-arrestin recruitment. Multiple GPCR kinases (GRK) phosphorylate the activated receptor at the C-terminal serine-threonine sites (Mehta, Griendling 2007). As is shown in **Figure I.19**, the receptor phosphorylation leads to the β-arrestin recruitment to terminate the GPCR signaling pathways (Mehta, Griendling 2007; Turu *et al.* 2019). In addition, non-conventional mechanisms referred as "biased agonism", might be involved in receptor inactivation, mediating independent GPCR mechanisms via β-arrestins (Wootten *et al.* 2018). This has been widely characterized in RAAS system with likely changes the desensitization dynamics. Based on this, recent analogues of AgII have been developed to selectively mediate one signaling pathway over other. Overall, this prevents ATR1 deleterious signaling and potentiates receptor desensitization in CVD (V. V. Gurevich, E. V. Gurevich 2019).

In HT, decreased internalization of ATR1 leads to abnormal activation of ATR1 signaling. Consequently, a prolonged vasoconstriction is found in VSMCs. In particular, altered steps in ATR1 internalization are described. For instance, an attenuation of receptor phosphorylation, reduction of receptor endocytosis, and increased receptor recycling (Bian *et al.* 2018). In summary, several studies have widely characterized the major changes in ATR1 desensitization and linked to HT. Because this is a regulatory mechanism associated after contractile machinery stimulation, this was not included as the major cornerstones in the project.

1.8.2 Receptor oligomerization

GPCRs are able to form homo or heterodimers (Rukavina Mikusic *et al.* 2020). In the contest of HT, ATR1 has been shown to interact with the bradykinin type 2 receptor (BR2) or the purinergic P2Y6 receptor.

Overall, this may modify GPCR function trough modifications in receptor internalization and/or downstream signaling pathways, among others (Breitwieser 2004). The general pattern observed after the receptor oligomerization is a decreased receptor desensitization together with a prolonged GPCR signaling (**Figure I.20**). Using both human and animal studies, a functional association between ATR1 and BR2 in pregnancy-induced HT has been described. Increased Ca^{2+} signaling in VSMCs, AgII hypersensitivity, and reduced arrestin-dependent internalization of B2R was reported by different independent groups (Quitterer *et al.* 2019; Wilson *et al.* 2013). Also, in the above mentioned work of Nishimura et al, the mechanism linking increased P2Y6R expression to HT relies on ATR1-P2Y6R heterodimer formation (Nishimura, Sunggip, Tozaki-saitoh, *et al.* 2016). This leads to enhanced AgII vascular remodeling and decreased ATR1 β-arrestin internalization. P2Y6R pharmacological disruption in these complexes suppressed AgII-induced HT, and mice deletion of P2Y6R attenuates increase of BP levels and vascular remodeling.

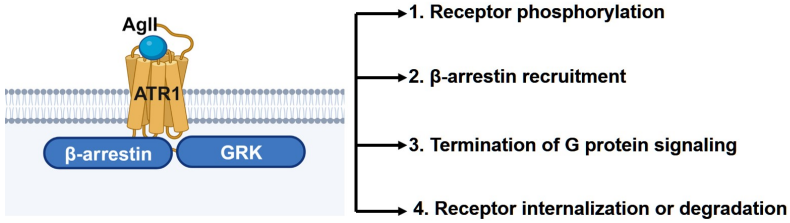

Figure I.19: *Steps of ATR1 desensitization and components involved. Over past years, the "barcode theory" emerged to describe the correlation between the phosphorylation patterns and the functional diversity of outcome pathways. Classically, GRK is the responsible for the phosphorylation and targeting of the active receptor. Recently, PKC can also phosphorylate an inactivated receptor.*

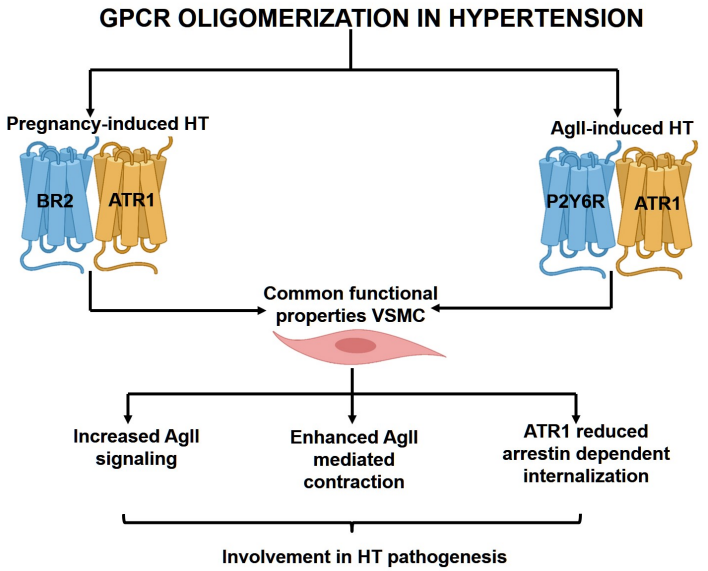

Figure I.20: *Overview of the GPCR oligomerization described in the literature. The general pattern observed after the receptor oligomerization is a decreased receptor desensitization together with a prolonged GPCR signaling.*

2 Hypothesis & Objectives

Changes in VSMC, leading to excessive vasoconstriction and concomitant elevation of vascular resistance lead to essential HT. Changes in the electrical activity of VSMCs and/or the interaction of vasoactive agents with PM receptors can modulate $[Ca^{2+}]_i$, thus modifying the contractile state of VSMC. Moreover, alterations in cellular mechanisms that regulate $[Ca^{2+}]_i$ homeostasis might also contribute to abnormal vascular function in pathological conditions, such as HT.

The likely molecular candidates responsible for these variations are PM ion channels in VSMC (Daghbouche-rubio et al. 2022) . The role of different PM ion channels in HT has been extensively explored in our laboratory over the last few years using BPH mice as a model for essential HT. Modifications in the expression and/or function of K^+, VDCCs, and TRPC channels have been identified as potential contributors to the HT phenotype. However, these studies did not investigate the modifications in VSMC contractility due to changes in agonist-mediated processes. These mechanisms can modulate $[Ca^{2+}]_i$ and cell responses, with little or no changes in resting V_M . The majority of ligands act through GPCR, whose expression and/or functional patterns might be altered in HT.

The overall objective of this project was to perform a detailed characterization of GPCR signaling pathways in HT. Microarrays using VSMCs from BPN and BPH mesenteric arteries provided a differential gene expression profile. From this starting point, a functional characterization of changes upon HT in some of these GPCR and their signaling pathways has been carried out. In this line, the study addressed two main questions:

1. To explore the contribution of purinergic transduction to increased vascular tone in the HT phenotype, by analyzing both the impact on changes in the expression and/or the contractile responses to ATP, UTP or their analogs. We will also explore the impact of increased purinergic response in the vasoconstriction induced by AgII, through the formation of P2Y6/AT1 receptor heterodimers, as previously described in KO models (Nishimura et al. 2016) , but not in HT models. Specifically we will study:

   (1.1) The changes in the functional expression of ionotropic P2X and metabotropic P2Y receptors in BPN and BPH mice.

   (1.2) The pharmacological characterization of P2Y receptors by exploring thecontractile responses to selective agonists and blockers.

   (1.3) The purinergic and angiotensin crosstalk signaling in BPH vessels via heterodimeric receptors, because of P2Y6R upregulation.

2. To characterize the downstream molecular components of the α-adrenergic signaling pathways in essential HT. We will explore potential changes in

GPCR downstream signaling pathways that could contribute to the increased contractility of BPH vessels. We will study:

(2.1) The contribution of several downstream elements of the α-adrenergic signaling pathway to agonist-induced contraction in essential HT.

(2.2) The potential differential contribution of these downstream elements in response to different agonists, both in control conditions and in the presence of HT.

(2.3) The differential contribution of G_{α}q11 and G_{α}12-13 signaling pathways in HT.

3 Materials & Methods

3.1 Schlager mouse model of essential hypertension

Adult male hypertensive mice (BPH/2J) and corresponding normotensive control mice (BPN/3J) were purchased from Jackson Laboratories (Bar Harbour, ME, USA). They were bred at the animal facilities of the Universidad de Valladolid. Mice were maintained on a 12:12 hour light-dark cycle at controlled temperature (21°C), fed standard rodent chow, and received fresh water *ad libitum*. All procedures were approved by the Institutional Care and Use Committee of the University of Valladolid and were performed in accordance with the European Community Guidelines for the Care and Use of Animals (Directive 2010/63/UE).

3.1.1 Non-invasive tail cuff measurements

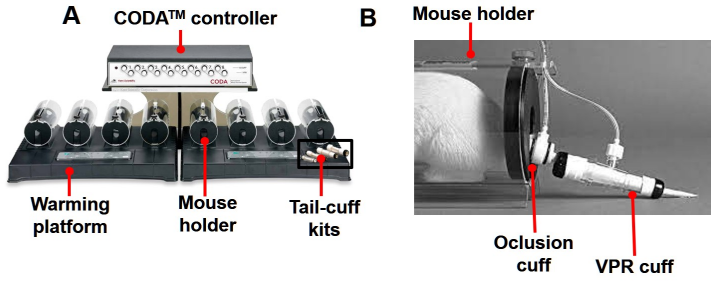

Figure M.1: *In A), CODA non-invasive high-throughput system BP and in B), mouse tail with occlusion cuff and the VPR cuff setup.*

BP was monitored using the CODA setup (Kent Scientific Corporation, Torrintgon, CT, USA) as described in (Krege *et al.* 1995) and illustrated in **Figure M.1**. Animals were restrained in a holder and acclimated to 32-35°C on a heat platform for 15 min (min) before data collection. Measurements were performed on awake mice at the same time each day to reduce animal stress and ensure reliable data. Each session consisted of 40 cycles of an inflation step to a maximum occlusion pressure of 250 mm Hg, followed by a deflation step of 15 s. A volume of 15 μL was used as the minimum tail volume for data collection. The first five cycles were considered part of the training and were not included in the analysis. This protocol was performed for 4-6 consecutive days and the first two days were not used for determinations as they were considered part of acclimatization. To obtain the BP average values, at least three sessions were performed. During the measurements, the occlusion cuff and volume pressure sensor (VPR) were used to detect changes in tail blood volume and then correlated with the desired parameters of interest. MAP was calculated as follows:

$$MAP = DBP - \frac{(SBP - DBP)}{3} \qquad \text{(Eq. 3.1)}$$

3.1.2 Mouse model of hypertension induced by AgII

To induce HT in BPN/3J and C57BL/6J normotensive mice, AgII was administered chronically for 2 weeks using minipumps (model 1007D, Alzet) placed subcutaneously.

The minipumps were placed in the intrascapular region under the skin. Isoflurane was administered with a SomnoSuite® Low-Flow Anesthesia System (Kent Scientific) at a dose of 2% for induction and 1-2% for maintenance of anesthesia (**Plumb, 2008**) at low flow rates of 500 mL/min and 45 mL/min, respectively. Eye drops were used to prevent corneal desiccation. The minipumps delivered AgII at a rate of 800 ng/kg/min. To ensure proper infusion, AgII was mixed with saline (0.9% NaCl).

In the experimental designs, mice were randomly assigned to either an experimental condition (AgII) or a control condition (saline). Control BP measurements were performed at least 3 days before the protocol and experimental data were obtained 3, 7 and 14 days after surgery.

3.1.3 Losartan administration *in vivo*

Adult male BPN and BPH were subjected to chronic treatment with losartan (0.6 mg/mL) for 6 weeks in drinking water, changing the bottles every two days. The age of the animals ranged from 3 up to 6 months. A random order crossover

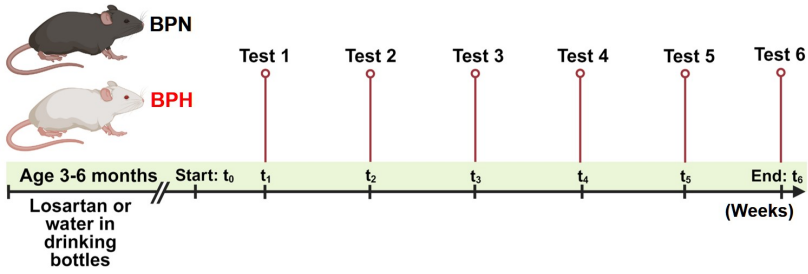

Figure M.2: *Experimental design for in vivo losartan administration procedure. Mice were subjected to either a control group (water) or an experimental group (losartan) in a random crossover assignment for 6 weeks. The BP measurements were running simultaneously and were performed weekly. At least three repeated measurements were performed for each animal in the study.*

design was used to expose animals to a control (without drug) or experimental (with drug) condition, as previously described (Huang *et al.* 2013). For the control condition, 3 BPN mice and 5 BPH mice were used. For the experimental condition, 4 BPN mice and 6 BPH mice were included. The overall experimental procedure is depicted in **Figure M.2**.

3.2 Surgical procedures

Adult BPN and BPH mice were anesthetized by inhalation of isoflurane (5% O_2 2.5 L/min) before decapitation. The animals were then placed in the supine position, and a surgical incision was made to gain access to the abdominal cavity, as previously described (Moreno-Domínguez *et al.* 2009). The mesenteric arcade was removed and kept in a Sylgard®-coated plate containing ice-cold (4 ºC) aerated (95% O_2-5% CO_2) smooth muscle dissociation solution (SMDS, see composition in **Table M.1**). Dissection was performed without further SMDS aeration. Due to protocol requirements, SMDS solution was used to obtain the arteries, whereas MgPSS (physiological magnesium solution) was used instead to obtain the cells.

Composition	SMDS-10 µM Ca^{2+} (mM)
NaCl	120
KCl	4.2
$NaCHO_3$	25
$MgCl_2 \cdot 6H_2O$	1.2
KH_2PO_4	0.6
Glucose	11
$CaCl_2$	0.010
pH	7.4

Composition	MgPSS (mM)
NaCl	140
KCl	5
HEPES	10
$MgCl_2 \cdot 6H_2O$	2
Glucose	10
$CaCl_2$	-
pH	7.4

Table M.1: *Composition of the solutions intended for isolation of both artery (SMDS) and VSMC (MgPSS) preparations.*

A dissecting microscope was used to distinguish veins from arteries; the V-shape of the bifurcations and the thicker SM layer in arteries were used as hints. Second- and third-order mesenteric arteries were harvested. Surrounding fat and connective tissue were removed, and clean arterial segments were used. Mechanical force was applied to the mesenteric arteries to remove the endothelium. A fine hair or bubbles were used for functional studies, while a pipette tip was used for gene expression studies. The experimental procedure is detailed is the **Figure M.3**.

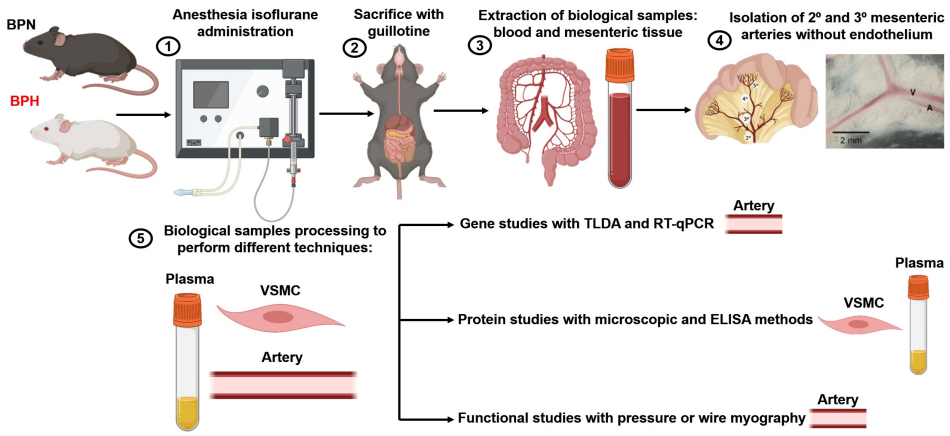

Figure M.3: *Overview of the experimental procedure performed in this study.*

3.2.1 Blood collection and plasma preparation

Most of the mice used in the different procedures were weighted before sacrifice (25.46 ± 0.48 g and 22.43 ± 0.29 g for BPN and BPH respectively, $p < 0.001$, n=40-80), and in many cases, after decapitation, blood samples of up to 1 mL were collected from the trunk into a tube containing ethylenediaminetetraacetic acid (EDTA). The blood tubes were centrifuged at 1500 g for 15 min at 4ºC.Three differentiated phases were separated: the lower part, which consisted of red blood cells; the interphase part, which resembled a thin white layer and contained mainly immune-type cells; and the upper part, which provided the cell-free plasma sample (**Figure M.4**). The plasma was transferred to a polypropylene tube to obtain a single aliquot with a final volume of ∼200 μL and stored at -80°C for subsequent ELISA assays The advantages of using plasma instead of serum were lower background noise and higher reproducibility (Yu *et al.* 2011).

3.2.2 VSMC isolation

To obtain freshly isolated VSMCs, mesenteric arteries were harvested in an ice-cold, 4ºC MgPSS buffer solution according to a previously published protocol (Prada *et al.* 2020). Mouse mesenteric arteries were digested in solution A and then in solution B (**Table M.2**). After 3 washes in ice-cold MgPSS buffer solution to stop the enzymatic digestion, mechanical trituration was performed with a wide-necked glass pipette to obtain fresh VSMCs. The enzymatic solutions were prepared daily. Arterial myocytes were stored in dissection buffer at 4ºC until further use.

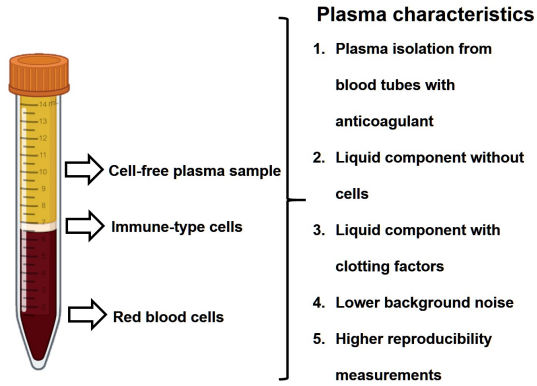

Figure M.4: *Overview of the three differential phases obtained by the plasma isolation procedure and the main characteristics of the obtained sample.*

3.3 Gene expression studies

Differences in mRNA expression were assessed using Affymetrix microarrays and confirmed by real-time polymerase chain reaction (RT-qPCR).

3.3.1 Affymetrix microarrays

An overall gene expression profiling was conducted with Affymetrix microarrays. Then, the pattern differences were confirmed by RT-qPCR. The total RNA from arteries was isolated with $MELT^{TM}$ Total RNA Isolation System Kit (Ambion, Inc., Austin, TX, USA). The quality of total RNA was assessed with the Agilent Bioanlayzer and samples were prepared for hybrization to the Affymetrix GeneChip®MG-430 2.0 Arrays according to Affymetrix instructions, in the Genomic Service of the CIC (Salamanca, Spain). Of note, RNA purification and

Composition	A solution (mg/mL in MgPSS)	B solution (mg/mL in MgPSS)
Papain (3119, Worthington)	1	
DTT (D9163, Sigma)	1	
Collagenase H (C8051, Sigma)	-	1.77
Elastase (2292, Worthington)	-	0.5
Trypsin inhibitor (T9003, Sigma)	-	1
Time (minutes) at 37ºC	9	9

Table M.2: *Protocol used for VSMC isolation from BPN and BPH mesenteric arteries.*

quantification is more detailed in the following sections. Differential gene expression was performed with the "LIMMA" R package (3.52.1) with log FC $\geq$ 0.5 and adjusted p-value $<$ 0.05 (Phipson *et al.* 2016; Ritchie *et al.* 2015). To elucidate the potential biological mechanisms of genes related to the hypertensive phenotype, enrichment analyses were performed using the "gprofiler2" R package (0.2.2), using the gSCS correction method, the expressed genes as background genes and Gene Ontology (GO), KEGG, Reactome (REAC), WikiPathways (WP), TRANSFAC (TF), and CORUM as data sources (Kolberg *et al.* 2020; Raudvere *et al.* 2019).

3.3.2 RNA purification

General steps in RNA purification included cell lysis, RNase-nuclease inactivation, and nucleic acid separation. The procedure consisted of 1) tissue homogenization, 2) phase separation, 3) extraction-precipitation, and 4) resuspension (**Figure M.5**). Briefly, second- and third-order denuded endothelium mesenteric arteries were harvested from 4-5 mice, as previously described (Cidad *et al.* 2010). The endothelial layer was removed mechanically with a pipette tip. The arteries were then cut into fragments less than 3 mm in length and stored in RNAlater™ (Invitrogen) until processing. The tissue homogenization was performed using a combination of a mechanical (with ceramic beads) and organic (with TRIzol®). In this regard, arteries were transferred to tubes with the TRIzol® reagent (Bertin Instruments, France) and ceramic beads of different sizes, CK14 and CK28 Precellys® Lysing Kit (Bertin Instruments, France). The sequential centrifugations were performed with Precellys® 24 homogenizer. Two consecutive cycles were then performed at 5000 rpm for 15 seconds. The debris was removed by centrifugation at 12000 g for 3 min at 4ºC. Incubation with TRIzol® was performed for 5 min at room temperature (RT) to allow complete cell lysis and dissociation of the nucleoprotein complex.

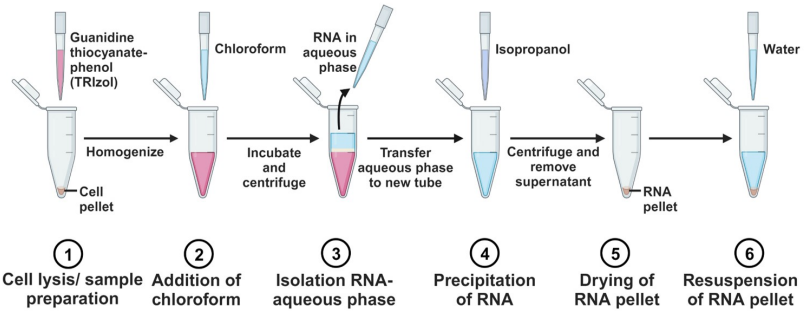

Figure M.5: *Total RNA isolation scheme.*

Phase separation was achieved by adding a phenol-chloroform solution. Under acidic conditions, denatured proteins remained in the lower organic phase, DNA was dissolved at the interface, and RNA was pelleted (Tan, Yiap 2009). RNA pellet was then carefully extracted and isopropanol mediated precipitation was performed. Impurities were removed with 75% ethanol. Resuspension was carried out in RNase-free water by heating at 60 ºC for 5 min, to allow the complete dissolution of the RNA pellet. Finally, it was stored at -80 ºC until processing or used to check RNA integrity the same day.

3.3.3 RNA quantification

The quality and quantity of isolated RNA was assessed by absorbance spectrophotometry. RNA concentration was determined by measuring optical density at 260 and 280 nm using a UV-Visible spectrophotometer (NanoDrop™ 1000, Thermo Scientific). A direct correlation was established between absorbance and concentration according to the Lambert-Beer law

$$c = \frac{A \cdot e}{b} \qquad \text{(Eq. 3.2)}$$

where c was the nucleic acid concentration (in ng/μL), A was the absorbance (in absorbance units, A), e was a standard coefficient (for RNA was 40 ng·cm/μL), and b was the sample length (1 cm). Values above two were considered purified RNA, while values below two indicated a sample contaminated by proteins or phenolic compounds.

3.3.4 Reverse transcription

Reverse transcription (RT) allows the conversion of an isolated single-stranded RNA template into a complementary strand of a DNA molecule (cDNA). RNA-dependent DNA polymerase (reverse transcriptase enzyme MuLvRT) catalyzed this step in the presence of specific primers that allow the starting point of the reaction.

RT was performed in a Rotor-Gene 3000 thermocycler (Corbett Research) according to the manufacturer's instructions. The reaction mixture indicated below was prepared in PCR buffer and used (**Table M.3**). All reagents were purchased from ThermoFisher Scientific. The cDNA synthesis was performed using random hexamers, to ensure complete synthesis of various RNA subtypes, including ribosomal RNA and both polyadenylated and non-polyadenylated species (Ginzinger 2002).

Composition	RT^+ Reaction mix	RT^- Reaction mix
Purified RNA	500-700 ng	200-350 ng
Random hexamers	2.5 µM	2.5 µM
$MgCl_2$	5 mM	5 mM
dNTPs	4 mM	4 mM
RNAse inhibitor	1 u/µL	
MuLvRT	2.5 u/µL	

Table M.3: *Reaction mix for experiment (RT^+) and genomic control (RT^-) conditions in a final volume of 80 µL for RT^+ and 20 µL for RT.*

cDNA was synthetized with the temperature protocol shown in the **Figure M.6**. The amplified cDNA was immediately stored at -20 °C.

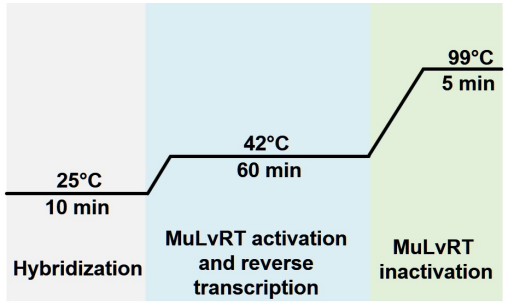

Figure M.6: *cDNA synthesis temperature protocol.*

3.3.5 RT-qPCR

TaqMan assays (Applied Biosystems, Life Technologies) were used to provide specific and sensitive detection of DNA sequences. A probe labelled with a fluorophore at the 5' end and a quencher at the 3' end hybridizes with the target sequence and is cleaved during amplification. This finally results in the release of the quencher and the emission of fluorescence. The general steps included repeated cycles of denaturation to separate DNA strands, annealing to bind DNA primers to the target sequence, and amplification to synthesize new DNA strands by Taq DNA polymerase (**Figure M.7**).

Increasing temperature allowed denaturalization of the double-stranded cDNA. Lowering the temperature allowed the primers and TaqMan probe to attach to their target DNA regions. cDNA synthesis was performed using TaqMan DNA polymerase with unlabeled primers and the DNA template. The

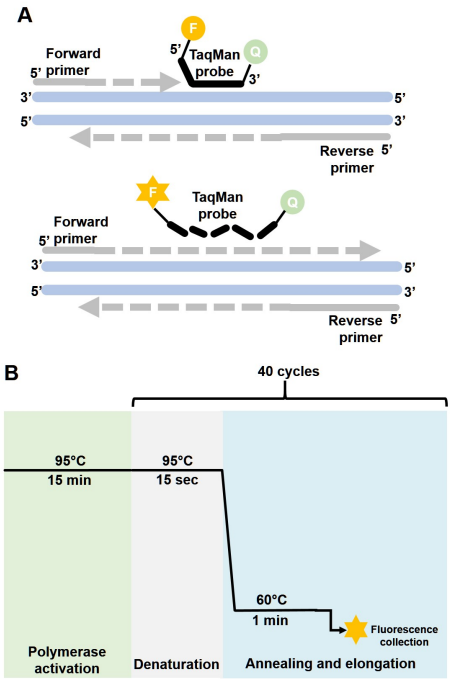

Figure M.7: *In A), Principle of taqMan assay and in B), Amplification temperature protocol.*

fluorophore indicator was separated from the quencher by the exonuclease activity of the TaqMan DNA polymerase. Therefore, the fluorescence detected in the thermocycler was directly proportional to the fluorophore released and the amount of DNA template present. For the qPCR reaction, 1X Maxima Probe qPCR Mix (ThermoFisher Scientific) was mixed with 1 μL of the TaqMan assay (two primers and the probe), the cDNA sample (1 or 2 μL) and nuclease-free water up to 20 μL. A no template control (NTC) in which cDNA was substituted by water was always included.

3.3.6 RT-qPCR normalization and quantification

Prior to gene quantification, background fluorescence was subtracted as a normalization procedure. For each assay, an experimental threshold (C_t) was determined, as is shown in the **Figure M.8**. The C_t value represents the number of cycles required to produce significant fluorescence relative to the baseline signal (Ginzinger 2002).

Data analysis was performed using the $2^{-\Delta\Delta C_t}$ relative quantification method (Livak, Schmittgen 2001). A C_t comparison was performed between the target

Gen name	Protein	Applied Biosystems identification number
P2rx1	P2RX1	Mm00435460_m1
P2rx4	P2RX4	Mm00501787_m1
P2ry1	P2RY1	Mm02619947_s1
P2ry2	P2RY2	Mm00435472_m1
P2ry2s1	P2RY2	Mm02619978_s1
P2ry4	P2RY4	Mm00445136_s1
P2ry6	P2RY6	Mm01275473_m1
P2ry6s1	P2RY6	Mm02620937_s1
Clca1	CLCA1	Mm01320697_m1
Clca2	CLCA2	Mm00724513_m1
Clcn3	CLCN3	Mm01348786_m1
Slc12a2	NKCC1	Mm01265951_m1
Tmem16a	TMEM16A/ANO1	Mm00724407_m1
Cnn1 (Calponin 1, smooth muscle)	CNN1	Mm00487032_m1
Gapdh (Glyceraldehide-3P-dehydrogenase)	GAPDH	Mm99999915_g1
Nos3 (Nitric oxide synthase 3, endothelial)	NOS3	Mm00435217_m1

Table M.4: *List of genes explored by TLDA assay and validated by RT-qPCR.*

gene and an endogenous gene (also referred to as housekeeping gene) to obtain the relative gene abundance, which is referred to as 2^{-C_t}.

$$\Delta C_t = C_{t(\text{target gene})} - C_{t(\text{housekeeping gene})} \qquad \text{(Eq. 3.3)}$$

The expression of the housekeeping genes RPL18 or GAPDH was not altered by the variable studied. Moreover, the amplification efficiency of target and housekeeping genes must be close to 1 and differ by less than 10%. To determine the reaction efficiency, a sample was serially diluted and then the C_t values were determined for each dilution (**Figure M.9**).

After this normalization, the variations in relative gene abundance between different preparations or experimental conditions were expressed as fold-change expression ($2^{-\Delta\Delta C_t}$) and calculated with the formula below:

$$\Delta\Delta C_t = \Delta C_{t(sample)} - \Delta C_{t(calibrator)} \qquad \text{(Eq. 3.4)}$$

The BPH model was considered as the sample, whereas the calibrator corresponded to the BPN model. For graphical representation, the changes obtained in the experimental BPH sample were expressed in $\log 2^{-\Delta\Delta C_t}$. Thus, zero values meant no changes in gene expression, positive values indicated higher expression in the BPH model, and negative values corresponded to lower expression in the BPH model. In cases where gene expression was undetectable in any of the conditions, a C_t value of 40 was used for comparisons.

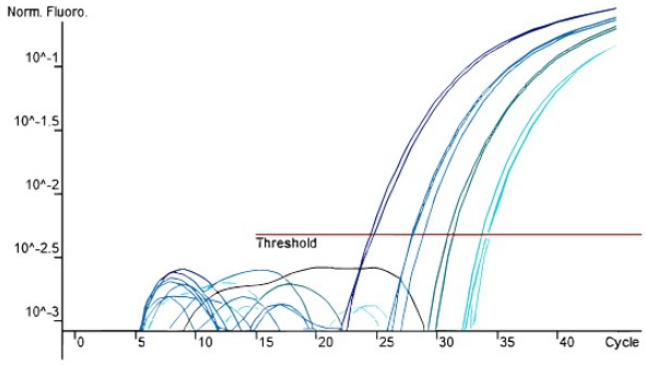

Figure M.8: *Example of qPCR amplification plot, where in the y-axis was represented the fluorescence signal in logarithmic scale versus in the x-axis the cycle number.*

3.4 Protein expression studies

The techniques used to evaluate protein expression were proximity ligation assays (PLA), ground state high-resolution microscopy (GSD) techniques and enzyme-linked immuno sorbent assays (ELISA).

3.4.1 Proximity ligation assay

PLA is a technique that combines both immunological and PCR-based approaches to detect protein-protein interactions (Fredriksson *et al.* 2002). Two primary antibodies raised in different species are used to identify two target proteins. Subsequently, two secondary antibodies, designated MINUS and PLUS, recognized constant regions of the primary antibodies. Short sequences of DNA strands were appended to each secondary antibody. When the two probes were close enough ($\leq$ 40nm), hybridization occur. Enzymatic ligation with two sequence-specific DNA oligonucleotides allowed the configuration of rolling DNA circle amplification. Amplification of the DNA circle was performed by DNA polymerase. Next, fluorescently labeled complementary oligonucleotide probes are added, and they interact with the amplified DNA. Discrete fluorescent spots can be visualized and quantified by image analysis. The experimental procedure is shown in **Figure M.10**.

3.4.1.1 PLA experimental procedure

A Duolink In Situ PLA Kit (Sigma-Aldrich) was used to detect complexes of P2Y6R and ATR1 receptors in VSMCs from BPN and BPH lines. Freshly iso-

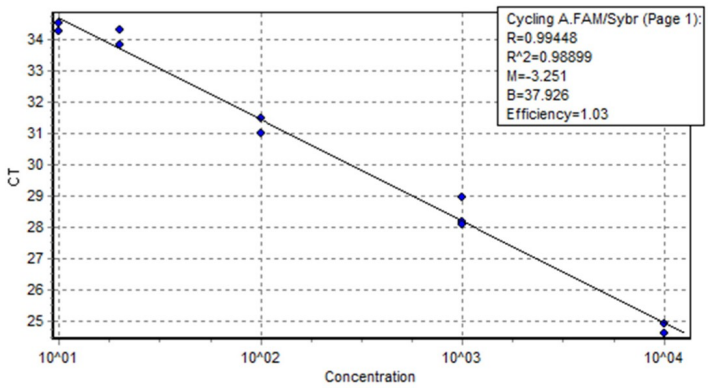

Figure M.9: *Standard curve of RPL18. (Housekeeping gene). The standard curve shows the C_t on the Y-axis and the starting quantity of cDNA template on the X axis. The Slope value is used to calculate the amplification efficiency of the reaction that was 1.03.*

lated cells were plated out and allowed to adhere for 1 hour on 25-mm-diameter glass coverslips at RT. Cells were fixed with 3% glyoxal for 20 min, then quenched with 100 mM glycine for 15 min, and then washed twice with the PBS protocol (x1). The permeabilization step was performed with 0.1% Triton X-100 for 20 min and then cells were blocked with 50% Odyssey Blocking Solution (LI-COR Bioscience) for 1 hour at RT. A 2-hour incubation at 4°C with a specific combination of the two primary antibodies was performed in 0.01% Odyssey + 0.05% Triton X-100 PBS solution. The working factor dilution of the primary antibodies was rabbit anti-P2Y6R (1:800; Genetex, GTX16289) and goat anti-ATR1 (1:800; Novus Biologicals NB100-57073). Samples with only one primary antibody were used as negative controls. After exposure of the primary antibody, cells were washed with Duolink buffer A (X2 for 5 min). Oligonucleotide-conjugated secondary antibodies (PLA probes: anti-goat MINUS and anti-rabbit PLUS) were incubated at 37°C for 1 hour. Last, cells were washed three times with buffer A and then a ligase enzyme solution (1U/uL, dilution 1:40) was incubated at 37°C for 30 min. After washing three times with PBS, amplification was performed by polymerase enzyme (10U/uL, dilution 1:80 in Duolink In site detection reagents orange) at 37°C incubation for 100 min. After washing twice with buffer solution B for 10 min and once for 1 minute with ultrapure water, samples were completely dried and mounted on a slide with Duolink mounting medium and stored protected from light at 4ºC until visualization by confocal microscopy. An Olympus FV1000 confocal microscope with a ×60 oil immersion objective (NA, 1.4) was used to visualize the fluorescence signals. Images were acquired in different optical planes (z-axis step = 0.5 μm) using Olympus Fluoview v1.4 software. For each sample, a single intensity projection image from the combined

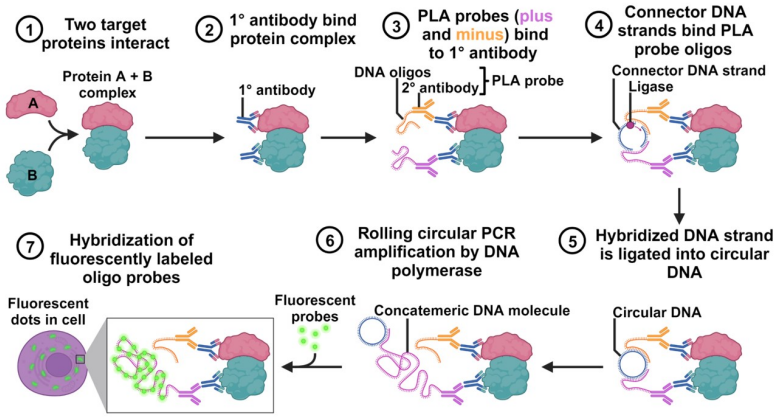

Figure M.10: *Representative experimental procedure of the PLA assay.*

image stack was used for analysis of the number of spots per cell area (μm2). The analysis was performed using NIH Image J v1.51 open software. Members of the team who were blinded to the conditions analyzed these data.

3.4.2 Ground State Depletion (GSD) Microscopy

GSD microscopy allows either the localization of individual proteins or protein association studies. Samples are labeled with fluorescent molecules that reversibly switch between a bright ("on", fluorescent) and a dark ("off", non-fluorescent) state. A random activation is induced and individual detection of fluorescent signals is emitted sequentially in time. High-resolution imaging by reconstruction localization maps is performed in the nanoscopic range (10-20 nm). This technique circumvents the diffraction limit by reducing the number of simultaneously emitting fluorophores (Dixon, Vivas, *et al.* 2017). Overall, GSD technique involved these sequential steps: ground state depletion, imaging, localization, and reconstruction (**Figure M.11**).

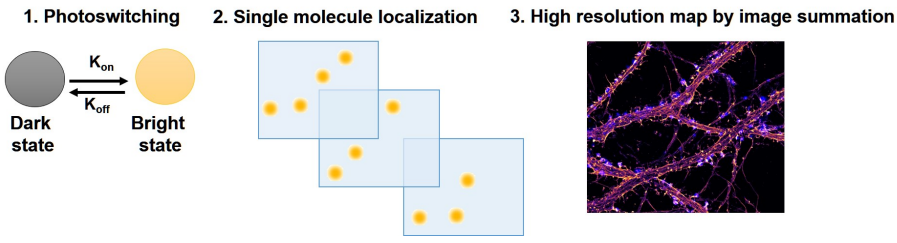

Figure M.11: *Overview of the major characteristics of GSD technique.*

Ground state depletion. High-energy laser is used to excite the fluorophore-labelled sample. The laser is tuned with a specific wavelength to induce a stable and reversible dark "off" state of the fluorophore. This process is called ground state depletion because the majority of the fluorophores are prepared to switch into the dark state, leaving a small fraction in the bright state.

Imaging. After ground state depletion step, individual molecules spontaneously returned to the bright "on" state. They emitted fluorescence stochastically for a short time before returning to the dark state. With less fluorophores emitting at any given time, the signals recorded become spatially and temporally distinct from neighboring fluorophores. This can be fitted with a Gaussian function. The calculated centroid corresponds to the position of the fluorophore with a localization precision that is dependent on the numerical aperture of the lens, the excitation wavelength and the number of photons emitted per fluorophore.

Localization and reconstruction. Since only a subset of fluorophores actively emits at any given time, thousands of images are collected over several min to build up a localization map. By using a mathematical algorithm, a high-resolution image was then provided and indicating the exact position of each fluorophore. GSD technique is only suitable for fixed samples because the long acquisition time combined with the high laser power requirements.

3.4.2.1 GSD experimental procedure

Mesenteric arterial myocytes were isolated from BPN or BPH mice. Cells were plated onto circular coverslips (#1.5, catalog no. 64-0715, Warner Instruments, USA). Cells were fixed using a glyoxal fixing solution for 20 min at RT and subsequently quenched for an additional 15 min in 100 mM Glycine (catalog #G8898, Sigma Aldrich). Permeabilization and epitope blocking was performed by incubating the cells with a blocking solution containing 50% fish serum blocking buffer (catalog #37527, ThermoFisher Scientific, USA) and 0.5% Triton X-100 (Sigma-Adrich) in PBS for 1 hour at RT. The cells were incubated with the primary antibodies goat anti-ATR1 (1:100, catalog #NB100-57073, Novus Biologicals, USA) and rabbit anti-P2Y6R (1:100, catalog #GTX16829, GeneTex, USA) diluted in antibody incubation block solution at a 1:4 ratio of fish serum blocking buffer:PBS and 0.5% of Triton X-100 for 2 hours at RT. After 5x washes with PBS, 15 min per wash cycle, the secondary antibody Alexa-Fluor 647 donkey anti-goat (1:1000, catalog #A21447, ThermoFisher Scientific, USA) was diluted in blocking solution and added to the cells for 1 hour at RT. After 5x washes with PBS, 15 min per wash cycle, the secondary antibody Alexa-Fluor 568 goat anti-rabbit (1:500, catalog #A11011, ThermoFisher Scientific, USA) was added to the cells for another hour at RT followed by another 5x 15 min wash. Cells were stored at 4° C until imaging was performed.

3.4.2.2 GSD imaging and analysis

Super-resolution imaging of ATR1 and P2Y6R was carried out using coverslips mounted on a round cavity microscope slide (catalog #BR475505, Sigma, USA). ONI B cubed buffers A+B (100:1, catalog #BCA0017, ONI) were added to the round cavity center, followed by the placement of the coverslips with the cells upside down. Localization maps images were acquired using a microscope coupled to a 100x Olympus oil-immersion UPlanApo TIRF 1.5 NA objective. Samples were imaged sequentially using 640 nm (1000 mW) and 561 nm (500 mW) lasers, with emission collected using the corresponding filter cubes. Images were acquired at 100 Hz with 10 ms of exposure rate. 30.000 images were acquired to construct a pointillist localization map image. Rendered images were filtered using the following parameter range values: photon count (600- 10000000), σlocx (0-25 nm), σlocy (0-25 nm), σX (100-400), σY (100-400), and p-value (0.6-1.0). Image acquisition was done using the ONI NimOS v.1.18.3 software.

Biophysical characterization of the ATR1 and P2Y6R clusters, including the intermolecular distance between the two receptors, was performed using pair and cross-correlation algorithms written in MatLab (R2023a, Mathworks, Natick, MA) as in (Sengupta, Jovanovic-Talisman, Skoko, *et al.* 2011; Sengupta, Jovanovic-Talisman, Lippincott-Schwartz 2013; Veatch *et al.* 2012). Autocorrelation (g(r)) and cross-correlation (c(r)) functions were obtained from regions of interest (ROIs) with an area of 6.25 μm2. Special care was taken to avoid placing the ROIs on visible "holes" in the cell image in order to minimize artifacts arising from membrane topography. Parameters such as cluster area, cluster density ($\Psi^{dcluster}$), molecules per cluster, and intermolecular distance were obtained by fitting the correlation functions with exponential models as in (Sengupta, Jovanovic-Talisman, Skoko, *et al.* 2011; Veatch *et al.* 2012).

3.4.3 Enzyme-Linked Immuno Sorbent Assays (ELISA)

A competitive *in vitro* enzyme-linked immunosorbent assay (ELISA) was performed to determine the plasmatic concentration of AgII (RayBio®, catalog #EIA-ANGII) and aldosterone (Invitrogen, catalog #EIAALD), whereas the concentration of renin (Invitrogen, catalog #EMREN1) was assessed using a sandwich ELISA assay. The conceptual differences between the two methods are shown in **Figure M.12**.

3.4.3.1 ELISA assay procedure

The ELISA competitive assay comprised different sequential steps: 1) target (antigen) detection by capture antibody, 2) colorimetric signal generation by a

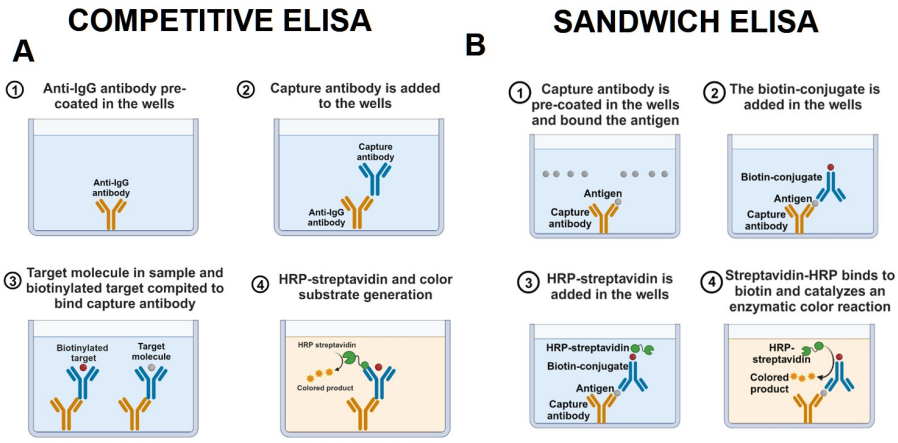

Figure M.12: *Conceptual differences of the two ELISA methods used. In A), The competitive ELISA, an anti-IgG antibody is pre-coated in the plate and a capture antibody is added to the wells. The target molecule in the sample and the biotinylated target compete to interact with the capture antibody. Finally, HRP-streptavidin is added to generate color. The intensity of the color reaction depends on the biotinylated target bound in the capture antibody. An inverse correlation between color and concentration is obtained, since higher intensities correspond to less target molecules in the sample. In B), The sandwich ELISA, the capture antibody is pre-coated in the plate. The target molecule binds to the capture antibody. The amount of molecules bound to the capture antibodies is calculated using biotin conjugated antibodies that recognize the target molecule. Finally, HRP-streptavidin is added to generate color, but in this case, the intensity depends on the amount of target molecules in the sample and a direct correlation is established.*

streptavidin chromogen system, and 3) termination of the colorimetric reaction by a stop solution. The protocol for the ELISA sandwich was quite similar. The 96-well plate (12 strips x 8 wells) precoated with the anti-IgG antibody was equilibrated at RT, the removable 8-well strips were labeled accordingly, and all reagents were mixed before experimental use. Importantly, this immunoglobulin protein was not present in the ELISA sandwich variant, although the experimental procedure was in common with the competitive type. For the 1) antigen detection phase, 100 μL of capture antibody of the target was added to each well and incubated for 1.5 hours at RT with gentle shaking. The solution was then discarded and a wash protocol (x4 times) was performed with x1 wash solution buffer, making up 200-300 μL per well. Complete removal of the liquid at each step was critical for successful performance of the assay. After the final wash step, all remaining buffer was removed by aspiration or decantation. The plate was inverted and blotted on a clean paper towel. Then, 100 μL of positive or negative control (buffer only) and diluted stock or sample solutions were pipetted into the wells. A standard curve was prepared for each experimental assay. The

target biotin conjugate was mixed into the above samples to subsequently compete with the endogenous target in the samples or standards. The 96-well plate was protected with a coverslip and incubated for 2.5 hours with gentle shaking at RT. The solution was discarded, and a wash protocol (x4) was performed as previously described. The 2) colorimetric signal response was generated by adding a prepared polyclonal antibody of HRP-streptavidin solution, 100 μL per well, and incubating for 45 min at RT. The solution was removed as previously described. A final volume of 100 μL TMB One-Step Substrate per well was added to perform a 30-min dark incubation at RT, avoiding any contact with aluminum foil or other metals. Finally, 50 μL of stop solution was pipetted to 3) stop the reaction, and the optical density was immediately measured at 450 nm using a plate reader.

3.4.3.2 ELISA assay analysis

The colorimetric signal value was used to estimate the mean absorbance for the samples. The working factor dilution was considered to estimate the absorbance (1/8 for both AgII and renin, while for aldosterone 1/5). After background subtraction, the percentage of absorbance was calculated as follows:

$$\text{Absorbance (\%)} = \frac{B\text{–blank OD}}{B_o\text{–blank OD}} \cdot 100 \qquad \text{(Eq. 3.5)}$$

Where B was corresponded to the OD of the sample or standard, while, B_o was related to the OD of the zero standard (total binding). Finally, the standard curve was plotted with the x-axis corresponding to the peptide concentration (in pg/mL for AgII or ng/mL for aldosterone and renin-1) and the y-axis corresponding to the percentage of absorbance. The standard curve was fitted to a logistic regression model.

3.5 Functional studies

Wire and pressure myography were used in the present study. The main differences are listed in **Figure M.13**.

The following sections describe the preparation of the mesenteric arteries, the mounting of the isolated resistance vessels, the normalization protocol, the assessment of tissue viability, and the different experimental protocols. All steps were the same for both techniques except for normalization, which was carried out only for wire myography.

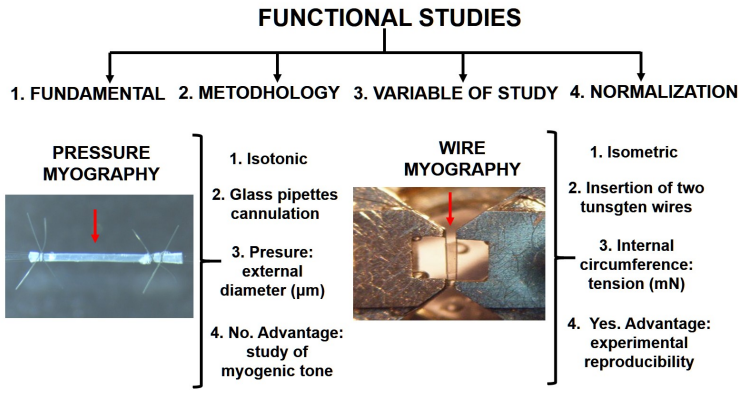

Figure M.13: *The main differences are represented between pressure and wire myography techniques.*

3.5.1 Wire myography

Mulvany and Halpern developed this method in 1977 to assess both passive and active functions of small resistance arteries under isometric conditions (Mulvany, Halpern 1977). The aim of this technique is to investigate the relationship between length and tension, which is crucial for actin-myosin cross bridge interactions. With this method several short segments of the same artery and the same animal can be used simultaneously, and a normalization procedure allow to do the experiments at the isometric condition where tension is maximal. However, the isolation of the vessel from the connective tissue together with the absence of pressure-length and pressure-diameter relationships inevitably disrupts the *in vivo* translation (Wenceslau *et al.* 2021).

3.5.1.1 Wire myography experimental procedure

After euthanasia, the mesenteric arcade was placed in ice-cold SMDS-Ca^{+2} solution and rapidly excised to prevent blood clot formation. In order to remove contaminants released into the solution, the buffer was changed as necessary. The second- and third-order denuded endothelium mesenteric arteries (∼2 mm long) were isolated by minimal manipulation without stretching. The vessel length should not exceed 2 mm. In case that was shorter than this value, it was measured with the calibration eyepiece in the dissecting microscope. Perivascular fat and connective tissue were removed. Because the dissection process can take longer than 2 hours, the vessels were stored in SMDS-Ca^{2+} at 4 ºC during the day. After washing the chambers four times with deionized water and cold physiological salt solution (PSS), they were filled with PSS heated to 37 °C and continuously aerated with 5% CO_2-95% O_2. The amount of air bubbling in each

chamber was appropriately controlled to avoid interference with force measurements. Throughout the experiment, PSS buffer solution was used to replenish the chambers and maintain the arterial preparations under control conditions. 5 mL was the volume added from the solutions, while the drugs were directly administered in the bath unit. Vascular preparations were viable for an average of 8 hours (**Figure M.14**).

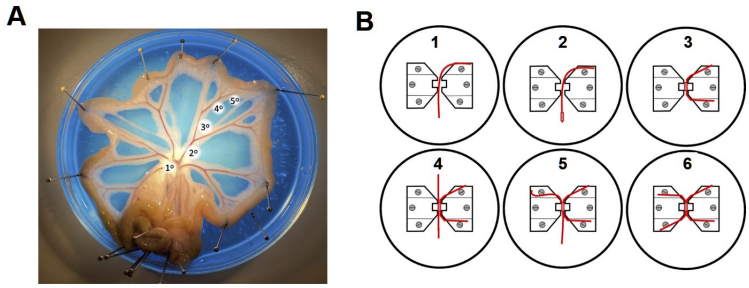

Figure M.14: *In A), Isolated mesenteric tissue placed in Petri dish with colored silicone elastometer, which was filled with SMDS solution. In B), Step-by-step description of mounting small resistance arteries on wire myography. Images extracted from (Wenceslau* et al. *2021).*

The mounting step began approaching the jaws together to gently hold the first wire in position and then secure the "top end" on the micrometer side jaw. The ends of both wires were attached in a clockwise direction when the artery was finally mounted in the chamber. A 2-cm tungsten wire with a 25-μm caliber was used according to the guidelines for mouse mesenteric arteries. The vessel was carefully picked up with fine forceps and transferred to the end of the wire at the unsecured section. The arterial lumen was gently opened with the wire. Then, the entire segment was slowly pushed into the space between the two myography jaws. The "bottom end" was secured on the micrometer side jaw. To remove the endothelium, a thin human hair was carefully inserted into the vessel lumen. The second wire was gently thread through the lumen of the vessel in one motion and using the previously attached wire as a reference. The jaws were bring together to hold the second wire in place. As noted before, the "top end" was secured on the force transduce side jaw. This step was performed with care because additional forces might damage the device. However, both wires should be tightened quite firmly to avoid experimental interferences. Finally, the "bottom end" of the wire on the force transducer side jaw was then secured. The forceps were used to check if the wires were parallel. Both wires should be closer and not generating any tension. The chamber was reinserted into the base unit and the transducer cables were connected to the instrument. PSS buffer solution was again added to the chambers to remove contaminants. Chambers were emptied individually or simultaneously by pressing the appropriate buttons

on the myograph interface display (Multi Wire Myograph System-model 820). Vessels were stabilized for 30 min prior to the normalization protocol to achieve bath-heating conditions. The commercial software (LabChart Pro-DMT, AD Instruments, Hastings, UK) was also calibrated before the first experimental approach according to the manufacturer's instructions. At the end of the protocol, the chambers were cleaned with 8% acetic acid and thoroughly rinsed with deionized water.

3.5.1.2 Wire myography normalization and vessel viability check

Normalization is the standardization procedure that optimizes the arterial responses when applying a pharmacological agent. Indeed, the resting stretch influences the study of the vascular functions, since the active responses are stretch dependent. Excessive or limited baseline stretch applied in each individual vessel might represent a critical factor to study the optimal contractile responses (SSpiers, Padmanabhan 2005). The objective of normalization is to define the internal circumference (IC) of the vessel that corresponds to the stretch where the artery generates the maximal tension upon stimulation (IC1). The procedure requires the characterization of the passive and active response of the artery to stretch. A passive stretch-tension graph was constructed for each artery measuring the tension generated from a gradual stretching protocol using the micrometer that controls the separation of the jaws where the artery is mounted. Tension was normalized by the length of the vessel (usually ∼2 mm long). The IC values (as a measure of stretch) were calculated from the micrometer readings in each step using the following formula:

$$\mathrm{IC} = 128.54\ \mu m + 2x_{\mathrm{gap}} \qquad \text{(Eq. 3.6)}$$

where 128.54 μm is the IC value when the two wires were just touching at the beginning of the normalization an the $2x_{\mathrm{gap}}$ is the value obtained from the incremental stretch from one micrometer reading to another. For any incremental force at a known IC, the corresponding transmural pressure can be determined by Laplace's equation

$$Pressure = \frac{\text{Wall tension}}{\text{internal circumference}/2 \cdot \pi} \qquad \text{(Eq. 3.7)}$$

The arteries were stretched at 1-minute intervals and the obtained tension were plotted against the corresponding IC (**Figure M.15**). For each vessel, the IC that mimics the wall force exerted at a physiological transmural pressure of 100 mmHg (IC100) was taken as the representative value that characterize the passive properties of that artery.

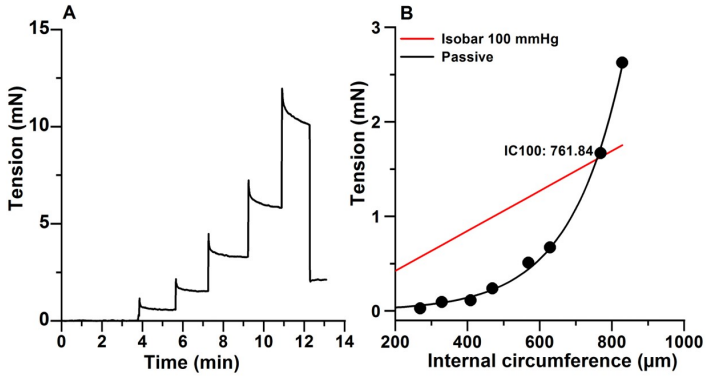

Figure M.15: *In A), Illustration of the stepwise stretching protocol applied in a daily normalization procedure. In B), Plot of wall force tension versus IC. Black line represents the tension corresponding to an arterial pressure of 100 mmHg (Laplace´s equation). IC100 is the IC obtained from the intersection between the isobar 100 mmHg and the passive curve.*

To obtain the IC that gives the maximal tension when there is active contraction (IC1) the ratio IC100/IC1 is assumed to be constant for arteries of the same bed and the same species, and therefore it was calculated in a set of experiments as depicted in **Figure M.16**. In these experiments, in addition to the passive stretch-tension, the active stretch-tension response was obtained using 120 mM K^+ as stimulus. The ratio IC1/IC100 obtained was 0.82, in good agreement with the 0.9 value obtained in a similar preparation, such as the mesenteric arteries from rat (Wenceslau *et al.* 2021).

After normalization, the arteries were kept at rest during 15 min. The average of the resting tension applied was around 1-2 mN. Arterial viability was tested using a standardized procedure to evaluate both vasoconstrictor and vasodilator responses, as previously described (Wenceslau *et al.* 2021). The mesenteric arteries were exposed to depolarization with high potassium solution (PSS-120 mM K^+) twice, and a 3-min pulse was followed by a 15-min washout. Subsequently, the absence of an endothelial layer was confirmed by the lack of relaxation in response to the maximum dose of Ach (10 μM) in vessels precontracted with Phe (10 μM). Vessels that did not contract with PSS-120 mM K^+ or relax more than 20% in response to Ach were excluded for further studies (**Figure M.17**).

3.5.1.3 Wire myography analysis

Experimental strategies used included 1) dose-response curves, 2) single pulse protocols and 3) paired protocols (see **Figure M.18**).

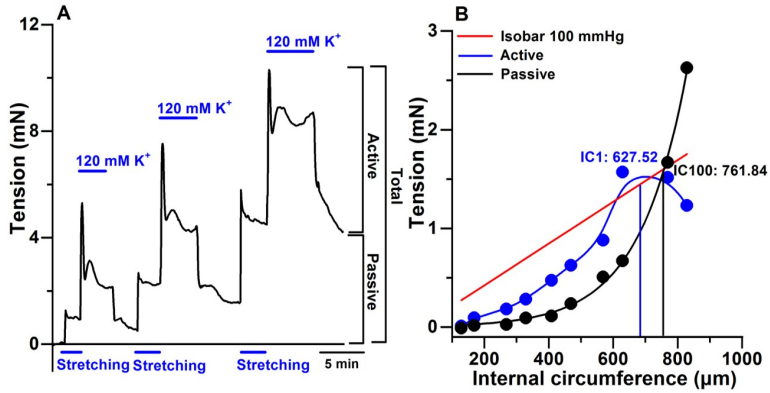

Figure M.16: *Stepwise stretching protocol allowed to determine the IC1/IC100 factor in mouse mesenteric arteries from BPN/BPH. In A), Illustration of the stepwise stretching protocol carried out to get the active responses using pulses of 120 mM K^+. In B), There are presented both the active (green) and passive (blue) forces generated in the vessel. IC1 was defined as the IC that produces the maximal tension in the active curve, while IC100 was the intersection between the 100 mmHg isobar and the passive curve. An average of 10 arteries from BPN and BPH were used for data collection. Passive curves were computed for every artery, and IC1 was estimated from the IC1/IC00 ratio obtained in this set of experiments.*

Several considerations were made before implementing the experimental strategies. Dose response curves were obtained by adding the agonist in an incremental manner with washouts between dose, except for the AgII dose-response curves. In this case, each individual vessel was exposed to a single dose to avoid interference from the desensitization phenomenon. **Figure M.19** illustrate how desensitization makes unfeasible to obtain a dose response curve in the same artery. After applying a pulse of AgtII 10 or 100 nM (S1), a second pulse with the same concentration (S_2) was applied 10, 30, 50 or 120 min later. On average, 120 min was needed to get the same response in the second pulse (S_2/S_1 ratio $\sim$ 100%) in BPH mesenteric arteries.

In single-dose protocols, several strategies were considered and further explained in each specific case. Agonists or antagonists were used either preincubating or applying in the stable tonic phase of the responses. Preconstriction was induced with maximal concentration of the agonist (Phe 10 μM, U46619 1 μM or UTP 10 μM). Finally, in paired protocols, two successive agonist-mediated contractions were applied in the arteries. Either control or experimental conditions were exposed to the vessels. In the latter, at least one control situation was generated to running simultaneously blocking and control conditions. 20-min contractile pulse followed by 30-min exposure to the control and 15-min of inhibitor preincubation. Same time references were considered without the

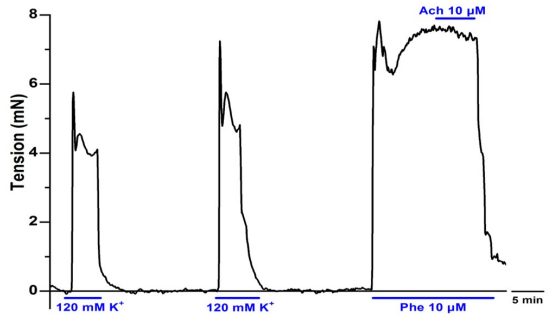

Figure M.17: *Overview of the activation procedure for verifying the viability of wire-mounted vascular specimens.*

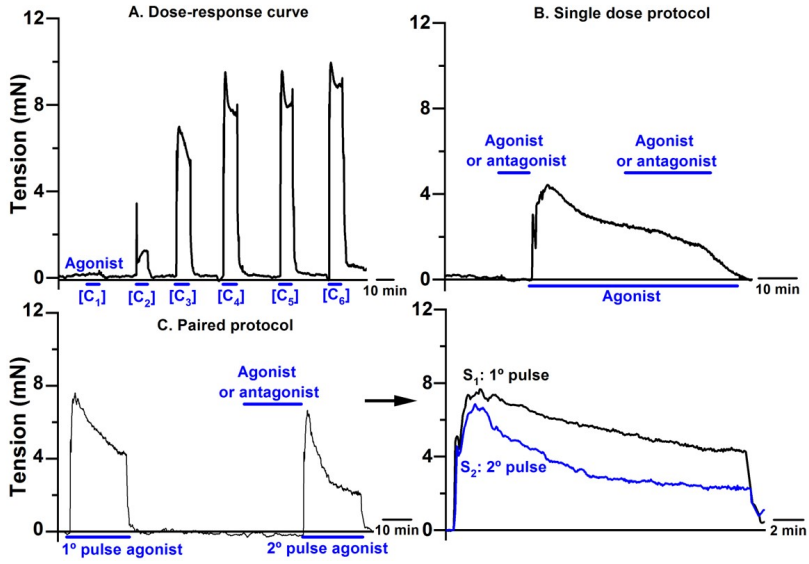

Figure M.18: *Set of experimental strategies performed in mounted wire myography vascular preparations.*

inhibitor application.

The reproducibility of the contractions was examined by measuring the ratio S_2/S_1 (%) for each of the agonists used. Two successive pulses with maximal concentration of Phe (10 μM) and UTP (500 μM) were administered in the vessels. With both agonists, the S_2/S_1 (%) ratio was close to 100% and no differences were detected between models. The data is illustrated in the **Table M.5**.

ADinstruments PowerLab software was used for data acquisition. It allowed the acquisition and conversion of analog force signals into digital ones, expressed in mN units. To normalize the data, contraction is usually expressed as a per-

Phe-S_2/S_1 (%)	Maximum (mN)	Stationary (mN)
BPN	92.90 ± 3.58	103.72 ± 6.17
BPH	100.26 ± 2.65	93.47 ± 2.37
Statistics	N.S.	N.S.

UTP-S_2/S_1 (%)	Maximum (mN)
BPN	89.05 ± 9.48
BPH	97.38 ± 8.03
Statistics	N.S.

Table M.5: *Analysis of paired protocols in control conditions from BPN and BPH mesenteric arteries. The vessels were exposed to either Phe or UTP and the S_2/S_1 (%) ratio was calculated. No significant differences were observed between groups. An average of 3 and 6 arteries were used for data collection.*

centage of high K^+ vasoconstriction (Wenceslau *et al.* 2021). However, in the present study, we use the absolute values of tension, because large differences between BPN and BPH were observed in the high K^+ vasoconstrictions. Tension was calculated by subtracting the active response and the resting tension for each vessel.

The pharmacological effects on contraction was compute as

$$Inhibition(\%) = \frac{\text{Parameter}_{\text{control}} - \text{Parameter}_{\text{inhibition}}}{\text{Parameter}_{\text{control}}} \cdot 100 \qquad \text{(Eq. 3.8)}$$

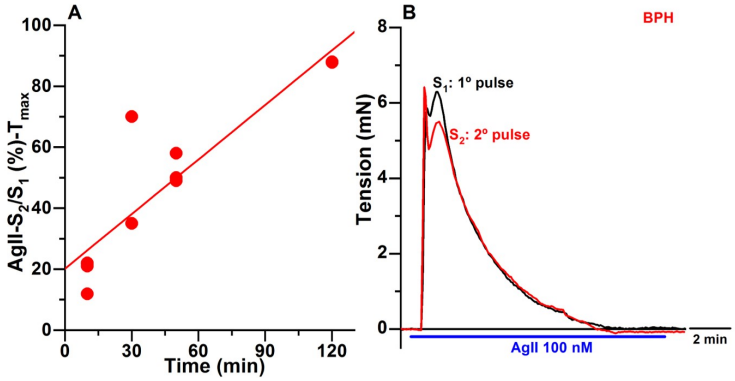

Figure M.19: *A), Linear correlation between time duration and S_2/S_1 (%) ratio. Different AgII concentrations were pooled and S_2/S_1 (%) ratio was estimated. Two hours was the time estimated to fully recover the second amplitude of the pulse regarding the first one. B), Representative trace of ∼100 % S_2/S_1 ratio after 2 hours of pause between the two consecutive pulses. An average of 10 arteries from BPH mesenteric arteries was used for data collection.*

3.5.2 Pressure myography

Pressure myography was also used to study vascular function under isobaric conditions. Arterial segments were cannulated between two glass pipettes, and physiological intraluminal pressure was applied. Agonist-mediated contractions were compared with wire myography data. However, differences were noted depending on which pressure or wire myography device was used. According to the literature, differences could be found in isometric and isobaric conditions using the same pharmacological agents (Buus *et al.* 1994; Wenceslau *et al.* 2021).

Several studies have indicated that pressure myography closely approximates physiological conditions because vessels are subjected to *in vivo* pressure rather than being stretched between wires. The choice of the appropriate technique depends on the experimental designs and the questions to be answered. In this regard, previous work by our group characterized the relationship between changes in BP and VSMC contractility in HT by pressure myography. One of the most important findings is that BPH mesenteric arteries showed an enhanced MT response compared with BPN (Tajada, Cidad, Moreno-Domínguez, *et al.* 2012). However, in the present study, the scenario was different. The main changes in GPCR-dependent pathways were examined in HT after agonist-receptor interactions. Because one of the main strengths of wire myography is experimental reproducibility and control of biological variability, most of the studies were performed using this setup. A smaller proportion of vascular reactivity studies were performed with pressure myography.

3.5.2.1 Pressure myography experimental procedure and vessel viability check

The second- and third-order denuded endothelium mesenteric arteries were isolated, and perivascular fat and connective tissue were removed. An average of two arteries per animal were mounted sequentially in the pressure myography device (Danish Myo technology, Aarhus, Denmark). The length of the vessels ranged from 1.5 to 3 mm. Before the procedure, the chambers were washed four times with deionized water and cold PSS solution. Then, they were filled with PSS, heated to 37°C, and continuously aerated with 5% CO_2-95% O_2. Throughout the experiment, PSS buffer solution was used to fill the chambers and maintain the arterial preparations under control conditions. 6 mL was the volume added from the solutions, while drugs were directly applied into the bath unit. Vascular preparations were viable for an average of 8 hours (**Figure M.20**).

The mounting step began with the approach and alignment of the two glass borosilicate pipettes. The pipettes were available in various sizes from commercial distributors. Four nylon sutures were loosely placed over the shaft of each

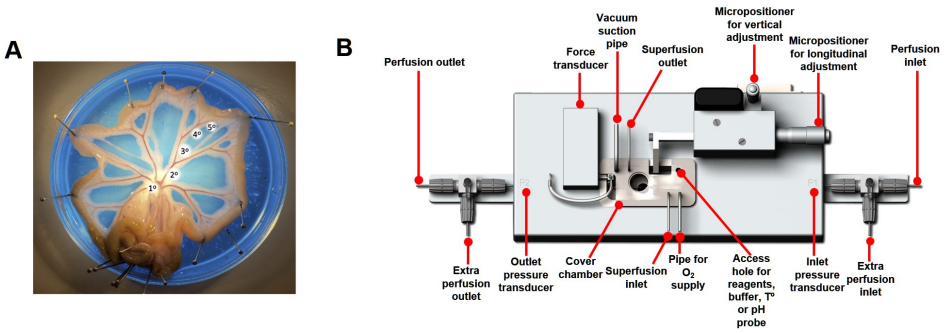

Figure M.20: *In A), Isolation of small mesenteric arteries for vascular studies with pressure myography, adapted from (Wenceslau* et al. *2021). In B), Representation of each of the components that configure the pressure device.*

glass pipette. The isolated artery was then brought into the pressure chamber and cannulated into the P1 inflow pipette. Nylon sutures were placed around the vessel to secure the sample in the glass pipette. The endothelial layer was removed by introducing air bubbles into the lumen of the artery with mechanical force. The outflow pipette P2 was advanced toward the inflow pipette P1 to allow cannulation of the distal portion of the artery without stretching. The other two sutures were used to connect and seal this section of the artery to the outflow pipette. Finally, the pressure myography device was carefully placed on the DMT microscope. The air tubing was connected to the air port of the lid so that the bath was constantly equilibrated with an air mixture of 95% O_2-5% CO_2. The chamber was heated to 37ºC, and the temperature was constantly recorded with a sensor in the myography chamber. A video camera coupled to the DMT inverted microscope (model 111P) continuously recorded the edges of the vessel. The computer frame grabber was set to continuously monitor the outer wall diameter of the artery. MyoViewTM DMT commercial software was used for data acquisition and subsequent analysis. Besides to the outer diameter recordings, temperature values were simultaneously recorded. A gradually increasing pressure protocol from 10 to 70 mmHg was performed to pressurize the arteries under physiological conditions. The procedure was performed every 5 min and in increments of 10 mmHg. Before data collection, the pressurized arteries were equilibrated for 20 min, and the bath solution was changed at least twice during the procedure. At the end of the experiment, the artery was removed from the chamber and the system was rinsed with deionized water. The pressure myography chamber was then cleaned with 8% acetic acid and thoroughly rinsed again with deionized water.

Vessel integrity and viability were checked. A PSS-60 mM K^+ depolarizing solution was administered once during 3 min followed by 15-min washout. The

absence of endothelium was confirmed by the absence of relaxation induced by Ach (10 μM) in vessels precontracted with Phe (10 μM) Arteries that did not contract in response to PSS-60 mM K^+ or Phe (10 μM) or did relax more than 20% with Ach were discarded (**Figure M.21**). At the end of the protocol, the maximum external diameter (maximal dilation) was achieved by applying the L-type calcium channel blocker nifedipine (Nif, 10 μM).

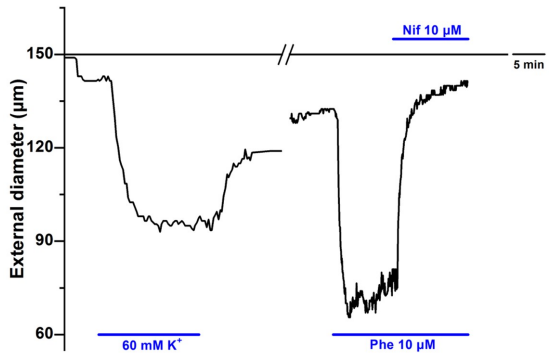

Figure M.21: *Representative experimental trace of an isolated pressurized vessel obtained from a daily experimental strategy.*

3.5.2.2 Pressure myography analysis

Experimental strategies were similar to those used in the wire myograph. For normalization corrections, the data was expressed considering as reference the maximal external diameter reached after the application of nifedipine, and the effect of agonists was calculated as:

$$Vasoconstriction\ effect(\%) = \frac{D_{\text{Nifedipine}} - D_x}{D_{\text{Nifedipine}}} \cdot 100 \qquad \text{(Eq. 3.9)}$$

Where $D_{\text{Nifedipine}}$ was the maximal vessel diameter, D_x was the diameter reached in presence of the drug. Dose-response curves obtained by both pressure and wire myography were fitted to a Hill function (**Figure M.22**). In some cases, data were best fitted to a model with two binding sites.

3.5.3 Myography solutions

The PSS, PSS-60 mM K^+, PSS-120 mM K^+, or PSS-free Cl- solutions were prepared to implement in the experimental strategies, as previously described (Boedtkjer *et al.* 2015; Wenceslau *et al.* 2021). The PSS-high K^+ solution was

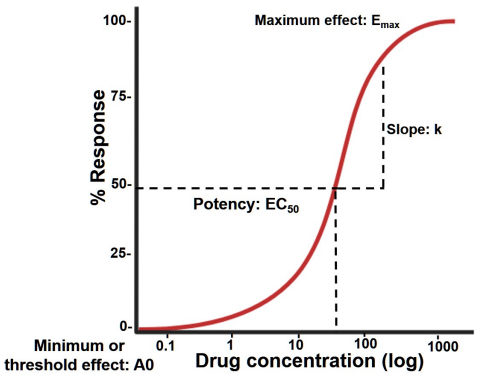

Figure M.22: *Graphical representation fitted to a Hill sigmoidal function. The parameters obtained were as the threshold effect (A0), the concentration to get 50% of the effect (EC_{50}), the slope (k), and the maximum effect (E_{max}).*

prepared by replacing NaCl with KCl. The PSS-free Cl^- solution was prepared by replacing NaCl and KCl with aspartate sodium and potassium salts, while $CaCl_2$ was substituted by $CaSO_4$. The same proportions were maintained as in PSS physiological condition. In this sense, the intracellular $[Cl^-]_i$ depletion was achieved via a prolonged substitution with the impermeant aspartate anion (Boedtkjer *et al.* 2015). The composition is listed below in the **Table M.6**.

Composition	PSS (mM)	PSS-60 mM KCL (mM)	PSS-120 mM KCL (mM)
NaCl	120	65	5
KCl	5	60	120
$NaCHO_3$	25	25	25
Na_2HPO_4	1.18	1.18	1.18
$MgSO_4$	1.17	1.17	1.17
Glucose	10	10	10
EDTA	1	1	1
$CaCl_2$	2.5	2.5	2.5
pH		7.4	

Composition	PSS-free Cl^- (mM)
$HO_2CCH_2CH(NH_2)CO_2Na{\cdot}H_2O$	5
$HO_2CCH_2CH(NH_2)CO_2K$	120
$NaCHO_3$	25
Na_2HPO_4	1.18
$MgSO_4$	1.17
Glucose	10
EDTA	1
$CaSO_4$	2.5
pH	7.4

Table M.6: *Composition of the solutions used in ex vivo wire and pressure myography techniques.*

3.6 Reagents

Most reagents were purchased from Sigma-Aldrich. **Table M.7** lists the agonists, and **Table M.8** lists the antagonists. These agents were used in *ex vivo* wire and pressure myography techniques, as well as, *in vivo* studies (uniquely in the

Agonist	Distributor	Effect	Dissolvent
Acetylcholine chloride, Ach	A6625, Sigma Aldrich	Vasodilator	Deionized water
Sodium nitroprusside, SNP	PHR1423, Sigma-Aldrich	Vasodilator	Deionized water
Isoproterenol hydrochloride, Iso	PHR2722, Sigma-Aldrich	Vasodilator	Deionized water. Light sensitive
Angiotensin II, AgII	A9525, Sigma Aldrich	Vasocontrictor	Deionized water
Phenylephrine hydrochloride, Phe	P6126, Sigma-Aldrich	Vasocontrictor	Deionized water
9,11-Dideoxy-11α,9α-epoxymethanoprostaglandin F2α, U46619	D8174, Sigma-Aldrich	Vasocontrictor	Deionized water
Uridine 5'-triphosphate trisodium salt, UTP	J63427, Alfa Aesar	Vasocontrictor	Deionized water
Uridine 5'-(γ-thio)-triphosphate trisodium salt, UTPγS	3279, Tocris Bioscience	Vasocontrictor	Deionized water
Uridine diphosphate disodium salt, UDP	27821-45-0, Tocris Bioscience	Vasocontrictor	Deionized water
PSB 0474	2715, Tocris Bioscience	Vasocontrictor	Deionized water
Methylene adenosine 5'-triphosphate lithium salt, αβMeATP	5054190001, Calbiochem	Vasocontrictor	Deionized water

Table M.7: *The list of vasoconstrictor and vasodilator agonists used in the present study.*

Antagonist	Distributor	Effect	Dissolvent
Nifedipine, Nif	481981, Calbiochem	Dihydropyridine LTCC blocker	DMSO. Light sensitive
N,N''-1,4-butanediylbis[N'-(3-isothiocyanatophenyl)thiourea, MRS2578	2146, Tocris Bioscience	P2Y6R blocker	DMSO. Light sensitive
1-[6-[[(17β)-3-Methoxyestra-1,3,5(10)-trien-17-yl]amino]hexyl]-1H-pyrrole-2,5-dione, U73122	662035, Calbiochem	PLCβ blocker	DMSO. Light sensitive
Gö 6983	2285, Tocris Bioscience	PKC broad spectrum blocker	DMSO. Light sensitive
(S)-(+)-2-Methyl-1-[(4-methyl-5-isoquinolinyl)sulfonyl]homopiperazine.2HCl, H1152	SC -203592, Santa Cruz	ROCK blocker	Deionized water
CCG215022	HY - 18991, Medchem	GRK1, GRK2, and GRK5 blocker	DMSO
Thapsigargin, TG	T9033, Sigma-Aldrich	SERCA blocker	DMSO. Light sensitive
TMEM16A inh	SML -0493, Sigma-Aldrich	TMEM16A blocker	DMSO
N-(4-(3,5-bis(trifluoromethyl)-1H-pyrazol-1-yl)phenyl)-4-methylbenzenesulfonamide, Pyr10	648494, Calbiochem	TRPC3 blocker	DMSO. Light sensitive
Losartan (potassium salt)	Normon 100 mg	ATR1 blocker	Deionized water

Table M.8: *The list of antagonists used in the present study.*

case of losartan).

3.7 Data processing and statistical analysis

Plots and Graphs were created with the Origin 7.5 program (OriginLab Corp., Northampton, MA, USA) and all illustrations and cartoons with BioRender. Data processing and analysis was carried out with Microsoft Excel, and statistical analysis was performed using R.

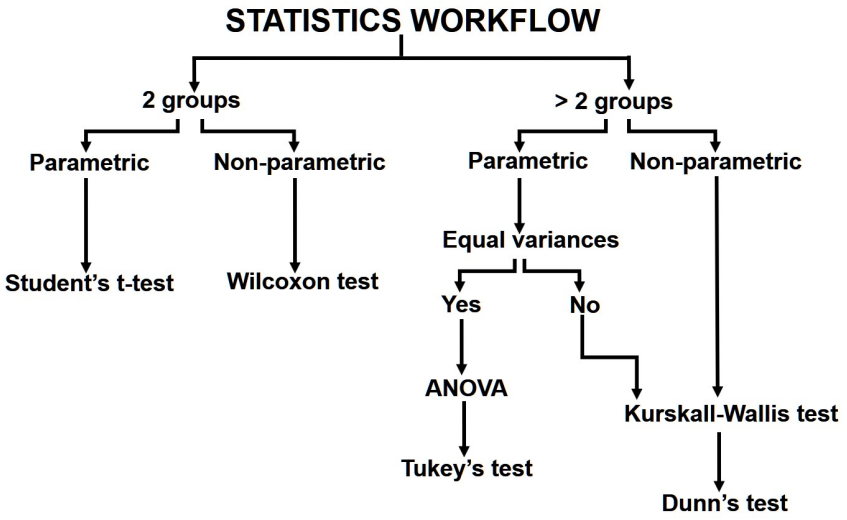

Figure M.23: *Overview of the workflow considered when performing the statistical analysis. Image created with biorender and adapted from (Mcdonald 2008).*

Data is represented as the mean and the standard error of the mean (SEM). For comparisons between two groups, a Student's t-test was applied for both paired and unpaired data when the distribution was normal. For non-normal distribution, the Mann-Whitney-Wilcoxon test was used for paired or unpaired data. For comparisons between more than two groups, one-way analysis ANOVA followed by Tukey's test was used when the distribution was normal and the variances were equal. Alternatively, Kruskal-Wallis analysis followed by Dunn's test was used. Shapiro-Wilk test and Bartlett test were used to test normality and homogeneity of variances, respectively. Linear correlation between variables was measured using Pearson coefficient. Throughout the Results section, p-values<0.05 were considered significantly different, where *<0.05, **<0.01, and ***<0.001. A summary is shown in the **Figure M.23**.

4 Results

4.1 The transcriptome of mesenteric arteries in essential hypertension

To study the molecular signatures determining the hypertensive phenotype in the VSMCs of mesenteric arteries from BPH mice, we compared the gene expression profiles of BPN and BPH using the Affymetrix GeneChip®MG-430 2.0 Array.

In BPH mice, 313 genes were more that 2-fold up regulated and 318 were more than 2-fold down regulated in comparison to BPN mice (adjusted p values <0.01). These 631 genes represent a 7.4% of the total genes expressed either in BPN or BPH VSMCs. Interestingly, P2YR and P2XR purinergic expression seem to be different in an opposite way (**Figure R.1**A). While P2Y6R was among the genes more up regulated (7.3-fold), P2XR1 expression was down regulated (2.3-fold). Purinergic receptor expression was also tested by RT-qPCR (**Figure R.1**B). Although we obtained similar results for P2Y6R, which expression is 7.1-fold higher in BPH, we could not validate the results for P2XR1, which seems to be similarly expressed in BPN and BPH. Data also showed that P2XR expression was ∼200 times higher than P2YR and that P2Y6R was the more abundant P2YR both in BPN and in BPH, despite the up regulation of

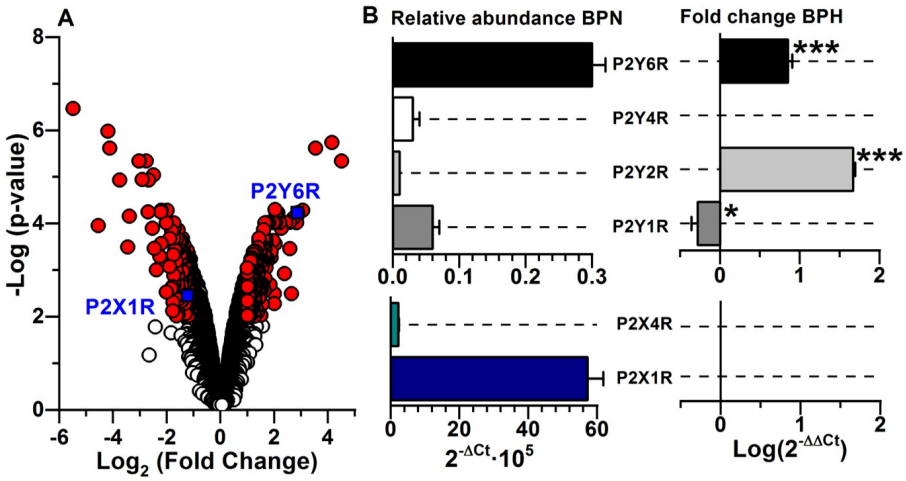

Figure R.1: *In A), The vulcano plot representing the significance [-log(p-value)] versus the differences in expression [log_2(Fold chance)] for the 8516 genes expressed in VSMC from BPN and BPH mice. Genes with a log_2(FC) >1 (up two fold) or <1 (down two fold) and a -log(adjusted p) > 2 (0.01) are considered significantly differentially expressed (red dots). In B), The RT-qPCR validation of gene expression profiles of P2X and P2Y receptors. The left panel shows their relative abundance in BPN estimated as $2^{-\Delta C_t}$. The right panel shows the differences of expression between BPN and BPH, expressed as $2^{-\Delta\Delta C_t}$. Data are the average of 4-5 animals of each strain.*

P2Y2R in BPH.

Gene ontology enrichment analysis based on biological process revealed more than 600 significant GO terms when the whole annotated mouse genome was used as background. However, when only the expressed genes were used as background, there was not any significant GO enrichment, suggesting that HT is not particularly associated with any pathway (Timmons *et al.* 2015). Nevertheless, several relevant genes related with VSMC contractility were expressed differentially. Those genes were identified manually and depicted graphically in **Figure R.2**.

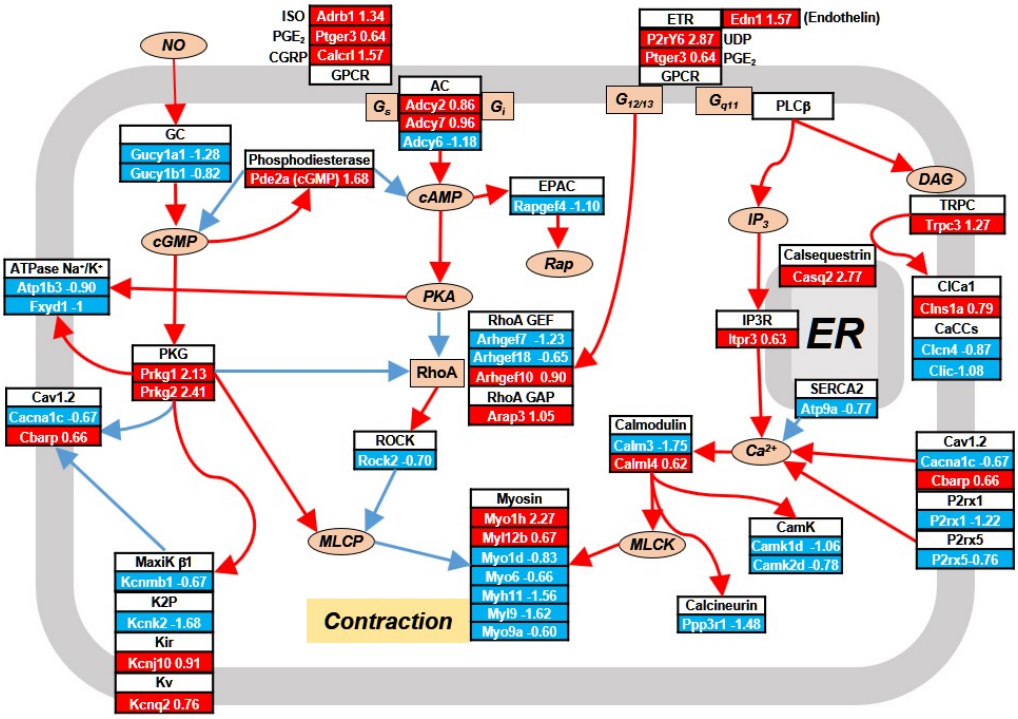

Figure R.2: *Differentially expressed genes in BPH related with contraction or with signaling pathways that modulates VSMC contractility. The cartoon shows the NO/GMPc/PKC, $G_{\alpha}s$, $G_{\alpha}q$ and $G_{\alpha}12$-13 signaling pathways, ER Ca^{2+} handling protein, ion channels and other proteins relevant for VSMC contraction that are differentially expressed in BPH mice. Genes were manually extracted from the list of 631 differentially expressed genes by inspecting their annotated functions. Proteins are depicted as white boxes and the related genes differentially expressed are depicted in red [logFC > 1] or blue [logFC<1] boxes.*

4.2 The purinergic system in essential hypertension

4.2.1 P2YR and P2XR mediated responses in BPN and BPH mesenteric arteries

High BP is associated with functional changes in the resistance vasculature. Indeed, an electrical remodelling was highlighted as key in HT by previous works of our group (Daghbouche-rubio *et al.* 2022). VSMC from BPH mesenteric arteries exhibited higher resting depolarized V_M values, which were linked to enhanced MT responses (Tajada, Cidad, Moreno-Domínguez, *et al.* 2012). These studies were performed in basal conditions without prior agonist stimulation. However, the differences in expression observed in several proteins participating in receptor dependent signalling pathways suggest a relevant role of those pathways in the genesis of the hypertensive phenotype. Based on mRNA profile variations shown above, we decided to focus on testing the functional differences of the purinergic system in the BPN/BPH model, evaluating the ionotropic (P2XR) and metabotropic (P2YR) components using pharmacological tools.

UTP dose-response curves were generated with BPN and BPH mesenteric arteries under isometric (wire myography) and isotonic (pressure myography) conditions, and the results are shown in **Figure R.3**. Greater contractions were obtained in BPH mice, with a significant leftward shift of the dose-response curves obtained with both techniques. Curves obtained in isometric conditions (**Figure R.3**B) were fitted with a Hill equation. In the case of BPH, a two-binding site model (red trace) gave a better fitting, with a high affinity component (EC_{50} = 2.27 ± 0.35 μM) characteristic of BPH (blue trace) and a low affinity component (EC_{50} = 124.35 ± 22.81 μM) similar to BPN (green trace). In addition, the high affinity component was larger than the low affinity one (T_{max} = 4.53 ± 0.32 vs. 2.34 ± 0.33). These results are consistent with the larger expression of P2Y6R and P2Y2R, and these receptors are the likely molecular candidates responsible for the augmented UTP contractions in BPH mice.

ATP dose-response curves were also obtained using the same methodological approach, and the results are shown in **Figure R.4**A and B. Unlike what occurred with UTP, responses to ATP were similar in BPN and BPH arteries. Nevertheless, UTP and ATP responses were kinetically very different. Whilst responses produced by UTP were tonic, those elicited by ATP were transient. This difference could be explained by the different activation of purinergic receptors of both agonist: UTP would activate P2YR and ATP would activate mainly P2XR. In any case, some experiments were performed to rule out any P2YR involvement in the ATP mediated responses, since ATP has been described as an agonist of both P2XR and P2YR receptors (Ralevic 2021). We have used the P2X1R agonist ($\alpha\beta$-MeATP, 5 μM) that produces a rapid and transient contrac-

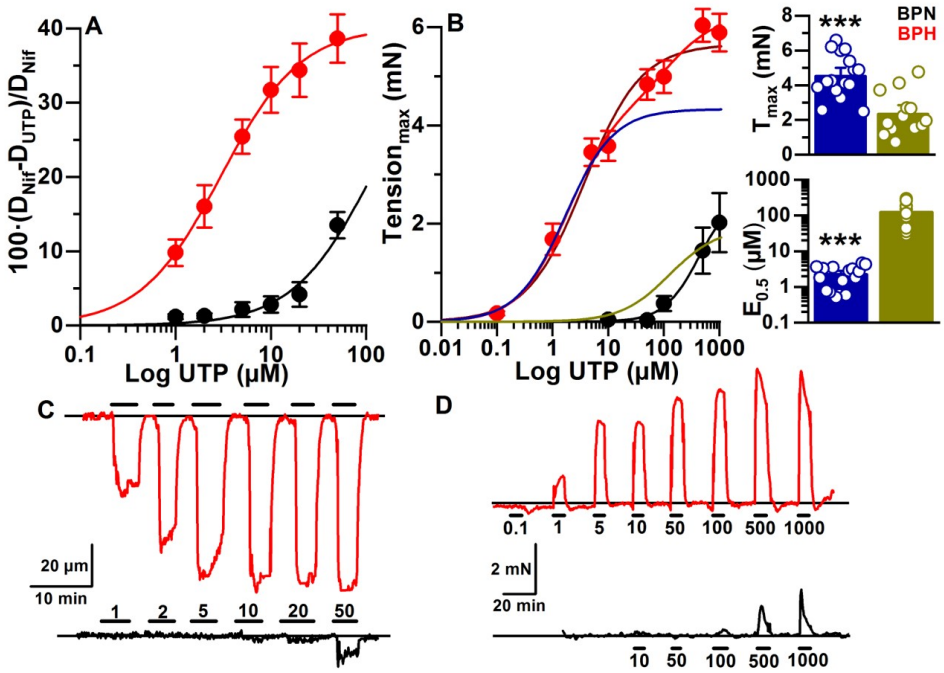

Figure R.3: *UTP-dose response curves obtained in mesenteric arteries from BPN and BPH mice using pressure (A) or wire myography (B). In A), The effect of the agonist at each concentration (% of vasoconstriction) was estimated as indicated in the axis label. DUTP is the diameter in the presence of UTP and* D_{Nif} *is the diameter in the presence of nifedipine (10 μM). In B), Maximal tension was fitted to a Hill function, with a single-binding site (red-BPH and black BPN-dashed lines) or with two-binding sites (red line-BPH). Dashed blue and green lines are the two components of the fit. The parameters of the fit to two-binding sites are shown in the box-plots. UTP was applied in pulses separated by at least 15 min in control solution using pressure (C) and wire myography (D). Black traces correspond to BPN and red to BPH arteries. An average of 13-16 arteries were used for data collection. Student's t-test was applied for unpaired parametric data, where p-value ***< 0.001.*

tion due to the complete desensitization of the receptor, as a tool to dissect the P2XR and the P2YR mediated responses (**Figure R.4**C). After desensitizing the P2XRs with $\alpha\beta$-MeATP, ATP (50μM) was unable of eliciting any response, whilst UTP (50μM) responses were identical to those obtained without applying $\alpha\beta$-MeATP in BPH. These results strongly suggest that ATP responses were mediated by P2XRs and UTP responses by P2YRs.

Since P2XRs are functionally equivalent in BPN and BPH mice, we decide to further characterize the functional differences in P2YR mediated responses, trying to identify if P2Y6R or P2Y2R, the two differentially up regulated receptors in BPH, are responsible of the observed different responses to UTP.

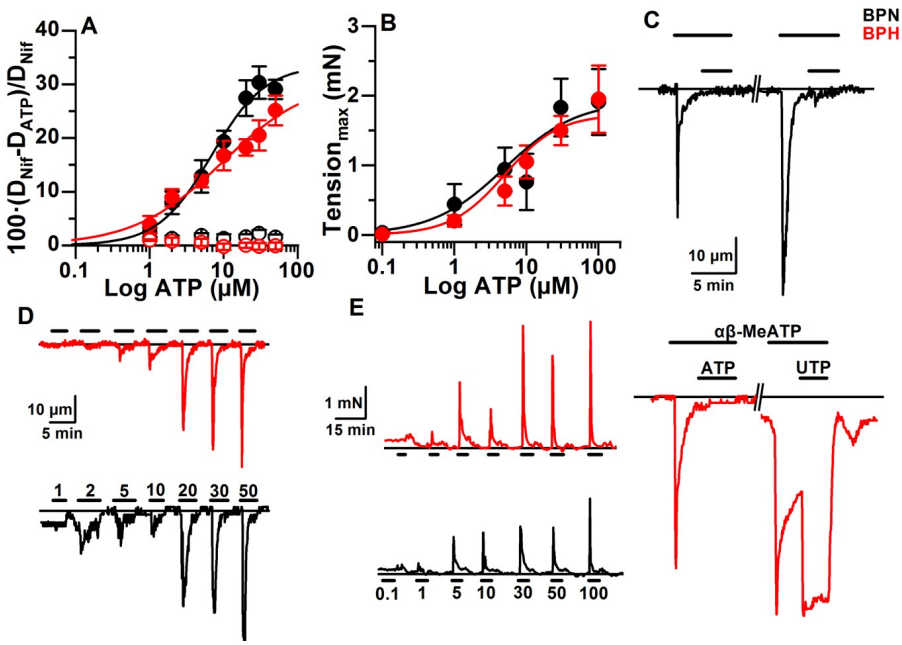

Figure R.4: *ATP-dose response curves obtained in mesenteric arteries from BPN and BPH mice using pressure (A) or wire myography (B). In A), The effect of the agonist at each concentration (% of vasoconstriction) was estimated as indicated in the axis label. DATP is the diameter in the presence of ATP and DNif is the diameter in the presence of nifedipine (10 µM). In B), Maximal tension was fitted to a Hill function, with a single-binding site (black–BPN and red-BPH). In C), The effect of 5 µM αβ-MeATP, and the effect of ATP or UTP in the presence αβ-MeATP tested in the pressure myograph. Red traces are BPH and black traces are BPN arteries. ATP was applied in pulses separated by several min in control solution, using pressure (D) or wire myography (E). Black traces correspond to BPN and red to BPH arteries.*

4.2.2 Pharmacological characterization of P2YR mediated responses in BPH mesenteric arteries

The putative role of several purinergic receptor subtypes (P2Y2R/P2Y4R/P2Y6R) was tested with different agonists in BPN and BPH mesenteric arteries with pressure myography (**Figure R.5**A). 10 μM UDP and 10 μM PSB0474 (selective agonists for P2RY6 (Kügelgen 2006)) induced responses in the pressure myograph that were ∼70% and ∼45% respectively of the response elicited by similar concentration of UTP. 10 μM UTP S (a selective agonist of P2Y2R/4R) elicited a response that was ∼27% of that of UTP. In all cases, responses in BPN were almost absent. Since we have not carried out a full dose curve characterization for all agonists, it is not possible to define precisely the amount of the response mediated by each receptor, although pharmacological data is compatible with a

dominant effect of P2Y6R. The responses to UTP and UDP are also sensitive to MRS2578, a specific P2Y6R blocker, but only when the inhibitor is applied after the agonist (**Figure R.5**B). When arteries were precontracted with the selective P2Y6R agonists, UDP or PSB0474, and MRS2578 was added, a significant inhibition was observed in both cases (27.13 ± 2.38 and 42.60 ± 7.39 respectively, **Figure R.5**C). Although MRS2578 is described in the literature as a potent P2Y6R blocker, in our hands, it has a limited effect, and we decided to use it as a qualitative rather than quantitative tool to examine the P2Y6R contribution in agonist-mediated responses.

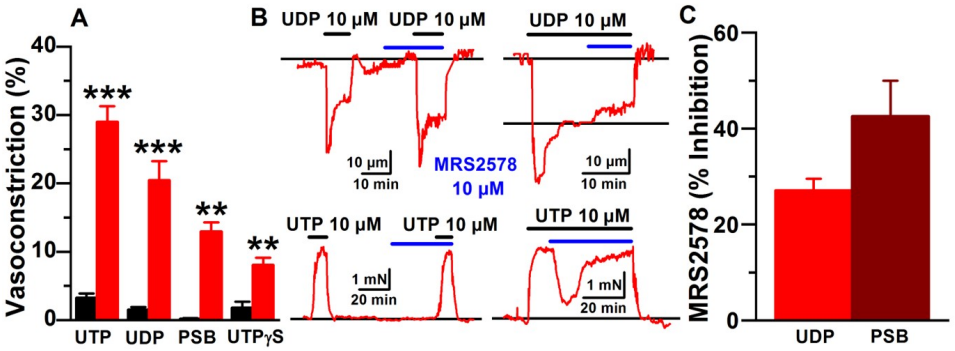

Figure R.5: *In A), Vasoconstrictor response elicited by different P2YR agonists (10 μM) in BPN (black) or BPH (red) arteries. Experiments were carried out in the pressure myography and were analysed as described in the previous figures. In B), Representative traces showing the effect of 10 μM MRS2578 (a P2Y6R antagonist) on the vasoconstrictor responses elicited by UDP or UTP under isotonic (upper traces) or isometric (lower traces) conditions. In C), Quantification of the effect of MRS2578 on the contractions elicited by 10 μM UDP or 10 μM PSB0474 when MRS2578 was applied in the stationary phase of the responses. Each bar is mean±SEM. An average of 8-10 arteries were used for data collection.*

Pharmacological and expression data clearly supported a higher P2Y6R functional role in BPH mesenteric arteries. However, the contribution of P2Y6R to the hypertensive phenotype is not so evident. A plausible hypothesis is to postulate a functional crosstalk between the purinergic system and RAAS, as has been recently published in a mouse model of HT-induced by AgII together with ageing (Nishimura, Sunggip, Tozaki-saitoh, *et al.* 2016). In the following set of experiments, we decided to test if this crosstalk is also present in the BPH model.

4.3 The purinergic and RAAS functional coupling in essential hypertension

4.3.1 P2Y6R and ATR1 are close enough to form heterodimers in BPH VSMCs

The PLA assay was used to investigate the distance between ATR1 and P2Y6R in VSMC from BPN and BPH mesenteric arteries. This technique does not demonstrate the existence of ATR1/P2Y6R heterodimers, but it helps to define the possibility of their existence, since positive labelling is obtained only when proteins are closer than 40 nm. As shown in **Figure R.6**A, significant differences in the number of puncta/μm2 were obtained in BPN and BPH VSMCs (0.08 $\pm$ 0.02 vs. 0.12 $\pm$ 0.01). Representative images from each group are shown in the lower panel (**Figure R.6**B). These results suggest that the formation of ATR1/P2Y6R heterodimers is not only possible, but also more probable in BPH VSMCs.

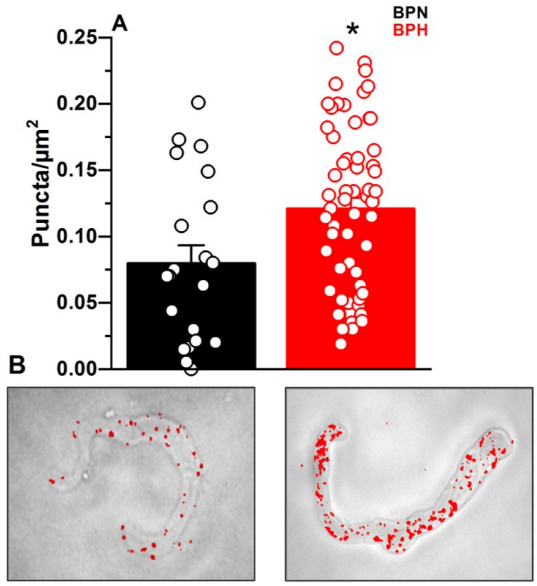

Figure R.6: *Analysis of PLA assays carried out with antibodies against ATR1 and P2Y6R in VSMC isolated from BPN and BPH mesenteric arteries. In A), The number of puncta/μm^2 obtained in each case is shown in the bar graph at the top. In B), Sample images of one BPN and one BPH VSMCs overlapping the PLA (red) and the transmission images are shown in the bottom. Each bar is mean$\pm$SEM. An average of 20-60 cells were used for data collection. The Wilcoxon test was used for unpaired non-parametric data, where the p-value * < is 0.05.*

This pattern was also confirmed by GSD high-resolution microscopy. **Figure R.7**A shows pointillist single-molecule images obtained after labelling BPN and BPH VSMCs with antibodies against ATR1 (red) and P2Y6R (green). The areas of interest (squares) labelled in the merge images are zoomed in the bottom. Analysis of the images (**Figure R.7**B) revealed significant changes for the AGTR1 clusters in BPH cells. Cluster area was smaller (6319 ± 768 in BPN vs. 2864 ± 360 in BPH), cluster density (Ψcluster) was higher (4.7 ± 0.7 in BPN vs. 39.9 ± 2.5 in BPH) and the number of molecules per cluster increased ∼7-fold (1.47 ± 0.32 in BPN vs. 10.2 ± 1.9 in BPH). However, P2Y6R clusters had similar areas in BPN and BPH, whilst cluster density (7.0 ± 0.9 in BPN vs. 25.2 ± 2.3 in BPH) and the number of molecules per cluster (0.36 ± 0.19 in BPN vs. 10.79 ± 2.49 in BPH) were also higher in BPH. Interestingly, the distribution of intermolecular distances between ATR1 and P2Y6R was quite different between BPN and BPH (**Figure R.7**C). Although the means of both distributions were quite similar (145.9 in BPN vs. 125.8 in BPH), medians (144.2 nm in BPN vs.

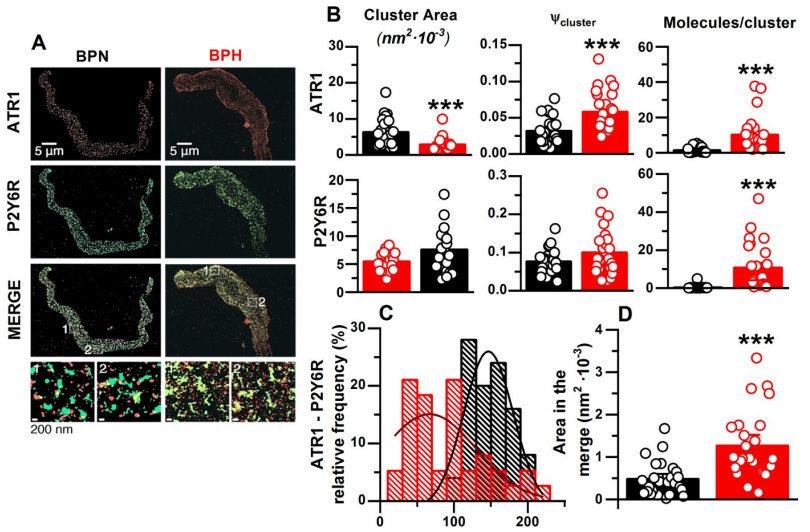

Figure R.7: *Analysis of colocalization of ATR1 and P2Y6R by GSD high-resolution microscopy in VSMCs from BPN and BPH mesenteric arteries. In A), Representative images, where P2Y6R is green and ATR1 red. The squares at the bottom correspond to the areas labelled as 1 and 2 in the merged images. In B), The cluster area ($mm^2 \cdot 10^{-3}$), the Ψcluster and the number of molecules/cluster obtained for each receptor in BPN (black) and BPH (red) VSMCs are shown as box plots. In C), The histogram of intermolecular distances between ATR1 and P2Y6R and the fit to Gaussian functions and in D), the area shared by the two receptors (colocalization) expressed as $mm^2 \cdot 10^{-3}$. An average of 20-50 VSMCs were used for data collection. Each bar is mean±SEM.*

70.8 nm in BPH) and skewness (0.4 in BPN vs. 2.6 in BPH) were quite different. Whilst the BPN distribution is quite symmetric, the BPH distribution is heavily right skewed, with a significant proportion of ATR1 and P2Y6R located at much closer distances in BPH than in BPN. The **Figure R.7**D represents the area shared between the two target proteins as an indicator of protein colocalization. This parameter was larger in BPH VSMCs (1.42 ± 0.22 $\mu m^2 \cdot 10^{-3}$) compared to BPN (0.48±0.08 $\mu m^2 \cdot 10^{-3}$).

PLA and GSD high-resolution microscopy demonstrated that P2Y6R and ATR1 are in close proximity (≤40 nm), enough to form heterodimers in VSMC from BPH mesenteric arteries. To test the existence of those heterodimers we decided to follow a functional approach, trying to disclose a possible interaction between purinergic and angiotensin responses in arteries from BPH mice.

4.3.2 Functional coupling of P2Y6R-ATR1 heterodimers in BPH mesenteric arteries

In order to examine the association of P2Y6R and ATR1, several functional parameters were investigated. First, we compared AgII responses in BPN and BPH arteries, studying the amplitude of the responses and the time course of the desensitization using wire myography.

AgII dose-response curves obtained in BPN and BPH mesenteric arteries are shown in the upper panel of **Figure R.8**A. AgII-mediated contractions were larger in BPH mesenteric arteries and a characteristic and distinctive U-shape curve was obtained with a maximal response at 100 nM. At this concentration, the difference between BPN and BPH arteries was maximal (5.08 ± 0.44 mN in BPH vs. 2.2 ± 0.47 mN in BPN). Both models showed common kinetic properties with fast and transient responses due to the ATR1 desensitization. However, the desensitization seems to be slower in BPH (see below). Overlapping representative traces obtained with 100 nM pulses of AgII in BPN and BPH mesenteric arteries are shown in the lower panel of **Figure R.8**B.

The recovery from desensitization in BPH mice is also kinetically different from that in BPN. **Figure R.8**D shows representative traces obtained in BPN (black) and BPH (red) arteries with a protocol of two 10 min AgII pulses separated by 30 min. Both traces are normalized respecting the maximal tension at the first pulse. The recovery from desensitization at 30 min was estimated as the ratio S_2/S_1 (**Figure R.8**C) and was significantly faster (S_2/S_1 closer to 1) in BPH arteries (66.13 ± 4.37in BPH vs. 34.43 ± 3.72 in BPN, $p<0.001$).

The time course of desensitization was measured as the time needed to get a tension half of the T_{max} ($t_{0.5}$) and was plotted against T_{max} in the scatter plot shown in **Figure R.8**E. The time course of desensitization was independent of

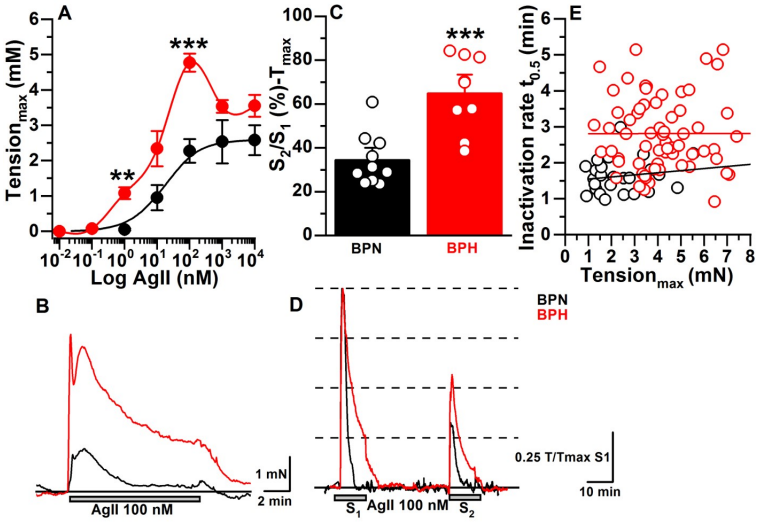

Figure R.8: *In A), AgII dose-response curves obtained in BPN and BPH mesenteric arteries. The vessels were exposed only once to the agonist to avoid the underestimation of the responses due to the receptor desensitization. In B), Sample traces obtained with 100 nM AgII in BPN (black) and BPH (red) are shown at the bottom panel. In C), And D), The recovery of desensitization was investigated with two 10 min pulses of 100 nM AgII separated 30 min and was estimated as the ratio S_2/S_1 (%). In E), The desensitization rate, expressed as the time needed to decay to a 50% of $T_{\max}$ is plotted against $T_{\max}$. Red dots correspond to BPH arteries and black dots to BPN. 13-16 arteries were used for data collection. Bars ares mean±SEM.*

T_{max} (at least for $T_{max} > 1$ mN) and was significantly slower in BPH ($t_{0.5} = 2.85 \pm 0.13$ min in BPH vs. 1.73 ± 0.13 min in BPN).

The enhanced AgII contractions and the slower ATR1 desensitization might be associated with changes in the expression of AgII receptors that were not disclosed in the microarray study. For this reason, expression of ATR1a and ATR1b isoforms was investigated in BPN and BPH arteries using RT-PCR. The relative abundance was estimated in BPN and the fold change was expressed in BPH compared to BPN. Unexpectedly, data showed a decreased expression of the ATR1a mRNA isoform in VSMC from BPH mesenteric arteries, as depicted in **Figure R.9**.

The lack of correlation between ATR1 expression and AgII responses and the kinetic differences in the desensitization process strongly suggest the interaction between ATR1 and P2Y6R as a possible explanation for the differences between BPN and BPH responses to AgII. Therefore, we design several protocols aimed to disclose the functional association between ATR1 and P2Y6R.

First, we explored the effect of blocking P2Y6R on the AgII contractile re-

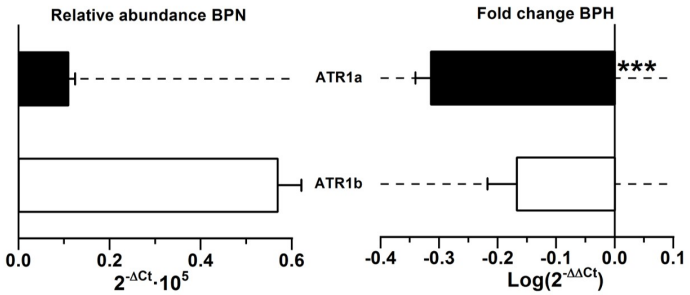

Figure R.9: *mRNA expression levels of ATR1a and ATR1b isoforms in mesenteric arteries from BPN and BPH mice. The left panel shows the relative abundance in BPN estimated as $2^{-\Delta C_t}$. The right panel shows the differences in expression between BPN and BPH expressed as $2^{-\Delta\Delta C_t}$. 4-5 animals were used for data collection. Bars are mean±SEM.*

sponse. **Figure R.10**C shows representative traces of 10 min pulses of AgII 100 nM obtained in BPN (left) and BPH (right) arteries with and without applying MRS2578 at the time indicated by the arrows. Traces are normalized to T_{max} to visualize the effect of the blocker on the time course of the desensitization of the AgII response. P2Y6R blockade had no effect on BPN but significantly sped up AgII desensitization on BPH arteries, strongly suggesting an enhancer effect of P2YR6 receptors on the AgII contractile response. The amount of desensitization was evaluated as the percentage of T_{max} remaining at the end of the 10 min pulse (**Figure R.10**B) or as the time interval between points where tension was 50 and 75% of the T_{max} (**Figure R.10**A).

Following the same rational, we hypothesize that P2Y6R simulation should have the opposite effect of MRS2578 slowing down the desensitization of the response. To test that hypothesis, we carried out a two-pulse protocol in pairs of BPH arteries in the wire myograph as shown in **Figure R.11**. Black traces were obtained in one artery stimulated by two pulses of 10 μM UDP (S_1 and S_2) separated by 60 min, whilst red traces were obtained in the second artery with a similar protocol but applying a 50 min prepulse of 100 nM AgII before the second pulse. Traces from both arteries are normalized to S_1T_{max}. The ratio of maximal tension amplitudes of pulses S_1 and S_2 in both arteries are shown in the bar graph to the right (**Figure R.11**A). **Figure R.11**B illustrates the results obtained in other pair of BPH arteries applying an identical protocol but using Phe 10 μM instead of UDP. **Figure R.11**C shows the box plots measuring the speed of desensitization of the AgII response as the percentage of the AgII T_{max} remaining after 50 min when only one pulse was applied (12.8 ± 2.8%, traces not shown) or when Phe (11.7 ± 3.4%) or UDP (24.8 ± 3.4%) were used as the stimuli for S_1 and S_2. Although previous stimulation with Phe (S_1) has no effect on

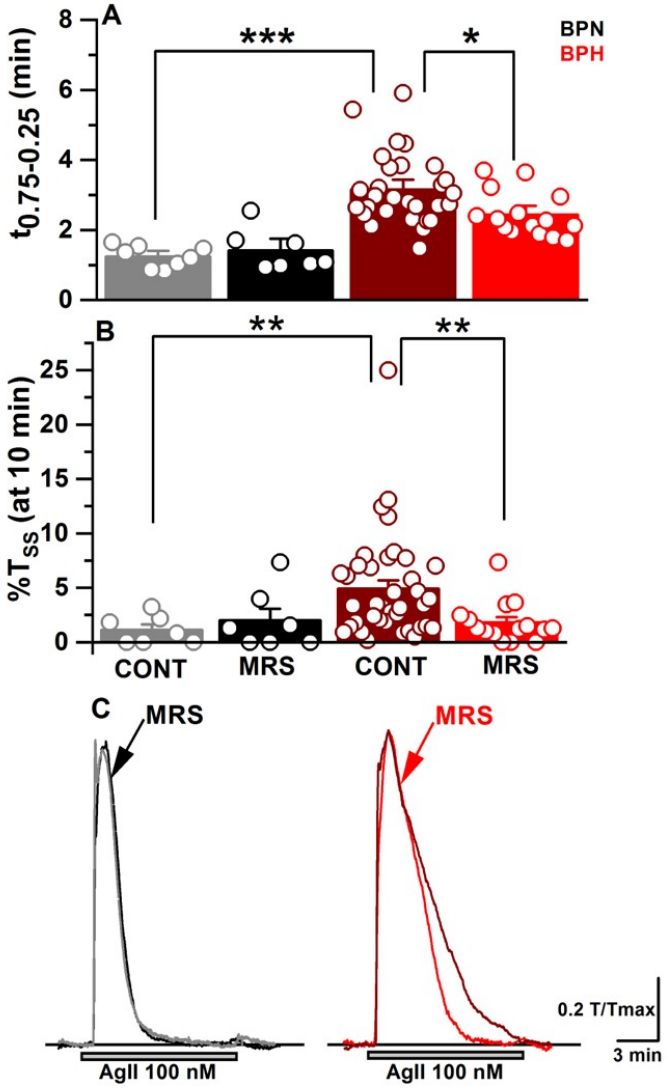

Figure R.10: *Effect of P2Y6R inhibition on the desensitization of the AgII response of BPN and BPH mesenteric arteries. Desensitization was measured either as the time for AgII response to decay from a 75% to a 25% of the $T_{\max}$ (in A) or as the % of $T_{\max}$ remaining at the end of the pulse (in B). Single pulses of AgII 100 nM were compared with identical pulses where MRS2578 was added at the onset of the decay of the response. Sample traces, overlapping the control and the MRS2578 trace and normalized to $T_{\max}$ are shown in C (BPN, left; BPH right). 5-15 arteries were used for data collection.*

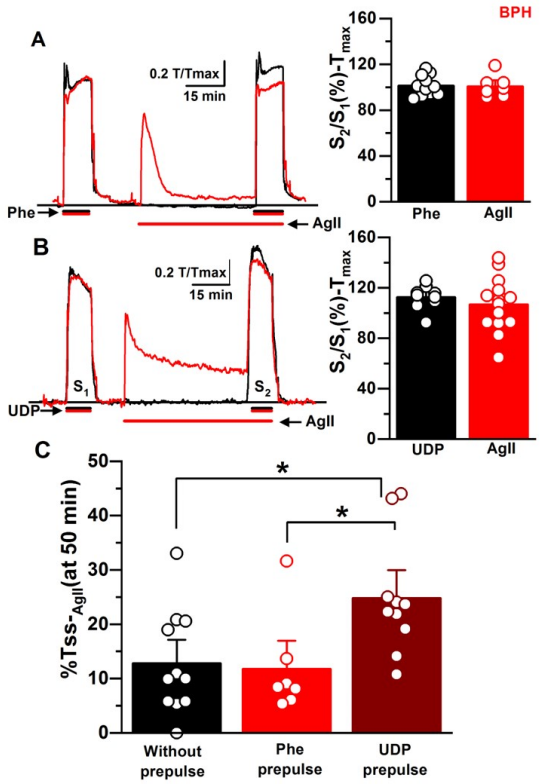

Figure R.11: *Effect of P2Y6R activation on AgII responses obtained in BPH mesenteric arteries. In A), Black traces were obtained in one artery stimulated by two pulses of 10 μM UDP (S_1 and S_2) separated by 60 min. Red traces were obtained in another artery with a similar protocol but applying a 50 min prepulse of 100 nM AgII before the second pulse. Traces from both arteries are normalized to $S1T_{max}$. The S_2/S_1 (%) ratio for each artery is also shown. In B), Same as in A but using 10 μM Phe as S_1 and S_2 stimulus. In C), Box plots quantifying the residual tension at the end of the AgII prepulse when Phe or UDP were used as stimuli (red boxes). The residual tension at the end of single 50 min AgII pulses (black box, traces not shown) is also shown. 5-15 arteries were used for data collection.*

AgII desensitization (no significant differences with single pulses of AgII), UDP almost double the contractile response of AgII remaining at 50 min, as expected if P2Y6R receptor activation potentiates the AgII response slowing down the desensitization. Unexpectedly, it seems that ATR1 activation has no effect on P2Y6R responses, since S_2/S_1 ratio for UDP was identical independently of applying the AgII prepulse before S_2 (**Figure R.11**A, bars graph).

These data clearly pointed to a specific functional coupling between P2Y6R and ATR1 receptors in BPH mesenteric arteries. The possible relevance of this

association for the hypertensive phenotype was explored by studying the RAAS system in the BPN/BPH model in the next set of experiments.

4.3.3 RAAS in the BPN/BPH model: A possible contribution of P2Y6R expression to the hypertensive phenotype

The higher responses to AgII of BPH arteries suggested a relevant role of RAAS in the genesis of the hypertensive phenotype. To explore that hypothesis, we tested the contribution of AgII to controlling BP levels in BPN and BPH mice measuring the effect of losartan (an ATR1 blocker) added to the drinking water (0.6 mg/mL). The obtained changes in mean, diastolic and systolic BP measured along 6 weeks are shown in **Figure R.12**. Losartan had a big effect on BP in both strains, but unexpectedly, the effect was larger in BPN mice, suggesting a more relevant role of RAAS in the normotensive mice.

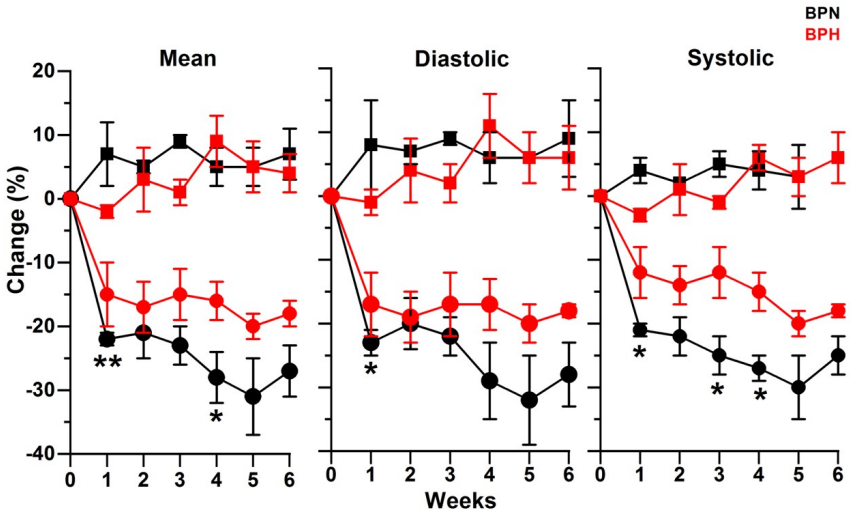

Figure R.12: *Contribution of RAAS to BP in the BPN/BPH model. Losartan was administered in the drinking water (0.6 mg/mL) during 6 weeks. BP were measured weekly with the tail-cuff system. At least three repeated measures were taken for each animal every week of the treatment procedure. Black symbols correspond to BPN and red to BPH mice. Open symbols were obtained in control animals (without losartan) and filled symbols in animals exposed to losartan. Each dot represents the mean±SEM. 5-8 mice were used in each condition.*

We explored this possibility by measuring basal levels of renin, AgII and aldosterone in plasma samples obtained from BPN, BPH and C57 mice (**Figure R.13**A). As expected, due to the reported bigger sympathetic drive of BPH mice (Davern *et al.* 2009), renin levels were ∼2-fold higher in that strain (21.6

± 2 ng/ml in BPH vs. 10.9 ± 0.4 ng/ml in BPN) but surprisingly, AgII was ∼2-fold higher in BPN (2.3 ± 0.2 pg/ml in BPH vs. 4.2±0.4 pg/ml in BPN). Aldosterone levels were not significantly different (0.4 ± 0.06 ng/ml in BPH vs. 0.36 ± 0.08 ng/ml in BPN). Interestingly, C57 mice levels of renin, AgII aldosterone and BP values (**Figure R.13**B) were intermediate between those of BPN and BPH mice, disclosing a surprising inverse relationship between AgII plasma levels and BP.

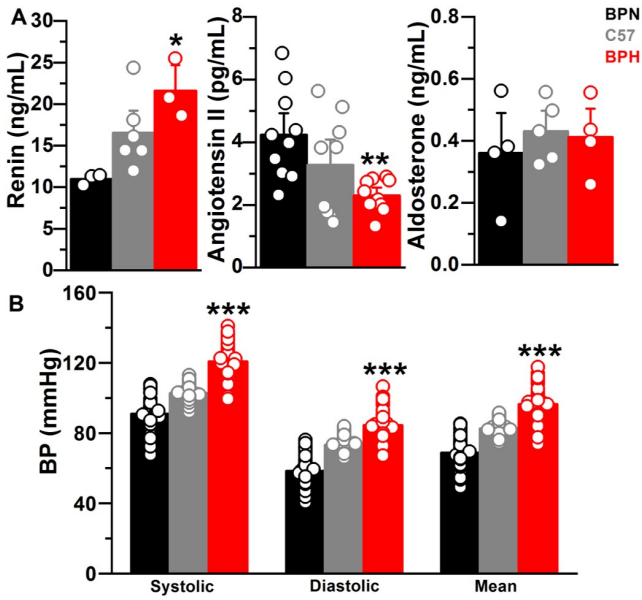

Figure R.13: *In A), Renin, AgII and aldosterone levels in plasma from BPN, C57 and BPH mice. In B), Mean, diastolic and systolic BP measured in the same three strains with the non-invasive tail cuff system. Bars are mean±SEM. An average of 3-6 plasma samples were used for ELISA, and 50 mice were used for BP measurements.*

Moreover, BPN mice, in addition to having the lower BP values with the higher levels of plasma AgII, were insensitive to the exogenous administration of AgII trough osmotic minipumps for 2 weeks. This protocol produced the expected results when carried out in C57 mice (**Figure R.14**). In this sense, it is interesting to note that a key difference between BPN and C57 is the sensitivity to P2Y6R activation, since UTP responses in C57 mesenteric arteries are almost identical to those recorded in BPH (EC_{50}=2.5 ± 0.2 μM and T_{max}=5.4 ± 0.2 mN).

Altogether, these data demonstrate a surprisingly negative correlation between AgII plasma levels and BP in the BPN/BPH model, as well as, a positive correlation between P2Y6R levels of expression in the resistance arteries and BP. The decreased participation of RAAS in BPH could represent a com-

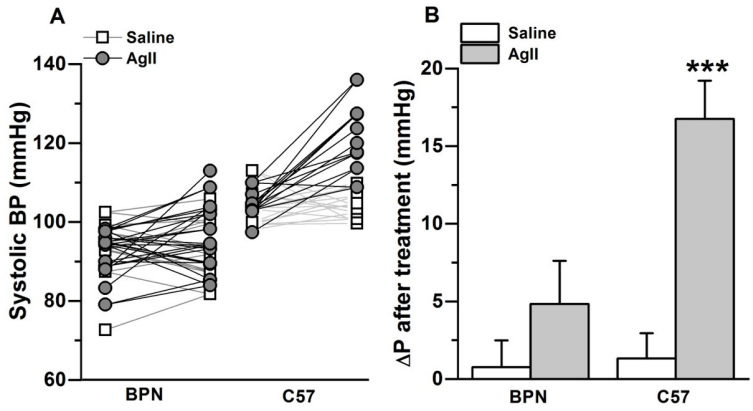

Figure R.14: *BP changes induced by AgII administration during 2 weeks with osmotic mini-pumps implanted subcutaneously in BPN and C57 mice. In A), Systolic BP measured before and after treatment is represented for each animal as a pair of symbols connected with a line. Filled symbols correspond to animals treated with AgII and open symbols correspond to animals having mini-pumps containing saline solution. In B), Average±SEM increase in pressure (ΔP) in each strain and condition. Mice were randomly assigned to the experimental or control condition. Control BP measurements were performed at least 3 days before the protocol and experimental data were obtained 14 days after surgery.*

pensatory mechanism to deal not only with the enhanced sympathetic drive characteristic of this strain, but also with the potentiating effect of the formation of P2Y6R/ATR1 heterodimers. Interestingly, BPN mice, which lacks of a functional expression of P2Y6R, have a low BP in spite of having high AgII in plasma. Since BPN mice are also resistant to the HT induced by AgII, it is tempting to postulate that the lack of P2Y6R is a relevant mechanism to explain the normotensive phenotype. That would convert this receptor in a promising target to treat HT. Nevertheless, our data certainly do not prove causality, and other effects of P2Y6R such as those described in endothelium (Bar *et al.* 2008) preclude a simple explanation to disclose the final role of these receptors *in vivo*.

4.4 Receptor-dependent modulation of vascular tone in the BPN/ BPH mesenteric arteries

4.4.1 Vasorelaxant pathways

Several changes in mRNA levels disclosed in the experiments with the Affymetrix microarrays were related with proteins belonging to vasorelaxant pathways (**Fig-**

ure R.2). Interestingly, several proteins related with the NO/cGMP/PKG pathway were significantly downregulated (gucy1b3, gucy1a3) or upregulated (prkg1). We tried to validate these results by RT-qPCR and to test functionally the pathway in the wire myograph (**Figure R.15**).

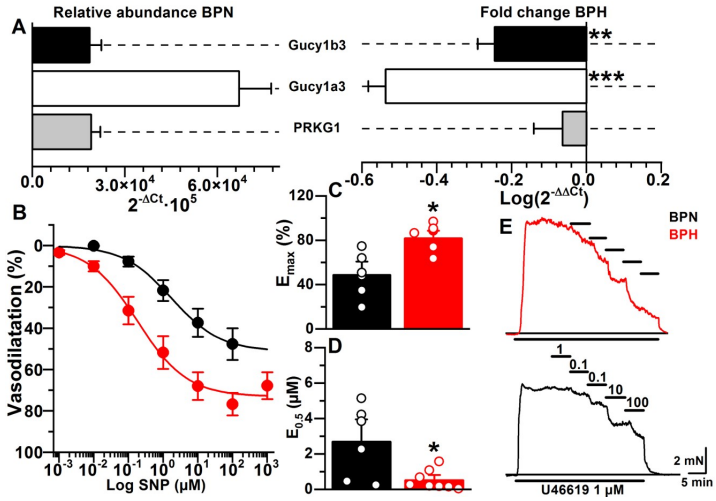

Figure R.15: *In A), mRNA expression profiles of guanylate cyclase α/β subunits and isoform I of PKG in VSMC from BPN and BPH mesenteric arteries. The left panel shows the relative abundance in BPN, estimated as $2^{-\Delta C_t}$. The right panel shows the differences in expression between BPN and BPH measured as $2^{-\Delta\Delta C_t}$. Data are the average of 4-5 animals. In B), Dose response curves of the vasorelaxant effect of SNP obtained in BPN and BPH arteries precontracted with 1 μM U46619. In C), Average of maximal effects ($E_{\max}$) and D) $EC_{0.5}$ obtained after fitting the data to a logistic function model. In E), Sample traces of the experiments carried on in BPH (red) or BPN (black) arteries. An average of 5-9 arteries were used in each case. Bars are mean±SEM.*

Whilst the downregulation of guanylate cyclase subunits (gucy1a3 and gucy1b3) was confirmed by RT-PCR, we could not reproduce the upregulation of PRKG (**Figure R.15**A). Since these results were compatible with an smaller response to NO of BPH arteries, we tested the vasodilator effect of the sodium nitroprusside donor (SNP) on arteries form BPN and BPH mice pre-contracted with the TXA_2 analogue U46619 (1 μM) (**Figure R.15**B-D). Incremental accumulative SNP dose response curves were obtained and the vasodilation relaxant effects were fitted to a sigmoidal logistic function. Unexpectedly, the vasodilator effect was larger in BPH arteries (E_{max} = 81.80 ± 4.47% in BPH vs. 48.63 ± 8.08% in BPN). Moreover, BPH arteries showed a greater sensitivity to SNP (EC_{50} = 0.52 ± 0.19 μM in BPH vs. 2.69 ± 0.83 μM in BPN).

Another surprising result disclosed in the experiments with the Affymetrix microarrays was the upregulation of β_1-AR in BPH arteries. Since there is

controversy in the literature regarding the possible role of β_1 receptors in the vasculature (Briones *et al.* 2005), we decided to explore the vasorelaxant adrenergic response. We did not replicate the microarray data with RT-PCR, but we found a significant downregulation of β_2-ARs (**Figure R.16**A). In this set of experiments, we also characterize the expression of α-AR. The more expressed isoforms (1A and 1D) are not different in BPH arteries, but the less expressed 1B is significantly upregulated.

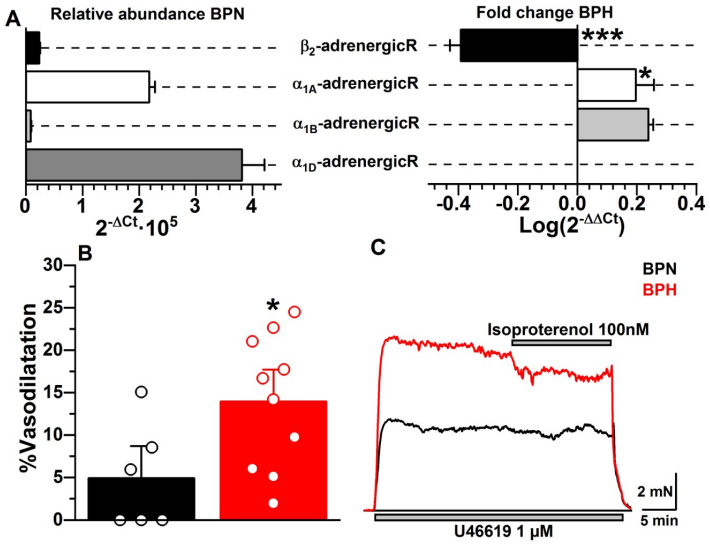

Figure R.16: *In A), mRNA levels of α and β-ARs in VSMC from BPN and BPH mesenteric arteries. The left panel shows the relative abundance in BPN of each component estimated as $2^{-\Delta C_t}$. The right panel shows the differences between BPN and BPH expressed as $2^{-\Delta\Delta C_t}$. An average of 4-5 animals was used for data collection. In B), Vasodilation elicited by isoproterenol 100 nM, expressed as % of full relaxation. n = 6-10 arteries in each group. Bars are mean±SEM. In C), Sample traces obtained in a BPN (black) and a BPH (red) arteries when the isoproterenol 100 nM was applied after precontracting the artery with 1 µM U46619.*

The functional effects mediated by the activation of β_2-ARs were tested in BPN and BPH mesenteric arteries by wire myography. Isoproterenol (a non-selective β-AR agonist) was used as stimulus. Vessels were pre-contracted with the U46619 (1 μM) and isoproterenol was applied when a constant tonic contraction was reached. **Figure R.16**C shows sample traces obtained with this protocol in BPN (black) and BPH (red) arteries. Quantification of the effect (**Figure R.16**B) revealed a significant enhanced vasodilatation in BPH mesenteric arteries (13.96 ± 2.49%) compared to BPN (4.92 ± 2.51%). Once again, expression data did not correlate with the functional response. Both vasodilator responses (NO/cGMP/PKG and β-adrenergic) were functionally potentiated in

BPH arteries, in spite of a clearly lack of correlation with the expression levels of at least some pathway components. These changes can be interpreted as compensatory mechanisms in the context of a hypertensive phenotype.

4.4.2 Vasoconstrictor pathways

The unexpected results obtained with the experiments that explored the vasorelaxant pathways prompted us to focus on the study of the receptor dependent vasoconstrictor responses. Several changes in mRNA levels suggested by the experiments with the Affymetrix microarrays were related with proteins belonging to these pathways (**Figure R.2**), and the experiments described in **Sections 4.2** and **4.3** clearly show a potentiation of some $G_\alpha q$ coupled receptors (P2Y6R and ATR1) dependent responses. We decided to characterize in more detail the contractile responses depending of $G_\alpha q$, exploring two additional receptors which activation shares that pathway: α_1-AR and TXA_2-R.

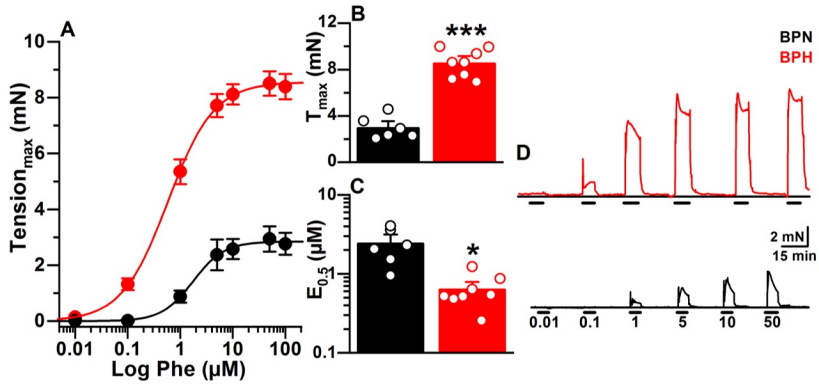

Figure R.17: *In A), Dose-response curves obtained using Phe as stimulus in BPN (black) and BPH (red) mesenteric arteries. In B), and C), Data were fitted to a Hill equation and the average of T_{max} and $EC_{0.5}$ are shown as box plots. N = 5-10 arteries in each case. In D), Sample traces of single experiments carried out in one BPN (black) and one BPH (red) arteries are shown in the right panel.*

The α_1-AR dependent contractile responses were evaluated using Phe (a selective α_1-AR agonist) in endothelium-denuded arteries through wire myography. Dose-response curves obtained in BPN and BPH mice are shown in **Figure R.17**. Curves were fitted to a Hill function and the average of the fitted parameters (T_{max} and EC_{50}) obtained in BPN and BPH arteries are depicted in the figure. A significantly larger contractile response (T_{max} = 8.53 ± 0.42 mN in BPH vs. 2.96 ± 0.39 mN in BPN) and a remarkable greater sensitivity to the agonist (EC_{50} = 0.63 ± 0.11 μM in BPH vs. 2.41 ± 0.49 μM in BPN) were observed in

BPH mesenteric arteries. Sample traces from these experiments are also shown in the figure.

The TXA_2-R dependent vasoconstrictor responses were assessed in a similar way using the TXA_2 analogue (U46619), and results are depicted in **Figure R.18**. In this case, the contractile responses were also larger in BPH (T_{max} = 6.82 ± 0.73 mN in BPH vs. 4.08 ± 0.44 mN in BPN), but the sensitivity was similar (no differences in EC_{50}). Representative traces are also shown in the figure.

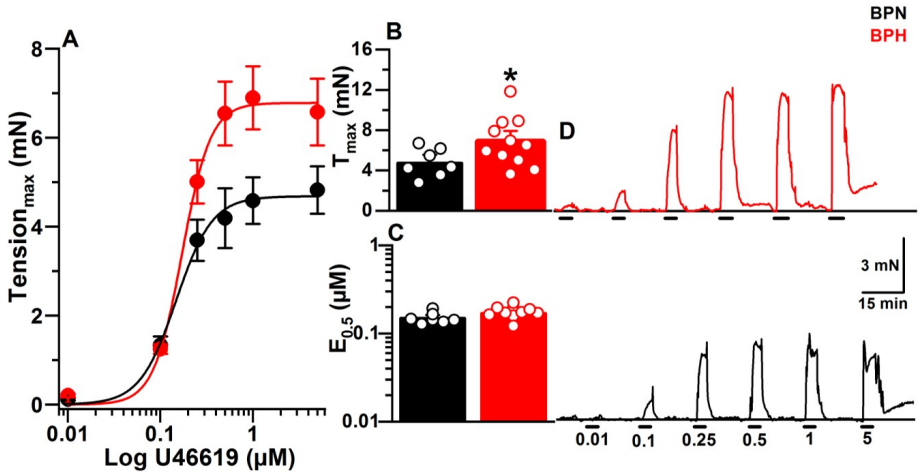

Figure R.18: *In A), Dose response curves obtained using U46619 (a TXA_2-R agonist) as stimulus in BPN (black) and BPH (red) mesenteric arteries. In B), and C), Data were fitted to a Hill equation and the average of T_{max} and $EC_{0.5}$ are shown as box plots. N = 5-10 arteries in each case. In D), Sample traces of single experiments carried out in one BPN (black) and one BPH (red) arteries are shown in the right panel.*

Altogether, presented data demonstrate larger responses in BPH arteries with all the receptors coupled to $G_{\alpha}q$ proteins we have tested. These results strongly suggest that in addition to differences in receptor expression, differences in other elements of the $G_{\alpha}q$ dependent contractile cascade must be considered in order to explain the enhanced responses observed in BPH arteries.

Figure R.19 shows a simplified scheme describing the elements that contribute to define the response from the receptor to the contractile machinery (see the introduction section for details). The scheme identify five key elements (bottom to top): 1) The Ca^{2+} entry dependent of the activation of LTCC, 2) the activation of CaCC and 3) TRPC channels, 4) the release of Ca^{2+} from the SR and 5) the relative contribution of $G_{\alpha}q$ and $G_{\alpha}12/13$ dependent pathways.

We decided to focus on those five elements in order to explore the different

responses in BPN and BPH arteries when the $G_{\alpha}q$ dependent pathway is activated. We used the stimulation of α_1-AR with Phe as the main tool. We chose the α adrenergic system because it is the principal regulatory system of vascular tone and because an increase in the sympathetic drive has been proposed as the main causal agent of high BP in the BPH model (Daghbouche-rubio *et al.* 2022).

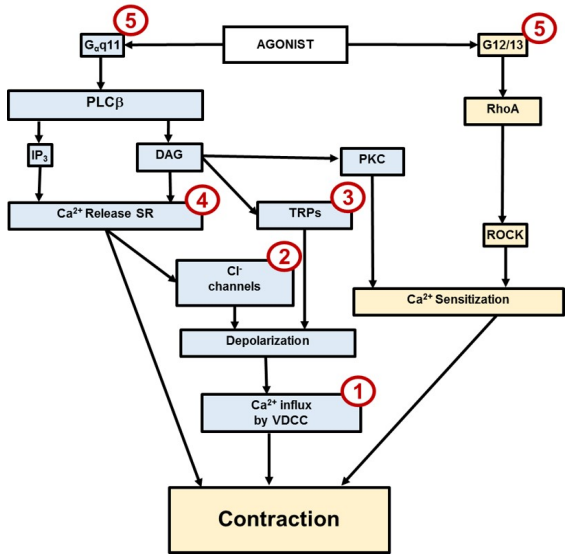

Figure R.19: *Scheme showing the $G_{\alpha}q$ (blue) and $G_{\alpha}12/13$ (yellow) dependent pathways activated by GPCRs. The key elements explored in this work are numbered from 1 to 5.*

4.4.2.1 Ca^{2+} influx by LTCC

The subunit composition of $Ca_v1.2$ channels and the differences in expression and function of these channels at the single cell level in BPN and BPH arteries have been extensively characterized in our lab (Tajada, Cidad, Colinas, *et al.* 2013). Briefly, a marked electrical remodelling is present in BPH cells and in spite of having smaller macroscopic currents, a different molecular composition of the LTCC channelosome is linked to a higher functional efficiency of the channels, promoting higher Ca^{2+} influx at resting membrane potential. However, these studies were carried out in unstimulated cells, and the functional contribution of LTCC activation to contraction elicited by agonist-receptor stimulation is unknown.

To test the role of LTCC in vasocontraction we decide to compare responses in BPN and BPH arteries stimulating LTCC just by pure depolarization (**Figure R.20**) or through the activation the $G_{\alpha}q$ dependent pathway with Phe

(**Figure R.21**) using the wire myograph.

High-K^+ solutions (120 mM K^+) were used as stimulus to induce Ca^{2+} entry mainly through activating LTCC by membrane depolarization. As shown in **Figure R.20**, the responses were clearly different in BPN and BPH. In agreement with the results obtained in unstimulated single cells (Tajada, Cidad, Colinas, *et al.* 2013), high-K^+ produced larger responses in BPH arteries, both when the initial peak (5.31 ± 0.23 mN in BPH vs. 3.00 ± 0.17 mN in BPN) or the steady-state (3.07 ± 0.18 mN in BPH vs. 1.62 ± 0.16 mN in BPN) were analyzed. These marked differences are consistent with a larger activity of LTCC in the BPH arteries.

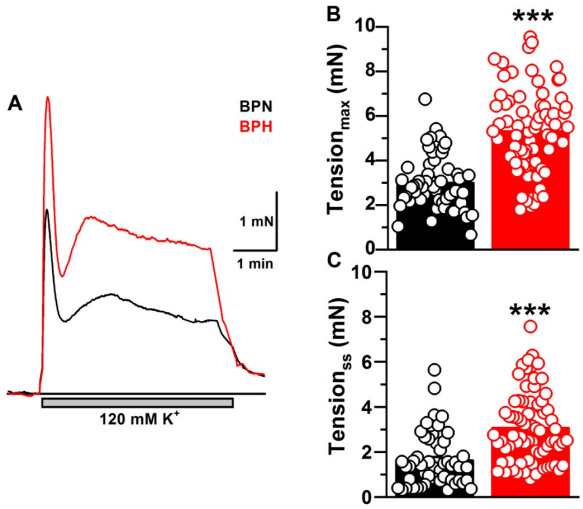

Figure R.20: *Contractile responses elicited by 3 min stimulation with 120 mM K^+ in BPN and BPH endothelium-denuded mesenteric arteries. In A), Representative traces obtained in BPN (black) and BPH (red) arteries are shown. In B), The average tensions measured at the peak (T_{max}) and in C), At the steady-state (TSS) are represented in the bar plots (mean±SEM). An average of 50-70 arteries were used for data collection.*

The contribution of LTCC to the contractile response dependent of $G_\alpha q$ was tested in BPN and BPH arteries measuring the effect of 1 μM nifedipine (that fully block LTCC) on the contraction elicited by 10 μM Phe (**Figure R.21**). In both strains, nifedipine had a significantly big effect on the response, but unexpectedly the effect was larger in BPN arteries. The difference was evident both, in the peak (68.16 ± 5.22 % in BPN vs. 42.76 ± 5.72% in BPH) and in the steady-state (86.79 ± 4.47% in BPN vs. 56.37 ± 4.93% in BPH) responses.

Therefore, VSMCs from BPH arteries have LTCC more active than BPN cells (larger responses with depolarization), but in their absence (after nifedipine blockade) the response is still larger in BPH (see sample traces of **Figure R.21**).

These results suggest that LTCC are not the main responsible of the larger contractions we see in BPH arteries after stimulating $G_{\alpha}q$ dependent receptors.

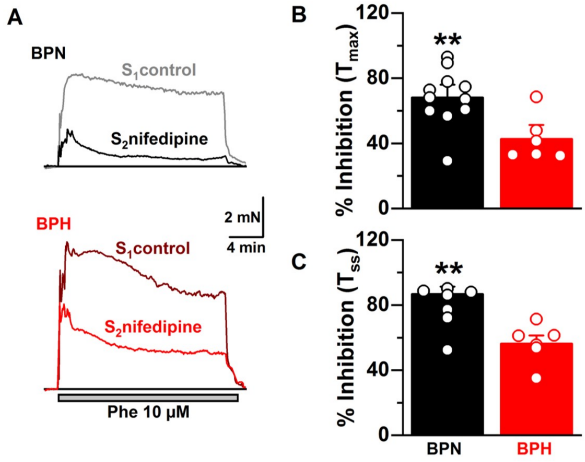

Figure R.21: *Relative contribution of LTCC to the contraction elicited by Phe in BPN and BPH mesenteric arteries recorded with wire myography. In A), Two 10 min pulses of Phe, separated by 30 min in control were applied. 15 min before, and during the second pulse, 1 µM nifedipine was added to the myograph chamber. In B), and C), The differences between the pulses in control and in the presence of the blocker were expressed as % of inhibition. Mean±SEM results obtained in BPN and BPH arteries are represented as bar plots. An average of 5-11 arteries were used for data collection.*

4.4.2.2 Ca^{2+} dependent Cl^- channels

The next element we explored, following the rational depicted in **Figure R.19**, was the role of CaCC. Since microarray data did not provide any information about the expression of Cl^- channels, we decided to test the expression of several genes related with Cl^- transport using RT-qPCR (**Figure R.22**). We found a significant expression of the channels TMEM16A, CLCN3 and CLCA1 and the $Na^+/K^+/Cl^-$ cotransporter NKCC1. Only TMEM16A and CLCA1 were upregulated in BPH arteries. Although there is some controversy in the literature regarding the molecular nature of CaCC, TMEM16A is a solid candidate to be the main responsible for carrying Cl^- currents through CaCC, and its upregulation supports the hypothesis that CaCC are relevant to explain the hypertensive phenotype.

Therefore, we tested the contribution of TMEM16A to the contractile response elicited by Phe in BPN and BPH arteries using the specific inhibitor of TMEM16A ($Inh_{TMEM16A}$). Results are depicted in **Figure R.23**. A small effect of the inhibitor was obtained when tested using the two-pulse protocol (**Fig-**

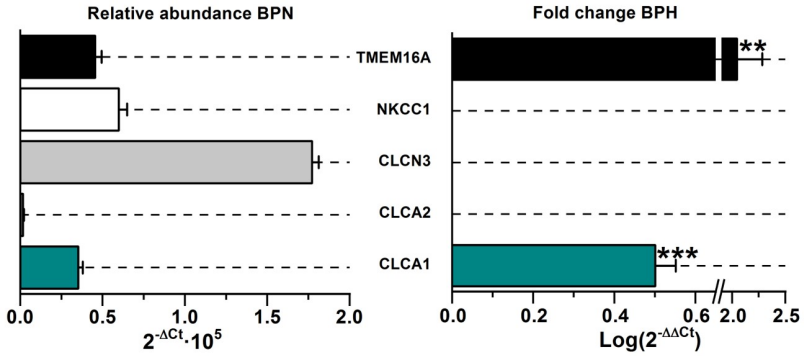

Figure R.22: *mRNA expression of several genes relevant in the transport of Cl^-. The left panel shows the relative abundance in BPN expressed as $2^{-\Delta C_t}$ and the right panel shows the differences between BPN and BPH expressed as $2^{-\Delta\Delta C_t}$. An average of 4-5 animals were used for data collection. Bars are mean±SEM.*

ure R.23A), and the inhibition was not significantly different between BPN and BPH (8.18 ± 2.96 % in BPH vs. 5.04 ± 2.77% in BPN). However, since the selectivity of this inhibitor has been put into question in the literature (Boedtkjer *et al.* 2015), we decided to test the effect in the presence of a Cl^--free solution. In this set of experiments, we used just BPH arteries. We applied the inhibitor using a single pulse protocol, when the contraction elicited by Phe had reached the steady-state (**Figure R.23**B). With this protocol the effect of the inhibitor was larger but the effect was identical in control and in Cl^--free solution (84.89 ± 0.59% in control vs. 88.01 ± 6.87% in Cl^--free solution), suggesting that the effect of the inhibitor is indeed completely unspecific.

The lack of a selective $Inh_{TMEM16A}$ hinders the study of the contribution of these channels to the contractile response. However, the approach of removing Cl^- from the bathing solution is at least a way of defining the importance of Cl^- dependent mechanisms in the contractile response, and the effect of Cl^- channels controlling depolarization is probably the principal impact of removing this ion. Therefore, we decided to use this approach and compare the responses to Phe in BPN and BPH when Cl^- was removed from the bath solution. The obtained results are depicted in **Figure R.24**. Responses in Cl^--free media were smaller both in BPN and BPH, but the effect was considerably larger in the case of BPN mice when measured at the peak (66.22 ± 4.62 % of inhibition in BPN vs. 17.24 ± 5.0 % in BPH) or at the steady-state (68.4 ± 5.1 % of inhibition in BPN vs. 14.3 ± 6.61 % in BPH).

These results strongly suggest that the contribution of Cl^- channels to the contractile response is larger in BPN arteries. However, the contribution of a channel to control the V_M depends not only of the number of channels that the

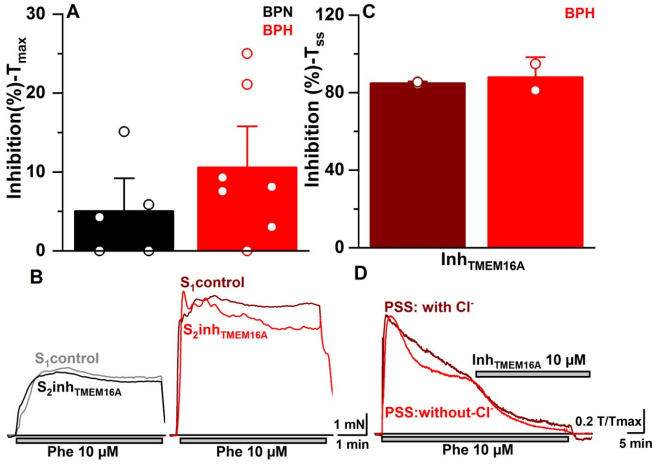

Figure R.23: *Effect of the InhTMEM16A in the contractile responses elicited by Phe in BPN and BPH mesenteric arteries. In A), Bars represent the % of inhibition (mean±SEM) in S_2, taking the response in S_1 as control. In B), Two Phe pulses of 5 min (S_1 and S_2) were applied separated by 20 min in control solution. 10 µM of the InhTMEM16A was added to the experimental chamber 5 min before and during S_2. An average of 5-7 arteries were used in each strain. In C), The effect of 10 µM InhTMEM16A, applied as indicated in the sample traces, was compared in BPH arteries bathed in control PSS with Cl^- or in PSS without Cl^-. Bars represent the % of inhibition (mean±SEM) obtained in control solution (garnet) or in solution without Cl^- (red). In D), Arteries were bathed with the free Cl^- solution 40 min before the experiment. N = 5-7 arteries.*

stimulus opens (permeability), but also of the difference between the V_M and the reversal potential for the moving ion (E_{Cl}). Using the Goldman-Hodgkin-Katz equation for the membrane potential, we can estimate the change in V_M (as ΔV_M) that would be produced by the sudden elimination of Cl^- from the extracellular medium (see **Appendix 8**):

$$\Delta V m_{Cl_i}^{Cl_o=0} = \frac{RT}{F} \ln\left(1 + \alpha_{Cl} \frac{[Cl]_0}{[K]_i}\right) \qquad \text{(Eq. 4.1)}$$

Interestingly, it follows from this equation that if we design a protocol where we suddenly eliminate the Cl^- from the extracellular solution, we should get a depolarization (ΔV_M) that only depends of $[Cl^-]_o$, $[K^+]_i$ and αCl (the permeability to Cl^-). Assuming that $[K^+]_i$ is similar in BPN and BPH, such protocol should give us information about the differences in αCl between BPN and BPH upon stimulation. Therefore, we tested the effect of removing Cl^- when the arteries were pre-contracted with Phe. The protocol and the results are shown in **Figure R.25**.

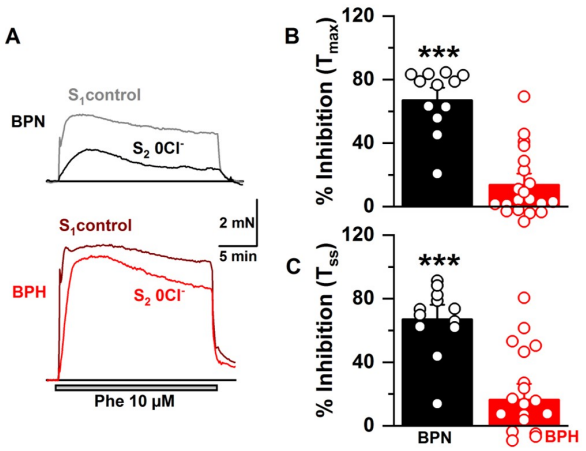

Figure R.24: *Contribution of Cl^- channels to the Phe contractile responses in BPN and BPH mesenteric arteries. In A), Two Phe pulses of 20 min (S_1 and S_2) were applied. At the end of S_1, the bathing solution was replaced by a Cl^--free solution, and after 40 min, the second pulse (S_2) was applied. In B), And C), Bars represent the response obtained in S_2 expressed as the % of S_1 (mean±SEM). An average of 5-7 arteries were used in each strain.*

The **Figure R.25**A shows representative traces of the effect of removing Cl^- from the bath ($0Cl_o$) on the contractile response of BPN (blue trace) and BPH (red trace) arteries pre-contracted with 10 μM Phe. Immediately after removing Cl^- there is an increase in contraction (ΔT_{peak}) that can be imputed to the depolarization of the V_M. With time, tension relax to an steady-state value (T_{SS}) that is reached when Cli equilibrates with the extracellular solution and $[Cl^-]_i$=$[Cl^-]_o$=0. The time course of this relaxation was estimated measuring $t_{0.5}$ (the time needed to get a contraction half of (T_{Peak}-T_{SS}).

The **Figure R.25**B shows the analysis of the described parameters in several arteries from BPN and BPH mice. No significant differences in ΔT_{peak} between BPH (1.16 ± 0.17) and BPN (0.94 ± 0.1) arteries were found, but $t_{0.5}$ was significantly smaller (which implies a faster decay) in BPH arteries (3.32 ± 0.27min in BPH vs. 4.45 ± 0.45 min in BPN). As expected, the % of inhibition of T_{SS} produced by the $0Cl^-$ solution (taking the tension before removing the Cl^- as control) was significantly smaller in BPH mesenteric arteries (27.41 ± 1.55 % in BPH vs. 58.52 ± 3.90 in BPN), in good agreement with the equivalent results obtained with the protocol depicted in **Figure R.24**.

The intrinsically non-linear nature of the contractile responses hinders a clear and unambiguous interpretation of the data. The simplest explanation is to consider that:

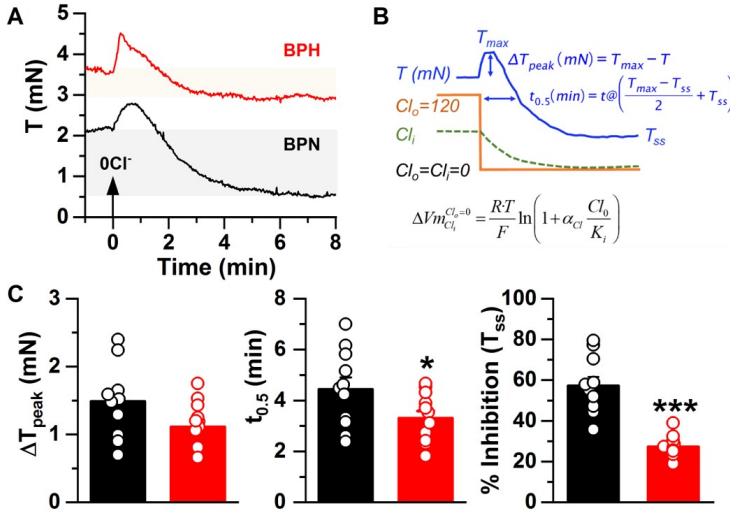

Figure R.25: *Effect of Cl^- removal from the bath solution on arteries pre-contracted with 10 μM of Phe. In A), Assessment of the likely differences in VSMC $[Cl^-]_i$ from BPN and BPH mesenteric arteries in wire myography. A single dose protocol was subjected to the vessels. A 20-min of the contractile pulse was followed by a prolonged 40-min of PSS-free Cl^- application in the stationary phase of the responses. In B), It shows the analysis of the described parameters in arteries from BPN and BPH mice. In C), The t0.5, the delta tension and the inhibitory (%) pattern was used in the analysis. An average of 10-20 arteries were used for data collection. Each bar is mean±SEM.*

$$\Delta \mathrm{T}_{peak} \sim \Delta \mathrm{V}_{\mathrm{M}} \cdot (\Delta Po_{LTCC} \cdot \beta_{Ca}) \qquad \text{(Eq. 4.2)}$$

Where $\Delta \mathrm{T}_{peak}$ and $\Delta \mathrm{V}_{\mathrm{M}}$ have the meaning described in **Figure R.25**, ΔPo_{LTCC} reflects the increase in open probability of LTCC because of $\Delta \mathrm{V}_{\mathrm{M}}$ and βCa is a factor reflecting the sensitivity of the contractile machinery to Ca^{2+}. Since $\Delta \mathrm{T}_{peak}$ is similar in BPN and BPH, the term $\Delta \mathrm{V}_{\mathrm{M}}$ $(\Delta Po_{LTCC} \cdot \beta\mathrm{Ca})$ must be similar in both strains. If we take into account that the contribution of LTCC to the steady-state response to Phe is smaller in BPH arteries (**Figure R.21**), the term $(\Delta Po_{LTCC} \cdot \beta\mathrm{Ca})$ is probably smaller in BPH arteries and then $\Delta \mathrm{V}_{\mathrm{M}}$ must be larger. Since $\Delta \mathrm{V}_{\mathrm{M}}$ is mainly determined by αCl, these results are compatible with a larger functional expression of Cl^- channels in BPH arteries (in agreement with the expression data described in **Figure R.22**). If that's the case, the faster decay of the contractile response (smaller $\mathrm{t}_{0.5}$) could reflect the larger permeability and perhaps a larger driving force for Cli (larger $[\mathrm{Cl}]_i$) leaving the cells to reach equilibrium (Fick's first law).

Nevertheless, as mentioned before, the contribution of Cl^- channels in a situation of normal intra and extracellular Cl^- is also very dependent of the difference between the V_M reached with the agonist and E_{Cl}. Results in **Figure R.24** are compatible with differences in both between BPN and BPH arteries. Although with our experimental setting it is impossible to distinguish between both alternatives, we decided to test the effect of removing Cl^- ions when other $G_\alpha q$ coupled receptor was stimulated (P2Y6R), since in that situation E_{Cl} is the same but the depolarization induced by the agonist could be in all likelihood different. Results of this set of experiments are shown in **Figure R.26**.

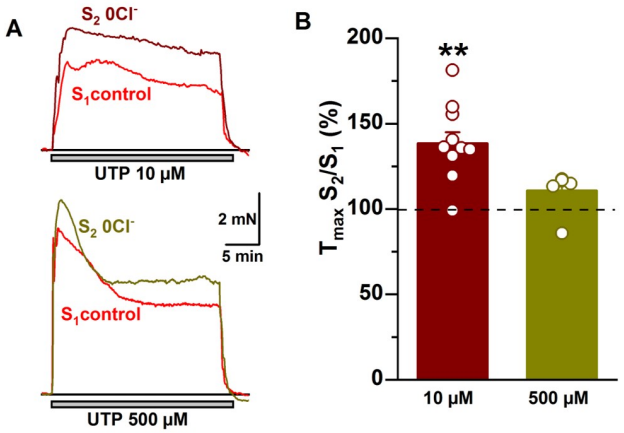

Figure R.26: *Effect of removing extracellular Cl^- on the contractile responses elicited by UTP in BPH mesenteric arteries. In A), Two 25 min pulses (S_1 and S_2) of UTP (10 μM or 500 μM) were applied, separated by 40 min. Immediately after finishing the first pulse the bathing solution was replaced by a free-Cl^- solution. Identical pair of pulses were applied in control experiments without removing Cl^- (not shown in the graph). In B), The effect of removing Cl^- was estimated as the S_2/S_1 ratio expressed as %. An average of 10-20 arteries were used for data collection.*

When UTP was used to activate the $G_\alpha q$ dependent contractile pathway, the effect of removing extracellular Cl^- was strikingly different to the effect obtained with Phe. In this case, Cl^- removal potentiated the contractile response when 10 μM UTP was used as stimulus (138.56 $\pm$ 6.5 % S_2/S_1 in $0Cl_o$ vs. 114.35 $\pm$ 6.80 $\%S_2/S_1$ in control), whilst the responses to 500 μM were essentially identical.

These experiments do not provide information about $[Cl]_i$, but clearly disclose an stimulus dependent role for CaCC. The potentiation of the response to UTP after removing Clo suggest an inhibitory effect of CaCC for this stimuli in control conditions, that can be explained if the depolarization elicited by the stimuli drives the V_M above E_{Cl}. In the case of Phe, the V_M would be close to E_{Cl} in BPH mice and bellow in BPN mice. Obviously, V_M and E_{Cl} (that is to say

$[Cl]_i$) need to be measured to fully understand the role of CaCC in the receptor dependent contractile responses.

4.4.2.3 TRPC3/6 channels

Following the rational of **Figure R.19**, we decided to explore the differences between BPN and BPH mesenteric arteries in the contribution of the unspecific cation channels activated by DAG that contribute to depolarize the V_M (see introduction). Previous data from our group showed a significant upregulation of TRPC3 in VSMC from BPH mesenteric arteries and a different TRPC3/C6 ratio composition (Álvarez-Miguel *et al.* 2017), but the effect of inhibiting these channels on agonist-induced contraction has not been tested.

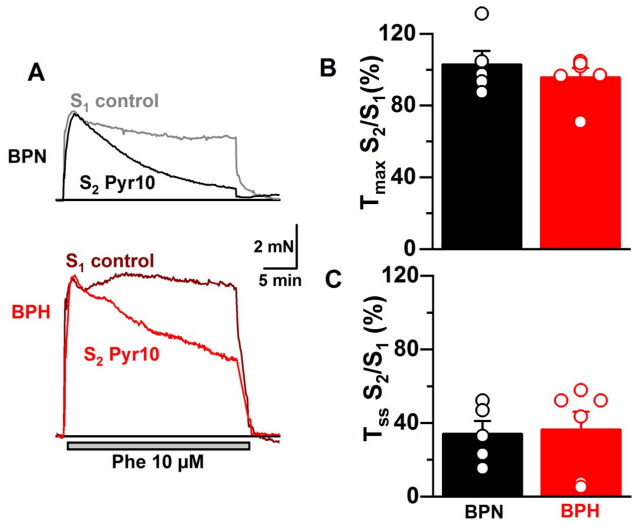

Figure R.27: *Contribution of TRPC channels to the contractile responses elicited by Phe in BPN and BPH mesenteric arteries. In A), Two 20 min pulses of Phe (S_1 and S_2) were applied separated by an interval of 30 min. 5 min before and during the second pulse, 10 µM Pyr10 was added to the bath. Traces are sample experiments carried out in BPN (up) and BPH (down) arteries. In B), And C), The S_2/S_1 (%) ratio was used to compute the effect of the inhibitor. Control experiments were carried out without adding the inhibitor to confirm that in that case the ratio S_2/S_1 is close 100% (data not shown). An average of 5-8 arteries were used for data collection. Bars are mean±SEM.*

We decided to compare the effect of the TRPC3 inhibitor Pyr10 on the contraction elicited by Phe using a two pulse protocol, where the contraction in the presence of the inhibitor (S_2) is compared with the contraction obtained in control conditions (S_1). Data obtained with this protocol are shown in **Figure R.27**. Interestingly, the inhibitor had no effect on the peak response (T_{max}), but pro-

duced a marked inhibition in the steady-state response (T_{SS}). These results suggest that although TRPC channels are no necessary to produce the initial response, they are critical to sustain the depolarization needed to keep LTCC active. However, we could not find any difference in the effect of Pyr10 between BPN and BPH arteries. The same inhibition was observed in the stationary phase (36.38 ± 9.71 % S_2/S_1 in BPH vs. 34.09 ± 6.97 % S_2/S_1 in BPN) and the same lack of effect on the peak response (95.75 ± 5.14 % S_2/S_1 in BPH vs. 102.88 ± 7.63 % S_2/S_1 in BPN).

Similar results were obtained in BPH arteries when UTP was used as stimulus (data nor shown). Altogether, these results confirm the relevant role of TRPC channel in the receptor-mediated contraction in mesenteric arteries, but in spite of the reported differences in expression, the differences in the contribution to agonists-mediated responses in the hypertensive phenotype seems to be very small.

4.4.2.4 SR Ca^{2+} release

The next step in the $G_{\alpha}q$ signalling cascade we tested, following the scheme of **Figure R.19**, was the contribution of Ca^{2+} release from intracellular stores to the contractile response. We compared the contribution of stores to the response in BPN and BPN using as stimuli Phe or UTP. The results obtained in this set of experiments are summarized in **Figure R.28**. Vessels were stimulated in the wire myograph with two pulses of the agonist, separated by an interval of 30 min. After the first pulse (S_1), thapsigargin (TG) 1 μM and ryanodine (Rya) 10 nM were added to deplete Ca^{2+} from the SR. TG is a non-reversible blocker of the Ca^{2+}-ATPase pump, and Rya at low concentrations activated the Rya receptor to accelerate SR Ca^{2+} depletion. The second pulse (S_2) was applied after depletion of SR, and the comparison of S_2 vs. S_1 was used to compute the % of inhibition produced by inhibiting Ca^{2+} release.

Immediately after adding the combination of TG/Rya to the bath, a contractile response was recorded (see **Figure R.28**A and B). This response was markedly larger in arteries from BPH mice (1.07 ± 0.15 mN in BPH vs. 0.14 ± 0.03 mN in BPN), suggesting a larger Ca^{2+} content in the SR. However, in spite of this striking difference, the depletion of Ca^{2+} stores had the same inhibitory effect in BPN and BPH, both when Phe (60.49 ± 5.32 % in BPH vs. 71.39 ± 1.24 in BPN, **Figure R.28**C) or UTP (70.65 ± 3.11 % in BPH vs. 67.21 ± 4.25 % in BPN, **Figure R.28**D) were used as stimulus.

These results strongly suggest the existence of larger Ca^{2+} stores in the VSMCs from the BPH arteries, but the contribution of Ca^{2+} release from the stores to the agonist-induced contraction seems to be equivalent in BPN and

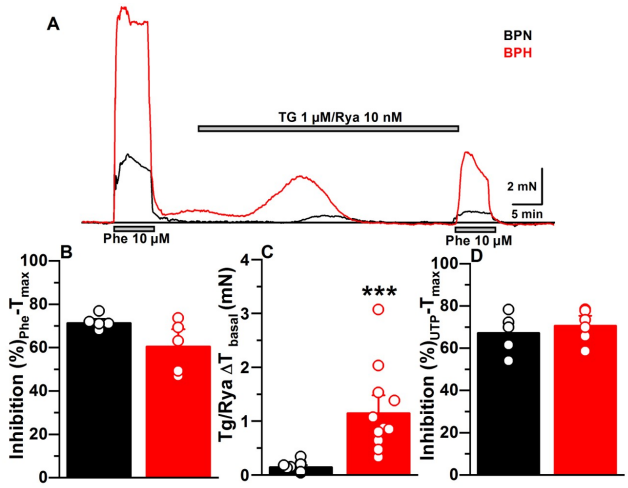

Figure R.28: *In A), Sample traces illustrating the protocol used to test the effect of inhibiting Ca^{2+} release from intracellular stores on receptor dependent contraction. BPN (black) and BPH (red). In B), Contraction elicited by the depletion of Ca^{2+} stores induced after applying TG 1 µM and Rya 10 nM as indicated. In C), Effect of depleting Ca^{2+} stores on the response elicited by Phe, expressed as % of inhibition. The pulse before applying TG/Rya was taken as control. In D), As in B, but using UTP as stimulus. An average of 5-6 arteries of each strain were used for data collection. Bars are mean±SEM.*

BPH arteries (the same % of inhibition is equivalent to the same % of contribution). There is not a simple explanation for these unexpected results. Further experiments are needed to directly asses the Ca^{2+} levels in the SR or to evaluate the efficacy of the releases Ca^{2+} to activate the contractile machinery.

4.4.2.5 $G_\alpha q11$ and $G_\alpha 12$-13 downstream effectors: PLCβ, PKC and ROCK

GPCR coupled to $G_\alpha q$ proteins are almost always also coupled to G12-13, and the activation of this pathway in VSMCs is especially relevant, since the consequent activation of ROCK mediate the Ca^{2+} sensitization of the contractile machinery (see introduction). Therefore, we decided to explore the relative contribution of these pathways in BPN and BPH arteries testing the effects of blocking PLCβ (the first enzyme in the $G_\alpha q$ cascade), ROCK (the effector of the activation of $G_\alpha 12$-13) and PKC (as an important enzyme participating in the crosstalk between both pathways). In order to inhibit each enzyme we used commercially available blockers at a dose that blocks completely the activity of the enzymes without losing specificity. The three blockers we have used are:

- The PLCβ inhibitor U73122, at 3 μM.
- The ROCK inhibitor H1152, at 0.3 μM.
- The PKC inhibitor Gö6983 at 0.1 μM.

First, we tested the effect of each blocker using a two pulse protocol and Phe 10 μM as stimulus. The obtained results are shown in **Figure R.29**. The three blockers produced a significant inhibition of the contractile response, and both in BPN and BPH the activation of PLCβ is the one that contribute the most to the contractile response, followed by ROCK and with a minor contribution of PKC.

However, the relative contribution of each enzyme was significantly different between BPN and BPH arteries. If we compare the inhibitory effect on T_{max}, it was larger in BPN either when PLCβ (77.11 $\pm$ 6.13% in BPN vs. 40.1 $\pm$ 8.29% in BPH), ROCK (56.5 $\pm$ 7.1% in BPN vs. 25.9 $\pm$ 3.42 % in BPH) or PKC (18.12 $\pm$ 2.38% in BPN vs. 9.47 $\pm$ 1.29 % in BPH) were blocked. Similar results were obtained when the inhibitory effects on T_{SS} were compared: PLCβ (95.52 $\pm$ 2.13% in BPN vs. 71.29 $\pm$ 6.07% in BPH), ROCK (82.83 $\pm$ 2.64% in

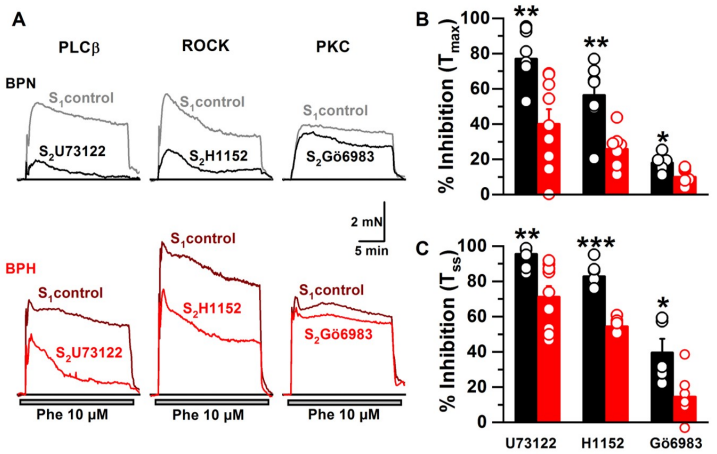

Figure R.29: *Relative contribution of PLCβ, ROCK and PKC to the contractile responses elicited by Phe. In A), sample traces obtained in BPN arteries. Two 20 min pulses of Phe (S_1 and S_2) were applied, separated by 30 min. 15 min before and during S_2 the different inhibitors were applied: PLCβ (U73122, 3 μM), ROCK (H1152, 0.3 μM) and PKC (Gö 6983, 0.1 μM). S_1 and S_2 are depicted superimposed. As in (A), But traces correspond to BPH arteries. In B), The % of inhibition produced in any case was measured taking the peak tension (T_{max}) obtained in S_1 as control. In C), As in (B), But measuring the effect on the steady-state tension (TSS). Black bars (BPN) and red bars (BPH) are mean$\pm$SEM. An average of 5-11 arteries were used in each case.*

BPN vs. 54.41 ± 1.32 % in BPH) and PKC (39.63 ± 7.77% in BPN vs. 14.64 ± 4.87 % in BPH). These results not only demonstrated larger effects of the three blockers in BPN arteries, but also disclosed a high level of crosstalk between the three pathways since the effects are far of being simply additive. Therefore, we decided to explore the effect of applying simultaneously two or three blockers. The results of these experiments are shown in **Figure R.30**.

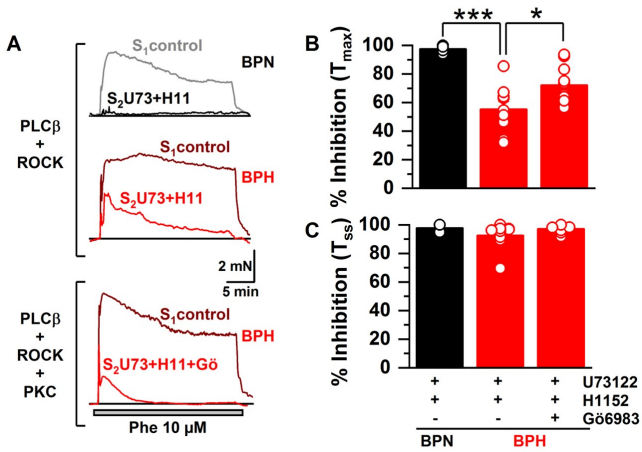

Figure R.30: *Effect of the additive blockade of PLCβ, ROCK and PKC. In A), The black bar shows the % of inhibition of* T_{max} *and TSS obtained in BPN when both, PLCβ and ROCK were inhibited with 3 μM U73122 and 0.3 μM H1152. The red bars show the effects obtained in BPH, either when PLCβ and ROCK were inhibited or when also PKC was inhibited (3 μM U73122±0.3 μM H1152±0.1 μM Gö 6983). The protocol used was identical to that described in Figure R29. Bars are mean±SEM. An average of 8-11 arteries were used for data collection. In B), and C), Sample traces of the double blockage in BPN and BPH and the triple blockage in BPH.*

In BPN arteries, the combination of the PLCβ and ROCK blockers fully abolish the contractile response to Phe, both when T_{max} (97.47 ± 1.29 %) or T_{SS} (97.67 ± 1.36 %) were used to estimate the effect (**Figure R.30**A and upper trace of part B). However, in BPH arteries that combination almost fully abolished the steady-state response (92.62 ± 3.06%), but was unable of fully blocking the peak response (55.35 ± 5.63 %). We tested if that residual response, after blocking PLCβ and ROCK, could be mediated by PKC combining the three blockers (**Figure R.30**A and lower trace in part B). The three blockers applied together fully block the steady-state response (96.21 ± 0.89% of inhibition), but only slightly increased the effect on the peak tension (72.25 ± 4.33 % of inhibition).

These results reveal interesting differences between BPN and BPH arteries. Whilst contraction in BPN arteries can be fully inhibited just blocking the

canonical pathways depending of PLCβ and ROCK, in BPH arteries there is another pathway, independent of PLCβ, ROCK and PKC that is at the moment unknown. Further experiments are need to explore this pathway. We also started the characterization of the contribution of $G_\alpha q$ and $G_\alpha 12$-13 pathways when other agonist were used. **Figure R.31** shows the effect of blocking PLCβ, ROCK or PKC in BPN and BPH arteries when UTP 500 μM was used as stimulus, and **Figure R.32** when Angiotensin II 100 nM was the agonist.

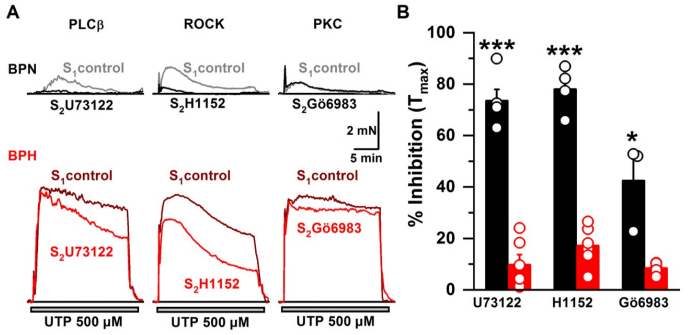

Figure R.31: *Relative contribution of PLCβ, ROCK and PKC in UTP-mediated responses from BPN and BPH mesenteric arteries. In A), The two pulses protocol was the same as described in previous figures. Black bars are obtained with BPN and red with BPH arteries. Sample traces at the bottom were obtained in BPN (upper row) or BPH (lower row) arteries. In B), Only the inhibition of the peak response is shown. Bars are mean±SEM. An average of 5-15 arteries were used for data collection.*

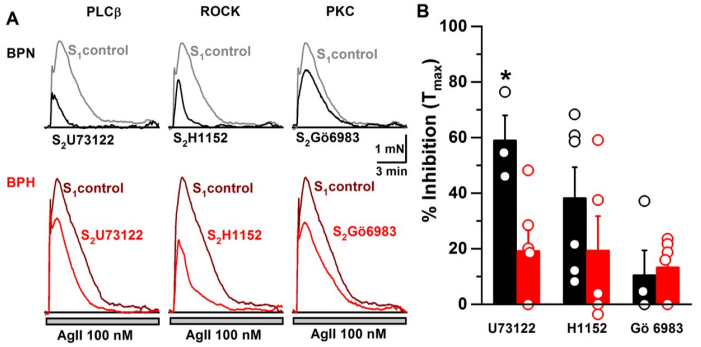

Figure R.32: *Relative contribution of PLCβ, ROCK and PKC in Angiotensin II-mediated responses from BPN and BPH mesenteric arteries. The two pulses protocol was the same as described in previous figures. Black bars are obtained with BPN and red with BPH arteries. Bars are mean±SEM. An average of 5-8 arteries were used for data collection. Only the inhibition of the peak response is shown. Sample traces at the botton were obtained in BPN (upper row) or BPH (lower row) arteries.*

When UTP was used as stimulus the inhibition of any of the three enzymes produced larger effects on T_{max} in BPN arteries: PLCβ (73.53 ± 4.44% in BPN vs. 9.78 ± 3.88% in BPH), ROCK (78.07 ± 4.51% in BPN vs. 17.15 ± 2.64% in BPH) and PKC (42.48 ± 9.91% in BPN vs. 8.37 ± 1.28% in BPH). However, when Angiotensin II was the agonist, only the blockade of PLCβ produced a significantly larger inhibition in BPN arteries (58.98 ± 9.03% in BPN vs. 19.21 ± 7.45% in BPH); the blockade of ROCK and PKC was smaller, and not significantly different in BPN and BPH arteries (**Figure R.32**).

5 Discussion

5.1 VSMCs mRNA expression in the BPH model of essential hypertension

The initial approach to study the molecular determinants of the hypertensive phenotype in VSMCs of mesenteric arteries from the BPN/BPH model has been the use of the Affymetrix GeneChip® Mouse Genome 430A 2.0 Array. This kind of arrays are less sensitive that the Low Density Taqman arrays we have used extensively in our laboratory to study the expression of ion channels (Álvarez-Miguel *et al.* 2017; Cidad *et al.* 2010; Moreno-Domínguez *et al.* 2009; Tajada, Cidad, Moreno-Domínguez, *et al.* 2012, Tajada, Cidad, Colinas, *et al.* 2013), but have the advantage of exploring the expression of 22690 genes. Among them, we only found 8516 significantly expressed either in BPN or BPH arteries. In BPH mice, 313 genes were more that 2-fold up regulated and 318 were more than 2-fold down regulated in comparison to BPN mice (adjusted p values <0.05). Gene ontology enrichment analysis based on biological process revealed more than 600 significant GO terms when the completely annotated mouse genome was used as background. In www.vsmcgroup.uva.es/UIC/Mesenteric.Arrays.rar two excel files are available: 1) One with the list of the 8516 genes expressed (including the average expression, the logFC and the adjusted P value obtained in the analysis of differential expression) and 2) another with a discretional selection of the 40 GO terms more relevant to the physiology of vascular smooth muscle cells.

The long list of GO terms obtained would imply that all those pathways are related with the hypertensive phenotype. However, when only the 8516 expressed genes were used as background, there were not any GO enrichment, suggesting that HT is not particularly associated with any pathway. The GO terms enriched when the whole mouse genome is used as background (as it is usually done) just reflect the pathways enriched in the smooth muscle tissue (see (Timmons *et al.* 2015) for an interesting discussion on the subject).

5.2 The remodeling of the purinergic system in the BPH model of essential hypertension

5.2.1 P2Y6R upregulation associates with the hypertensive phenotype

The alterations in the purinergic system were determined by expression and functional assays in HT. A decrease in P2Y1R and a significant increase in P2Y2R and P2Y6R receptors were found (**Figure R.1**). Functional studies showed significantly increased responses to UTP (larger and more sensitive) in BPH

arteries (**Figure R.3**). Pharmacological characterization revealed that P2Y6R was the likely candidate for the enhanced UTP-dependent contractions in BPH mesenteric arteries (**Figure R.5**). Taken together, these results suggested that the increased P2Y6R functional expression might be key in the pathogenesis of HT. Although the increased expression of P2Y6R has been demonstrated in several pathological contexts (**Figure D.1**), few studies have been conducted in HT. In endothelial cells, P2Y6R upregulation was associated with vascular inflammation (Riegel *et al.* 2011). In cardiomyocytes, P2Y6R upregulation was associated with pressure overload and cardiac fibrosis (Nishida *et al.* 2008). In VSMCs, P2Y6R upregulation was associated with AgII-induced HT and ageing of mouse aorta. In the latter case, the authors emphasized that the triggers of P2Y6R upregulation in AgII-induced HT conduit vessels are not fully understood. A combination of the above-mentioned factors such as inflammation, mechanical stress and aging increased the likelihood of developing HT through P2Y6R upregulation (Nishimura, Sunggip, Tozaki-saitoh, *et al.* 2016). This explanation is also consistent with our results.

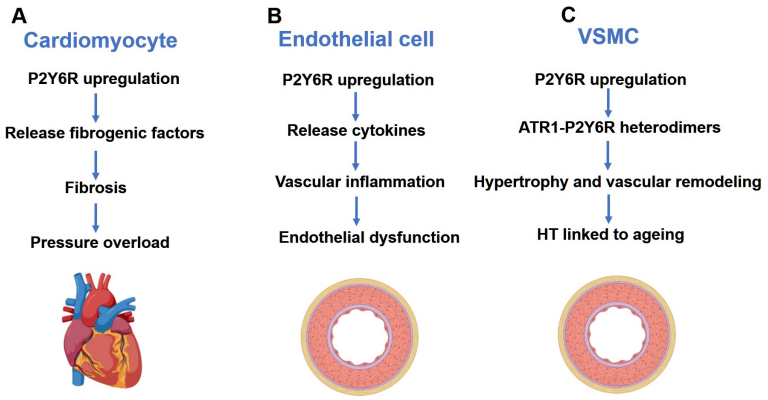

Figure D.1: *Pathophysiological role of P2Y6R upregulation in several contexts. In A), Pressure overload induces upregulation of P2Y6Rs and is involved in cardiac fibrosis. In B), Inflammation promotes P2Y6R expression in vascular endothelial cells and mediates cytokine responses. In C), Aging enhances P2Y6R expression in VSMCs via AT1R-P2Y6R heterodimers, which could participate to HT and vascular remodeling.*

5.2.2 P2Y6R-ATR1 functional coupling in the BPH model of essential hypertension

P2Y6R and ATR1 were located closer to each other in VSMC from BPH mesenteric arteries, as confirmed by both PLA and GSD high-resolution techniques (**Figure R.6** and **Figure R.7**). These patterns suggested a higher probability of heterodimer formation in BPH. Furthermore, the functional studies confirmed

the assembly of P2Y6R-ATR1 complexes in BPH VSMCs. Indeed, P2Y6R-ATR1 heterodimers seems to be involved in the stronger AgII contractions obtained in BPH arteries promoting a lower ATR1 desensitization (**Figure R.10** and **Figure R.11**).

GPCR oligomerization has been described in several pathological contexts. However, not many papers have been focused on HT. A functional interaction between ATR1 and B2R was found in human placental biopsies from pregnancies with preeclampsia (Rukavina Mikusic *et al.* 2020). ATR1-B2R heterodimers were involved in the increased contraction and the altered receptor desensitization in VSMC from both human and animal models (Quitterer *et al.* 2019; Wilson *et al.* 2013). These patterns were consistent with our results. A functional coupling between ATR1 and P2Y6R was also described in the resistance vessels of a model of HT induced with AgII and ageing. ATR1-P2Y6R heterodimers contributed to the sustained AgII-mediated signaling and the attenuated ATR1 desensitization (Nishimura, Sunggip, Tozaki-saitoh, *et al.* 2016). These authors hypothesized that the presence of the heterodimers were implicated in the transition from the physiological to the pathological scenario. In particular, the structural changes caused by hypertrophic remodeling in response to AgII were involved in the development of HT (Nishimura, Sunggip, Tozaki-saitoh, *et al.* 2016).

In summary, our data demonstrated the importance of P2Y6R-ATR1 heterodimers in the pathophysiology of HT in a genetic model. These complexes contribute to the increase of AgII contractions by reducing ATR1 desensitization in the BPH mesenteric arteries. This could be a consequence of attenuated ATR1 phosphorylation, a reduction in ATR1 endocytosis and/or increased ATR1 recycling, as previously described (Bian *et al.* 2018).

5.2.3 Decreased RAAS system as a compensatory mechanism in BPH

The study of the RAAS system is complex and contradictory results can be found in the literature (K. L. Jackson, Head, *et al.* 2019). An earliest work reported equal plasma renin levels between BPN and BPH (Iwao 1984). However, in a more recent work, a higher plasma renin level was found in the SHR genetic model (J. W. Yang *et al.* 2017). The higher renin secretion could be explained by the increased sympathetic activity trough renal β1-ARs described in both patients and HT animal models (Noh *et al.* 2020). This greater amount of plasma renin was consistent with our results. However, the increased renin levels did not promote increased AgII production. In fact, a lower plasma AgII concentration was observed in BPH (**Figure R.13**).

Of note, other studies have described similar results. For example, Uddin and

Harris-Nelson also found a higher concentration of renin and a lower concentration of AgI in the submandibular gland of the BPH model (Uddin, Harris-Nelson 2004). The authors proposed a faster metabolization of AgI in BPH as a possible explanation for this controversy. Indeed, altered AgI metabolism by endopeptidase/aminopeptidase has already been described in the corresponding genetic SHR model (Sim, Qiu 1994). This mechanism could also be involved in BPH.

Another possible explanation would be an increased rate of AgII degradation in HT. AgII is hydrolyzed by ACE2 to angiotensin 1-7, which acts as a vasodilator. Several works have measured ACE2 in both tissue and plasma of HT animal models and patients. ACE2 inhibition was implicated in HT development, while ACE2 potentiation was associated with HT resistance (Patel *et al.* 2014). Based on these patterns, increased ACE2 activity in BPH could represent a compensatory mechanism to prevent further increases in BP by lowering AgII levels. We have not explored further this hypothesis, but ACE2 is expressed both in endothelial and VSMCs of many vascular beds (Kuriakose *et al.* 2021), and in our arrays ACE2 was downregulated in BPH $\sim$ 7 fold (logFC = -2.75).

Altogether, our data suggest that RAAS system overstimulation is not implicated in the development of high BP in the BPH model. The reduced hypotensive effect of losartan in BPH is consistent with the reduced circulating AgII levels in this model (**Figure R.12** and **Figure R.13**).

Similar results have been reported by other groups, studying the RAAS system in the BPH model (Palma-Rigo *et al.* 2011). This work suggested that while the RAAS is an important contributor to BP, it has little or no involvement in the development of high BP in BPH mice. In contrast to our results, they found no differences in the hypotensive effect of losartan between BPN and BPH. This slight discrepancy could be due to the shorter treatment period used in this study (two weeks of losartan treatment in drinking water). We have found that the plateau of effect takes a longer time (up to 4 weeks) to develop and that it remains unchanged with treatments over longer periods of up to six weeks. In addition, another potential difference could be the interpretation of the data. These authors reported no changes in BP levels after two weeks losartan treatment, comparing the absolute values. MAP was reduced in BPN 23 mmHg and in BPH mice 25 mmHg (Palma-Rigo *et al.* 2011). However, considering that MAP are significantly higher in BPH data, these changes in absolute terms most likely reflect a smaller decrease of BP in BPH mice when expressed as % of change compared to time 0, as we did in our analysis (**Figure R.12**). In fact, they acknowledge this effect in a more recent work in which they explored the contribution of the sympathetic and RAAS system in these mice during the active (night) and inactive (light) period, as they conclude that there is a decreased % contribution of the RAAS to BP in BPH during light (K. L. Jackson, Marques, *et al.* 2013) as we found here. Altogether, these data suggested that HT was

independent of the RAAS system in the BPH mice. Of note, BPH represents a model of HT that has increased sympathetic drive and most likely enhanced sympathetically induced renin synthesis with decreased AgII levels. In this regard, BPH mice may prove to be an excellent animal model to investigate the mechanism mediating the hypotensive effect of renal sympathetic nerve ablation observed in treatment-resistant patients with HT (Esler *et al.* 2010). In any case, the reduced RAAS contribution could be interpreted as a compensatory mechanism aimed at preventing further increases in BP.

5.2.4 P2Y6R as a molecular switch in essential hypertension

The increased P2Y6R functional expression was related to the greater UTP contractions in BPH mesenteric arteries. We suggested that this change was also involved in the modulation of AgII desensitization through P2Y6R-ATR1 heterodimers, potentiating the AgII responses in BPH mesenteric arteries. Our data emphasized the pathophysiological role of this purinergic receptor in HT. We proposed that P2Y6R levels could represent a molecular switch in pathological conditions. Thus, the increased P2Y6R functional expression is a crucial factor in the development of certain forms of HT. Our data suggest that increased P2Y6R expression boost BP levels through P2Y6R-ATR1 heterodimers. Moreover, in the absence of P2Y6R functional expression, the mice are resistant to develop HT with AgII. This hypothesis was supported by the data obtained in the three mice strains (BPN, BPH and C57), where a correlation was shown between P2Y6R abundance and the susceptibility to develop AgII-dependent HT.

The sensitivity to UTP and the contractile responses elicited by this agonist were decreased in BPN mesenteric arteries. Conversely, responses to UTP were similar in BPH and C57 mesenteric arteries (**Figure D.2**). Therefore, the magnitude of the UTP responses correlate with the functional expression of P2Y6R in the resistance vessels. These findings were in good agreement with the previous data in the literature. P2Y6R was reported to be the dominant purinergic component involved in MT responses mediated by extracellular nucleotides, as UTP or UDP. These MT responses were abrogated in mesenteric arteries in KO P2Y6R mice (Kauffenstein *et al.* 2016).

After 2-week infusion of AgII in the normotensive BPN and C57strains, only C57 showed a significant increase in BP (**Figure R.14**). We hypothesize that the low expression levels of P2Y6R observed in BPN mice could contribute to this resistance to develop AgII-dependent HT. This role of P2Y6R is also indirectly supported by data from the literature. In this regard, KO P2Y6R mice showed decreased BP levels after AgII infusion-dependent HT, which was consistent with our results (Nishimura, Sunggip, Tozaki-saitoh, *et al.* 2016). We propose that P2Y6R upregulation might predispose to form P2Y6R-ATR1 het-

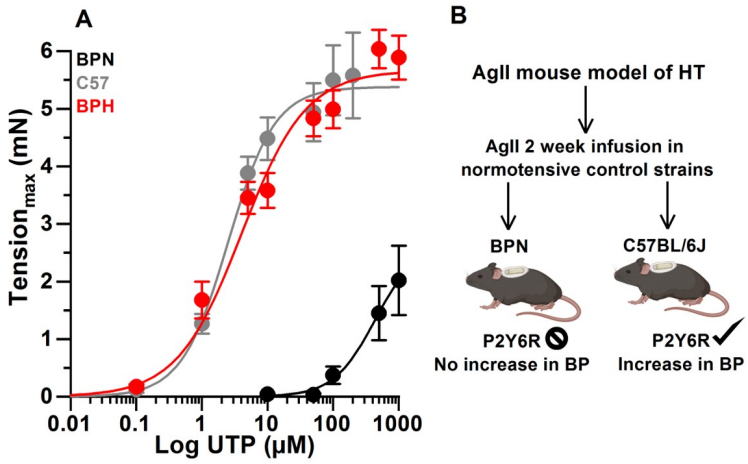

Figure D.2: *In A), Dose-response curves of the contractile effect of UTP in BPN, BPH and C57. UTP responses in C57 and BPH mice were identical, while UTP sensitivity of BPN mice is significantly decreased. In B), Illustration of the hypothesis linking the ability to induce AgII-dependent HT in normotensive mice to the expression levels of P2Y6R in each strain.*

erodimers, which in turn modulate the abnormal activation of GPCR signaling pathways in BPH. In this sense, P2Y6R will be acting as a molecular switch of the disease (**Figure D.3**). Elevated AgII levels could therefore only lead to the development of HT in the presence of high expression levels of P2Y6R, as this would determine the formation of P2Y6R-ATR1 heterodimers. In the event that this hypothesis were true, this receptor would become a promising target for the treatment of HT, as blockers of P2Y6R could prevent AgII-induced HT. Nevertheless, our data certainly do not prove causality, and other effects of P2Y6R such as those described in endothelium should be considered to disclose the final role of these receptors *in vivo* (Bar *et al.* 2008). In addition, additional experimental approaches directed to demonstrate the effects on BP of the blockade of P2Y6R or its genetic manipulation will be required to give support to the hypothesis.

5.3 The remodeling of the adrenergic system in the BPH model of essential hypertension

A mosaic of hormonal and cellular changes has been described in HT, many of which play a role in the development and maintenance of the disease (Z. Liu, Khalil 2018). Increased peripheral resistance is the key hemodynamic change

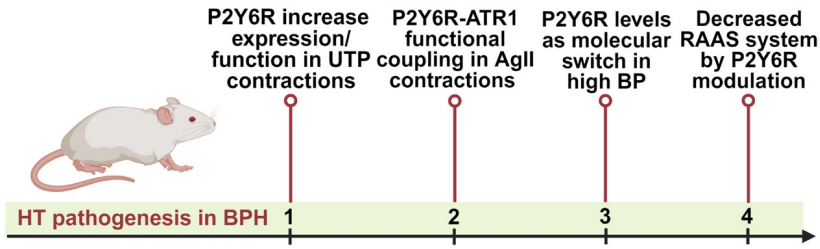

Figure D.3: *Representation of the main alterations that take place in the purinergic and RAAS system in HT.*

observed in high BP. The balance between vasoconstrictor and vasodilator mechanisms determines the net result on the peripheral resistances. The enhanced vasoconstriction and thus, the increased peripheral resistance have been widely characterized in several studies. In fact, larger sympathetic activity was attributed as a causal agent of the increased vasoconstriction in the BPH model (Palma-Rigo *et al.* 2011). Nevertheless, the underlying mechanisms are not fully understood. In addition, the impairment of the vasodilator responses might also contribute to produce a functional shift, increasing the peripheral resistances (Feldman, Gros 1998). Of note, controversial results could be found in the literature. Overall, the present study investigated the potential functional changes in both vasoconstrictor and vasodilator mechanisms, including in some cases the correlation between gene expression and function.

5.3.1 β-adrenergic relaxation as a compensatory mechanism

A significant downregulation of β2-AR mRNA was found in VSMC from BPH mesenteric arteries (**Figure R.16**). An impaired vasodilator response was expected in BPH arteries, but surprisingly, isoproterenol-mediated vasodilatation was potentiated (**Figure R.16**). These results probably reflect a compensatory mechanism aimed at preventing a further increase in BP and attenuating the increased activity of the sympathetic nervous system in BPH. To our knowledge, this is the first report of showing increased vasodilator responses in HT. The general dogma in the literature associated an impaired vasodilatation with high BP development, and that has been shown in several HT animal models (Feldman, Gros 1998). Attenuated β-AR relaxations were observed in mesenteric arteries from the DOCA-salt HT rat model (Matsumoto *et al.* 2012). Conversely, no differences in β-adrenergic relaxations have been noticed in mesenteric arteries from the equivalent SHR model (Valovič *et al.* 2023). Altogether, no changes or

reduced β-adrenergic relaxation were described in HT rat animal models, which was not in agreement with our findings. In most of these studies, the reported impaired vasodilator responses occur without changes in the expression levels of β-AR. In these cases, a reduced function of $G_\alpha s$, a defective coupling of β-AR to AC, or a reduced activity of AC have been considered the main reason for the impairment (Fujii *et al.* 1999; Masuzawa *et al.* 1989). We did not measured the differences in AC activity in the VSMCs of BPN and BPH mice, but in this context it is worth to note that several AC subunits are differentially expressed in BPH mice (**Figure R.2**). In other studies the impairment of the vasodilator response may also result from an attenuation of β-AR function due to agonist-induced receptor desensitization. For instance, an increased GRK2 receptor phosphorylation can lead to an increased receptor desensitization. An impaired β-AR vasorelaxation was then shown in the forearm resistance vasculature from HT patients (Izzo *et al.* 2008).The phosphorylated β-AR may in turn trigger new signals and activate different intracellular pathways, a mechanism that has also been involved in the impaired vasorelaxation observed in HT aged arteries (Werstiuk, Lee 2000; Feldman, Gros 1998). The impairment of β-AR mediated responses does not appear to be secondary to the increase in sympathetic activity in HT. β-AR function increased to normal levels when HT patients are fed a low-sodium diet and despite a concomitant increase in sympathetic activity, suggesting that this defect in β-AR function is unrelated to a "classic" process of agonist-mediated desensitization (Ferguson, Feldman 2014). However, the details of these mechanisms are still unresolved.

Despite baseline impairment in β-AR response in HT, it is notable that β-adrenergic antagonism is still an effective therapeutic approach. This probably reflects several considerations. First, the major effects of β-AR blockers in BP regulation are through their actions in reducing cardiac output. Second, notwithstanding the impairment in receptor responses, the net β-AR effect in HT (the product of both receptor expression/function and hormone levels) is normal or increased in many groups of patients with HT, due to higher sympathetic activity (Ferguson, Feldman 2014).

5.3.2 α-adrenergic contractile responses in the BPH model of essential hypertension

RT-qPCR assays indicated a significant upregulation of α_1B-AR in VSMC from BPH mesenteric arteries (**Figure R.16**), and consequently, Phe-mediated contractions were larger in BPH (**Figure R.17**). The augmented Phe-mediated contractions have been also described in intact BPH mesenteric arteries, in good agreement with our results (Jelinic *et al.* 2023). Of note, since the basal sympathetic activity is bigger in BPH mice (K. L. Jackson, Head, *et al.* 2019), the

effect of the sympathetic drive could be even larger since BPH vessels are more responsive to α_1-AR stimulation.

The mechanisms involved in the potentiation of the α1-adrenergic pathway were investigated focusing on the steps shown in **Figure R.19**. In terms of Ca^{2+} entry, we found an enhanced contractility in response to high-K^+ in BPH mesenteric arteries, likely attributed to the larger relative contribution of LTCC in HT (**Figure R.21**). A distinctive hallmark of high BP is LTCC upregulation. Higher functional efficiency of $Ca_v1.2$ channels was previously described by our group in BPH VSMCs (Tajada, Cidad, Colinas, *et al.* 2013). However, in spite of these observations, the relative contribution of LTCC in Phe-mediated contractions is smaller in BPH arteries (**Figure R.21**). If there is an increased activity of LTCCs in BPH, and if BPH responses to depolarization are larger (high-K^+ data), the most likely explanation of the decreased contribution of LTCCs to Phe-induced contraction in BPH is a decreased Phe-induced depolarization in the hypertensive vessels.

5.3.2.1 Differential role of CaCC and ROCs

CaCC channels seem to be good candidates to explain the increased contractile response induced by Phe based on previous data in the literature (Boedtkjer *et al.* 2015). Upregulation of TMEM16A gene was described in several HT animal models. In fact, an increased functional expression of TMEM16A was linked to high BP in the equivalent genetically SHR model (Goto, Kitazono 2022). However, some controversial results can also be found, and the lack of selective antagonists complicated the channel function characterization. To cope with this limitation, we decided to use an external PSS solution without Cl^- to test the role of Cl^- channels in the Phe-induced contractions. The $[Cl^-]_i$ depletion was assumed to take place after a prolonged incubation, as previously described (Boedtkjer *et al.* 2015). More recently, a novel specific TMEM16A inhibitor (TMinh-23) has been developed, and in intact mesenteric arteries from SHRs it lowered BP (Cil *et al.* 2021). However, this blocker was not available when we carried out the experiments described in this thesis.

In agreement with these previous studies, our expression data showed an increased mRNA expression of the TMEM16A channels in BPH arteries (**Figure R.22**). However, a diminished relative contribution of Cl^- channels was evidenced in Phe-induced contractions from BPH mesenteric arteries when Cl^--free solutions were used (**Figure R.24**). Actually, these results showed Phe-induced contractions in BPH quite similar in the presence and the absence of Cl^-. The almost independency of Cl^- of the response in BPH have two possible explanations. First, Cl^- permeability (αCl) is close to 0 in spite of the increased expression of the TMEM16A gene. Second, the V_M values reached in the pres-

ence of Phe and the equilibrium potential for Cl^- (E_{Cl}) had a similar value in BPN but not in BPH, so that it could be a larger α_{Cl} that has no effect in the response because the electrochemical gradient for Cl^- is close to 0.

To try to distinguish between these two options, we explored the increase in tension observed in the presence of Phe in response to an acute depletion of extracellular Cl^- (**Figure R.25**). The analysis of these experiments shows that the acute replacement of Cl^- induced a transient increase in tension (ΔT_{peak} in the figure) that has a similar amplitude in in BPN and BPH. According to our estimations, this Δ_{peak} upon exposure to a Cl^--free solution depends on the magnitude of membrane depolarization (which is mainly determined by αCl) and on the opening probability of LTCCs:

$$\Delta T_{peak} \sim \Delta V_M \cdot (\Delta Po_{LTCC} \cdot \beta_{Ca}) \sim \alpha_{Cl} \cdot (\Delta Po_{LTCC} \cdot \beta_{Ca}) \qquad \text{(Eq. 5.1)}$$

Our previous experiments indicate a decreased contribution of LTCC to Phe-induced contraction in BPH, that is, a decreased ΔPoLTCC in BPH. The lack of a significant difference in the Δ_{peak} value between BPN and BPH, led us to conclude that in fact αCl must be larger in the BPH mesenteric arteries, which is in agreement with our expression data. The diminished contribution of CaCCs to Phe-induced contraction in BPH vessel has to be a consequence of the decreased driving force for Cl^- ions in hypertensive vessels (that is, $E_{Cl} \sim V_M$). Interestingly, the results obtained with UTP (**Figure R.26**) showed a different pattern, and the activation of CaCC is clearly inhibitory (larger responses in Cl^--free solution) when this agonist is used instead of Phe. At this point, we can only speculate that a different depolarized V_M value is reached during stimulation (way below E_{Cl} for Phe in BPN, close to EC for Phe in BPH and above E_{Cl} for UTP in BPH). Another possibility is to have a different $[Cl^-]_i$ (and then a different E_{Cl}) in BPN and BPH). In any case, it is evident (and many times underestimated) that to really understand the role of Cl^- channels not only the permeability (the number of channels in the membrane) but the driving force (V_M-E_{Cl}) need to be measured.

One caveat of the use of Cl^--free solutions is the effect of the possible changes in intracellular pH because of the inhibition of the Cl^-/CO_3H- exchanger. The smaller responses in Cl^--free solutions when Phe was used as stimulus could be imputed to an effect of pH on contractility, but this is unlikely if we take into account that responses in Cl^--free solutions are larger when UTP is the stimulus.

Previous data in the literature indicate that in physiological conditions $[Cl^-]_i$ is controlled by NKCC1 cotransporter and Cl^-/HCO_{3-} exchanger, and it seems to be increased under pathological conditions such as HT (Goto, Kitazono 2022). In particular, an increased $[Cl^-]_i$ in VSMC from femoral arteries of HT DOCA

rat animals was reported due to the higher activity of NKCC (Davis *et al.* 1993). However, we have no direct measurements of $[Cl^-]_i$ in VSMC from BPH and BPN vessels to confirm these changes. Regarding V_M values, we have previously reported that BPH VSMC were depolarized compared to BPN by $\sim$ 10 mV at rest (from $\sim$ 45 mV in BPN to 35 mV in BPH (Moreno-Domínguez *et al.* 2009). However, we have not measured the value of V_M reached in the presence of Phe or UTP in both preparations, which will be the relevant point for this argument. Further characterization of these variables should be carried out to reach a more solid conclusion.

Other elements involved in Ca^{2+} mobilization mechanisms were also studied to complete this functional characterization. An altered TRPC expression and function has been linked with HT progression in several experimental models (Daghbouche-rubio *et al.* 2022). A significant upregulation of TRPC3 gene was related to an increased cation permeability at rest, contributing to the membrane depolarization of BPH VSMCs. In addition, a different TRPC3/C6 ratio composition was also described (Álvarez-Miguel *et al.* 2017). Although, we found that TRPC3/6 channels were relevant in holding the steady state in Phe-mediated contractions, no differences were evidenced in the relative contribution between BPN and BPH mesenteric arteries (**Figure R.27**).

Our previous data indicated an upregulation of TRPC3 channels in BPH arteries. mRNA and protein expression data supported changes in TRPC3 and TRPC6 proportions and assembly, with a higher TRPC3 channel contribution in BPH VSMCs that could favor cell depolarization, as TRPC3 channels showed larger unstimulated basal activity. However, we also reported that TRPC currents were sensitive to the selective antagonist Pyr10 only when TRPC6 was present. In mesenteric VSMCs, basal and agonist-induced currents were more sensitive to Pyr10 in BPN cells. Consistently, myography studies showed a larger Pyr10-induced vasodilatation in BPN mesenteric arteries (Álvarez-Miguel *et al.* 2017). Putting these data together, we have less effect of Pyr10 in BPH arteries, but no differences in Pyr10 contribution to Phe-induced contraction in BPN and BPH vessels. An explanation to these contradictory results could be a reduced depolarization in response to Phe in BPH mesenteric arteries, as proposed above. In this case, the decreased activation of TRPC channels upon agonist stimulation will determine less depolarization, smaller recruitment of LTCC and lower Ca^{2+} influx that will produce less CaCC activation.

5.3.2.2 Differential role of Ca^{2+} stores and Ca^{2+} release

Functional differences in LTCC, CaCC and TRPC channels did not fully explain the enhanced α1-AR mediated contractions in HT. For this reason, the potential differences in SR-Ca^{2+} mechanisms were also explored. Interestingly, although

we disclosed a larger SR Ca^{2+} storage capacity in BPH mesenteric arteries, the contribution of SR Ca^{2+} release was relatively similar in the Phe-mediated contractions in BPN and BPH arteries (**Figure R.28**).

The larger Ca^{2+} storage capacity has been also observed in other HT experimental models. An increased Ca^{2+} storage due in part to the increased Ca^{2+} reuptake into the SR was found in mesenteric arteries from the equivalent genetically SHR model (Nomura, Asano 2002). Linked to that, a larger IP_3R gene and protein expression was described in mesenteric arteries from AgII-induced HT rats. A larger IP_3R functional contribution to Phe-mediated contractions was also observed in this model, which was not consistent with our results (AAbou-Saleh *et al.* 2013). However, these disparities are not surprising as the model of AgII induced HT shows clear differences with the BPH mice (they found for example upregulation of IP_3R1 and the α1C subunit of the LTCC), indicating the involvement of different mechanisms in the development of HT.

The role of Ca^{2+} SR-release mechanisms is undisputed in the pathway activated by α1-ARs. However, some striking results can be found in the literature. In physiological conditions, KO mice for the three IP_3Rs isoforms did not dramatically affect the Phe-mediated responses in intact mesenteric arteries (Lin *et al.* 2016), suggesting that other elements apart of the canonical $G_\alpha q/PLC\beta/IP_3/Ca^{2+}$ SR-release are relevant mechanisms involved in the contractile responses mediated by Phe.

5.3.2.3 Differential role of PLCβ, ROCK and PKC

It is well known that the canonical $G_\alpha q11$ dependent pathway is not the only one activated by GPCRs. In addition to $G_\alpha q11$, most of the $G_\alpha q11$ coupled receptors also activate $G_\alpha 12$-13. Activation of the $G_\alpha q11$ induce MLC phosphorylation via stimulation of PLCβ, resulting in the Ca^{2+} and calmodulin-dependent activation of MLCK. The $G_\alpha 12$-13 activate the Rho/ROCK pathway, resulting in the inhibition of myosin phosphatase. Thus, the dual regulation of MLC phosphorylation through Ca^{2+}-dependent MLCK activation and Rho/ROCK-mediated myosin phosphatase inhibition is initiated by the dual coupling of receptors to $G_\alpha q11$ and $G_\alpha 12$-13 respectively (see introduction and **Figure R.19**).

In previous data in the literature, greater efficiency of the contractile machinery has been described in HT animal models, particularly related to changes in Ca^{2+} sensitization mechanisms. In fact, an enhanced ROCK-mediated Ca^{2+} sensitization mechanism in α_1-AR was observed in mesenteric arteries of HT rats on a high-salt diet (Crestani *et al.* 2017). However, the use of VSMC restricted genetic ablation of each of these two proteins ($G_\alpha q11$ KO and $G_\alpha 12$-13 KO) does not support these observations (Wirth *et al.* 2008).

They show that G_αq11–mediated signaling in VSMCs is required for maintenance of basal blood pressure and for the development of salt-induced HT, while VSMC restricted G_α12-13 KO mice did not have any alteration of BP under basal conditions but also show impairment in the development of HT. However, they also show clear differences in the responses to different vasoconstrictors in both KO mice. In aortic segments prepared from G_αq11 KO mice, Phe had no contractile effect, whereas its ability to induce contraction was unaffected by G_α12-13 deficiency. They proposed that α_1-AR effects on VSMCs are exclusively mediated by G_αq11, whereas the effects of other vasoconstrictors such as AgII, or TXA2 also involve G_α12-13.

Activation of RhoA through G12-13 is mediated by a subgroup of Rho guanine nucleotide exchange factors (RhoAGEFs) and GTPase-activating proteins (RhoAGAPs). We have found in the Affymetrix arrays changes in the expression of some RhoAGEFs (*Arhgef7*, *Arhgef18* and *Arhgef10*) and the RhoaGAP *Arap3*. We have not characterize these results further, and they are pending of being validated by RT-PCR. We also found in the arrays a moderate downregulation of Rock2 ($\log_2$FC = -0.70). This result has been validated by RT-PCR ($2^{-\Delta\Delta C_t} = -0.8 \pm 0.006, p < 0.05$), but a detailed description of the transcriptional changes associated to the activation of ROCK remains to be done.

We have tested the relative contribution of G_αq11 and G_α12-13 in BPN and BPH using U73122 (PLCβ inhibitor) and H1152 (ROCK inhibitor) at concentrations assumed to completely block each target without having unspecific effects. Therefore, we assume that the response seen in the presence of the PLCβ inhibitor is mediated by G_α12-13 (ROCK) and that the response seen in the presence of the ROCK inhibitor is mediated by G_αq11. This set of experiments provide several relevant conclusions regarding the functional contribution of these pathways to the adrenergic vasoconstriction in BPN and BPN arteries. First, the contribution of PLCβ or ROCK to Phe-induced contraction in BPN vessels was significantly larger than in BPH vessels, since larger inhibitions were obtained in BPN when any of the two enzymes were blocked (**Figure R.29**). Second, the combined effect of blocking PLCβ and ROCK could explain in full the contractile response elicited by Phe in BPN arteries, but only half of the response in BPH, suggesting that additional mechanisms, independent of elements downstream of these enzymes, are needed to explain the larger responses in BPH arteries (**Figure R.32**). It has to be noted that inhibiting ROCK do not affect the upstream activation of G_α12-13, so that we cannot exclude other targets of the G_α12-13 proteins as responsible of the difference.

Third, if we add the effects of blocking PLCβ and ROCK separately in BPN (both if we analyze the effect on Tmax or TSS) the effect were way above 100 % ($\sim$ 133% for Tmax and $\sim$ 178% of TSS), suggesting a large crosstalk between both pathways. The effect of combining the two inhibitors in BPN is

		PLCβ inhibition	ROCK inhibition	*Theoretical additive response*	Combined inhibition
T_{max}	BPN	77.1±6.1 %	56.5±7.1 %	*~ 133%*	97.5±1.3%
	BPH	40.1±8.3 %	25.9±3.4 %	*~ 66%*	55.3±3.6 %
T_{ss}	BPN	95.52±2.13%	82.83±2.64%	*~ 178%*	97.67±1.36%
	BPH	71.29±6.07%	54.41±1.32	*~ 125.69%*	92.62±3.06%

Table D.1: *Overview of the inhibitory patterns of PLCβ and ROCK in adrenergic signaling pathways in from BPN and BPH.*

close to 100% (97.5 ± 1.3), suggesting that both pathways are the sole mechanisms involved in Phe-induced contraction in BPN. However, the effect of such combination in BPH is less that the added effect of the blockers when applied separately (55.3 ± 3.6% vs. ∼ 66%), suggesting once again the crosstalk between the pathways and the existence in BPH of different mechanisms behind the larger responses to Phe. The effects of the inhibition of the peak and steady-state tensions with each blocker, the theoretical addition of both and the combined effect (extracted from the data of **Figures R.29** and **R.30**) are summarized in the Table D1 below:

Due to the position of PKC as a bridge between $G_{\alpha}q11$ and $G_{\alpha}12$-13 signaling pathways (see introduction and **Figure R.19**), we have explored if this additional mechanism or the crosstalk between both pathways could at least partially imputed to PKC. To test that hypothesis we have used the PKC blocker Gö 6983. Indeed, PKC activation seems again to be more relevant in BPN arteries, and certainly it can be responsible of part of the crosstalk, but PKC was not able to abolish in full the contractile response in BPH arteries when combined with PLCβ and ROCK blockers (**Figure R.30**).

We did not carried a full analysis of the contribution of $G_{\alpha}q11$ and $G_{\alpha}12$-13 pathways when other GPCR agonist are used, but preliminary results are obtained for UTP (**Figure R.31**) and AgII (**Figure R.32**). Clearly, the first conclusion is that the relative contribution is very dependent of the agonist. As an example, just to compare one effect, the relative contribution of ROCK on the response on Tmax in BPN is ∼56% with Phe, ∼78% with UTP and ∼35% with AgII. In addition, the second conclusion is to reinforce the idea that a new mechanism is needed to explain the enhanced responses in BPH arteries, since the effect of the three blockers are around only 10% when UTP was the stimulus, and around 20% when it was AgII.

Overall, this work demonstrate that the increased contractile responses to vasoconstrictor agonist that activate GPCRs in HT is the result of a complex

dysregulation of multiple molecular components rather than caused by changes in single elements. This pattern is in clear agreement with the multifactorial nature of the disease. Further research is needed to deeply characterize the responses and find the putative new molecular candidates responsible for the increased responses in BPH. Nevertheless, another important conclusion derived from our data is the need of exploring the effect of every molecular element in the proper context of the pertinent pathway and considering the very probable concomitant changes of its partners in the pathway.

5.4 Limitations and future perspectives

Experimental models of HT have been developed over the years and have filled some of the gaps in our knowledge of the regulation of BP. Advantages and disadvantages are present in each model, and depending of the election, different aspects of the physiopathology of the disease can be highlighted. The underlying mechanisms of the disease have been widely studied in genetically or induced HT animal models. The most commonly used model is associated with AgII infusion (Campbell, Henry 2013). However, the RAAS overstimulation is not the general pattern observed since other factors might be involved in high BP. Here we used the Schlager BPH mice as a model of essential HT. As these strains share some common characteristics with HT in human patients we have been using this model as a tool for describing causal agents in HT. However, there is not an animal model that can fully explain HT pathophysiology and complications, and this limitation should be taken into account. As an example, the BPH mice model do not show age-related HT, as the high BP values are established very early in life and remain unchanged over their whole lifespan. Another difference, in this case common to all rodent models, is that some common complications of HT in humans, such as stroke, are never seen in rodents (with the notable exception of the stroke-prone hypertensive rat model, which is a unique genetic model of severe HT (Nabika *et al.* 2012).

As our line of research was initiated more than ten years ago, the search for the molecular determinants of HT in our animal model was initiated with an overall gene expression profiling conducted with Affymetrix microarrays, which was the technology available at that time at an affordable cost. If we had to initiate our study now, clearly RNAseq will offer clear advantages, detecting low abundance transcripts that are missed in microarrays. In fact, the recent technical improvements for single-cell RNAseq could provide very relevant information in the field of HT, as we could obtain the expression profile specific of cell type and also of vascular bed. These studies could help to identify novel targets and provide more mechanistic insight.

5.4 Limitations and future perspectives

In this work, the experimental approach was based on the study of agonist-mediated responses in the resistance vessels. In some cases, a maximal agonist concentration was used to explore the effects, without a systematic characterization of the dose-response effects. This approach might represent a technical limitation. In addition, isolated endothelium-denuded mesenteric arteries have been used to examine the biological differences in VSMCs, hence eliminating the potential effects of the endothelium. However, we have tested the effect of some endothelial vasoactive agents such as NO, **Figure R.15**. This simplified scenario was created to facilitate the functional dissection of molecular mechanisms in the VSMCs, but it complicates the extrapolation of the results to explain the physiology of the vascular system. Finally, we have used only one type of vessel (mesenteric arteries) as model of a resistance vessel, but it is well known that differences between vascular beds are notable.

Functional assays were performed using pressure and wire myography. In the latter, a 120 mM K^+ solution was used to check the vessel viability. However, higher contractile responses to high K^+ were observed in the mesenteric arteries of BPH, precluding the use of this parameter as normalizer, as conventionally done in this technique.

Increased vasoconstriction and increased systemic vascular resistance are characteristic features of HT. Alterations in the functional expression of various elements of the purinergic, RAAS and sympathetic signaling pathways have been studied in BPH. However, the distinction between cause and consequence is difficult to establish in complex systems. Therefore, the functional changes can be categorized as "contributory" or "compensatory" mechanisms in HT, as previously described (K. L. Jackson, Head, *et al.* 2019).

It should be noted that the correlation between mRNA and protein changes is not always straightforward. Clearly, alternative splicing and regulatory factors are involved in altering gene expression levels and generating protein diversity under pathological conditions. Moreover, trafficking and localization of the protein could modify its function in the absence of expression changes. Although these processes have been described in the field of vascular remodeling (Green *et al.* 2021) further research focused on the contractile alterations in HT is needed

Regarding the pathophysiological role of P2Y6R, further studies are needed to provide additional support for our hypothesis. P2Y6R overexpression in BPN or P2Y6R downregulation in BPH might be among the *in vivo* genetic manipulations that might be carried out to test the P2Y6R involvement in HT. Alternatively, P2Y6R pharmacological manipulation might also provide complementary information. However, we have not managed to apply the P2Y6R blocker (MRS2578) *in vivo* for technical reasons that need to be solved in the future.

Also, more detailed studies exploring the correlation of the changes in the contractile responses to the different agonist in our BPH and BPN model with direct measures of resting V_M and or cytosolic Ca^{2+} levels both in intact arteries or isolated VSMC would represent a valuable addition to our study, contributing to strengthen the current findings and provide more insight into the molecular mechanisms involved.

6 Conclusions

1. **The remodeling of the purinergic system contribute to generate the hypertensive phenotype in the BPH model.** We found a significant P2Y6R upregulation in the hypertensive phenotype. Pharmacological characterization reveals that this receptor is the responsible for the enhanced UTP-dependent contractions in BPH mesenteric arteries.

2. **A functional coupling of P2Y6R-ATR1 is shown in the BPH model.** These complexes are involved in decreasing ATR1 desensitization in BPH mesenteric arteries, which can contribute to explain the increased AgII contractions in this preparation.

3. **HT development is independent of the RAAS system in the BPH model.** We obtained a reduced hypotensive effect in response to chronic application of the ATR1 blocker losartan in BPH mice, together with a decreased circulating levels of AgII. The reduced RAAS function could represent a compensatory mechanism to prevent further increases in BP.

4. **P2Y6R levels may represent a molecular switch for high BP development.** The higher P2Y6R expression favors the formation of P2Y6R-ATR1 heterodimers which contribute to increase AgII-dependent responses, leading to increased BP. We propose that increased levels of P2Y6R might be a necessary condition for the development of certain types of HT. Our data suggest that not only the increased P2Y6R functional expression, through the formation of P2Y6R-ATR1 heterodimers, would contribute to BP increase, but also that in the absence of this increased P2Y6R expression AgII exposure fails to develop HT.

5. **The remodeling of the adrenergic system also contribute to essential HT in BPH mice.** α_1-AR stimulation with Phe leads to larger contractions in BPH mesenteric arteries, but the vasodilation in response to β-AR stimulation with isoproterenol is also increased. This latter effect could represent a compensatory mechanism directed to prevent further increases in BP in the presence of the high sympathetic activity in BPH mice.

6. **The relative contribution of LTCC to Phe-mediated contractions is decreased in BPH arteries.** The most likely explantion is a decreased Phe-induced depolarization in the hypertensive vessels.

7. **There is a decreased contribution of CaCCs to Phe-induced contraction in BPH vessel.** However, our expression and functional data suggest an increased Cl^- permeability in these mice. We propose that the diminished contribution of CaCCs to Phe-induced contraction is a consequence of the decreased driving force for Cl^- ions in hypertensive vessels.

Either a more depolarized E_M value during Phe stimulation in BPH, or an increase in intracellular Cl^- concentrations (or both) could led to the observed results.

8. **TRPC3/6 channels were relevant in holding the steady state in Phe-mediated contractions**, but no differences in their contribution were observed between BPN and BPH mesenteric arteries.

9. **Our data suggest larger SR Ca^{2+} stores in BPH mesenteric arteries.** However, the contribution of SR Ca^{2+} release to Phe-mediated contractions was similar in BPN and BPH arteries.

10. **The contribution of PLCβ or ROCK to Phe-induced contraction in BPN vessels was significantly larger than in BPH vessels.** The combined effect of blocking PLCβ and ROCK could explain in full the contractile response elicited by Phe in BPN arteries, but only half of the response in BPH, suggesting that additional mechanisms, independent of elements downstream of these enzymes, are needed to explain the larger responses in BPH arteries. Our data also evidenced a large crosstalk between these two pathways both in BPN and BPH

11. **The contribution of PLCβ or ROCK to agonist-induced contraction is dependent on the agonist.** We found a different contribution of these two enzymes to UTP or AgII-induced contraction. However, in all cases the effects of blocking PLCβ or ROCK was reduced in BPH arteries, reinforcing the idea of an additional mechanism, different from PLCβ or ROCK-mediated pathways, to explain the enhanced responses in BPH arteries.

12. **Overall, our data demonstrate that the increased contractile responses to agonists of GPCRs in HT is the result of a complex dysregulation of multiple molecular components, reflecting the multifactorial nature of the disease.** While some of these changes contribute to the development of HT, other represent compensatory mechanisms directed to prevent further increases in BP.

7 References

1. Aaronson, P. I., Ward, J. P. T., Wiener, C. M. *(2004). The Cardiovascular System, 2nd ed. Oxford.* (2004).
2. Abou-Saleh, H. *et al. Inositol 1,4,5-trisphosphate (IP3) receptor up-regulation in hypertension is associated with sensitization of Ca2+ release and vascular smooth muscle contractility.* Journal of Biological Chemistry **288,** 32941–32951 (2013).
3. Aird, W. C. *Phenotypic heterogeneity of the endothelium: I. Structure, function, and mechanisms.* Circulation Research **100,** 158–173 (2007).
4. Álvarez-Miguel, I., Cidad, P., Pérez-García, M. T., López-López, J. R. *Differences in TRPC3 and TRPC6 channels assembly in mesenteric vascular smooth muscle cells in essential hypertension.* Journal of Physiology **595,** 1497–1513 (2017).
5. Bar, I. *et al. Knockout mice reveal a role for P2Y6 receptor in macrophages, endothelial cells, and vascular smooth muscle cells.* Molecular Pharmacology **74,** 777–784 (2008).
6. Bian, J., Zhang, S., Yi, M., Yue, M., Liu, H. *The mechanisms behind decreased internalization of angiotensin II type 1 receptor.* Vascular Pharmacology **103-105.** Publisher: Elsevier, 1–7 (January 2018).
7. Boedtkjer, D. M., Kim, S., Jensen, A. B., Matchkov, V. M., Andersson, K. E. *New selective inhibitors of calcium-activated chloride channels - T16Ainh-A01, CaCCinh-A01 and MONNA - What do they inhibit?* British Journal of Pharmacology **172,** 4158–4171 (2015).
8. Born, B. J. H. van den, Koopmans, R. P., Montfrans, G. A. van. *The Renin-Angiotensin System in Malignant Hypertension Revisited: Plasma Renin Activity, Microangiopathic Hemolysis, and Renal Failure in Malignant Hypertension.* American Journal of Hypertension **20,** 900–906 (2007).
9. Brayden, J. E., Nelson, M. T. *Regulation of Arterial Tone by Activation of Calcium-Dependent Potassium Channels.* **256,** 532–535 (1992).
10. Breitwieser, G. E. *G Protein-Coupled Receptor Oligomerization: Implications for G Protein Activation and Cell Signaling.* Circulation Research **94.** ISBN: 1524-4571 (Electronic) 0009-7330 (Linking), 17–27 (2004).
11. Briones, A. M. *et al. Direct demonstration of 1- and evidence against 2- and 3-adrenoceptors, in smooth muscle cells of rat small mesenteric arteries.* British Journal of Pharmacology **146,** 679–691 (2005).
12. Brozovich, F. V. *et al. Mechanisms of vascular smooth muscle contraction and the basis for pharmacologic treatment of smooth muscle disorders.* Pharmacological Reviews **68,** 476–532 (2016).

13. Bulley, S., Jaggar, J. H. *Cl- channels in smooth muscle cells.* Pflugers Archiv European Journal of Physiology **466.** ISBN: 0042401313, 861–872 (2014).

14. Burnstock, G. *Discovery of purinergic signalling, the initial resistance and current explosion of interest.* British Journal of Pharmacology **167,** 238–255 (2012).

15. Burnstock, G. *Purinergic Signaling in the Cardiovascular System.* Circulation Research **120.** ISBN: 0009-7330, 207–228 (2017).

16. Buus, N. H., VanBavel, E., Mulvany, M. J. *Differences in sensitivity of rat mesenteric small arteries to agonists when studied as ring preparations or as cannulated preparations.* British Journal of Pharmacology **112.** ISBN: 0007-1188 (Print), 579–587 (1994).

17. Campbell, R. J., Henry, J. P. *Animal models of hypertension.* **6.** Publication Title: Handbook of Psychology and Health: Volume III: Cardiovascular disorders and behavior. 155–197 (2013).

18. Caputo, A., Caci, E., Ferrera, L., Pedemonte, N., Barsanti, C. *TMEM16A, A Membrane Protein Associated with Calcium-Dependent Chloride Channel Activity.* Science, 590–594 (October 2008).

19. Cat, A. N. D., Touyz, R. M. *Cell signaling of angiotensin II on vascular tone: Novel mechanisms.* Current Hypertension Reports **13,** 122–128 (2011).

20. Catt, K. *et al. Angiotensin II blood levels in human hypertension.* The Lancet, 459–464 (1971).

21. Chen, X. *et al. Targeting deletion of angiotensin type 1B receptor gene in the mouse.* American Journal of Physiology - Renal Physiology **272** (1997).

22. Chen, Z. J., Minneman, K. P. *Recent progress in 1-adrenergic receptor research.* Acta Pharmacologica Sinica **26,** 1281–1287 (2005).

23. Chrissobolis, S., Sobey, C. G. *Evidence that Rho-kinase activity contributes to cerebral vascular tone in vivo and is enhanced during chronic hypertension: Comparison with protein kinase C.* Circulation Research **88,** 774–779 (2001).

24. Cidad, P. *et al. Characterization of Ion Channels Involved in the Proliferative Response of Femoral Artery Smooth Muscle Cells.* Arteriosclerosis, Thrombosis, and Vascular Biology **30,** 1203–1211 (2010).

25. Cil, O. *et al. pressure in spontaneously hypertensive rats.* **100,** 311–320 (2021).

26. Compeer, M. G., Janssen, G. M., De Mey, J. G. *Endothelin-1 and endothelin-2 initiate and maintain contractile responses by different mechanisms in rat mesenteric and cerebral arteries*. British Journal of Pharmacology **170,** 1199–1209 (2013).

27. Cox, R. H., Lozinskaya, I., Dietz, N. J. *Differences in K+ Current Components in Mesenteric Artery Myocytes From WKY and SHR*, 897–907 (2001).

28. Cox, R. H., Rusch, N. J. *New expression profiles of voltage-gated ion channels in arteries exposed to high blood pressure*. Microcirculation **9,** 243–257 (2002).

29. Crestani, S., Webb, R. C., Da Silva-Santos, J. E. *High-salt intake augments the activity of the RhoA/ROCK pathway and reduces intracellular calcium in arteries from rats*. American Journal of Hypertension **30,** 389–399 (2017).

30. Daghbouche-rubio, N., López-lópez, J. R., Pérez-García, M. T., Cidad, P. *Vascular smooth muscle ion channels in essential hypertension*. Frontiers in Pharmacology, 1–9 (September 2022).

31. Davern, P. J., Nguyen-Huu, T. P., La Greca, L., Abdelkader, A., Head, G. A. *Role of the sympathetic nervous system in schlager genetically hypertensive mice*. Hypertension **54,** 852–859 (2009).

32. Davis, J. P., Chipperfield, A. R., Harper, A. A. *Accumulation of intracellular chloride by (Na-K-Cl) co-transport in rat arterial smooth muscle is enhanced in deoxycorticosterone acetate (DOCA)/salt hypertension*. ISSN: 00222828 Issue: 3 Pages: 233–237 Publication Title: Journal of Molecular and Cellular Cardiology Volume: 25. 1993.

33. Dietrich, A. *et al. Increased Vascular Smooth Muscle Contractility in TRPC6 − / − Mice*. Molecular and Cellular Biology **25,** 6980–6989 (2005).

34. Dixon, R. E., Navedo, M. F., Binder, M. D., Fernando Santana, L. *Mechanisms and Physiological Implications of Cooperative Gating of Clustered Ion Channels*. Physiological Reviews **102,** 1159–1210 (2022).

35. Dixon, R. E., Vivas, O., Hannigan, K. I., Dickson, E. J. *Ground state depletion super-resolution imaging in mammalian cells*. Journal of Visualized Experiments **2017,** 1–9 (2017).

36. Earley, S., Brayden, J. E. *Transient receptor potential channels in the vasculature*. Physiological Reviews **95,** 645–690 (2015).

37. Ercu, M. *et al. Phosphodiesterase 3A and Arterial Hypertension*. Circulation **142,** 133–149 (2020).

38. Esler, M. D. *et al. Renal sympathetic denervation in patients with treatment-resistant hypertension (The Symplicity HTN-2 Trial): A randomised controlled trial*. The Lancet **376.** Publisher: Elsevier Ltd, 1903–1909 (2010).

39. Feldman, R. D., Gros, R. *Impaired vasodilator function in hypertension: The role of alterations in receptor-G protein coupling*. Trends in Cardiovascular Medicine **8,** 297–305 (1998).

40. Ferguson, S. S., Feldman, R. D. *-Adrenoceptors as molecular targets in the treatment of hypertension*. Canadian Journal of Cardiology **30.** Publisher: Canadian Cardiovascular Society, S3 (2014).

41. Flack, J. M., Adekola, B. *Blood pressure and the new ACC/AHA hypertension guidelines*. Trends in Cardiovascular Medicine **30.** Publisher: Elsevier Inc., 160–164 (2020).

42. Fredriksson, S. *et al. Protein detection using proximity-dependent DNA Ligation Assays*. Nature Biotechnology **20,** 473–477 (May 2002).

43. Fujii, K., Onaka, U., Goto, K., Isao, A., Fujishima, M. *Impaired isoproterenol-induced hyperpolarization in isolated mesenteric arteries of aged rats*. Hypertension **34,** 222–228 (1999).

44. Gabella, G. *Structural apparatus for force transmission in smooth muscles*. Physiological Reviews **64,** 455–477 (1984).

45. Gasc, J. M., Shanmugam, S., Sibony, M., Corvol, P. *Tissue-specific expression of type 1 angiotensin II receptor subtypes: An in situ hybridization study*. Hypertension **24,** 531–537 (1994).

46. Ginzinger, D. G. *Gene quantification using real-time quantitative PCR: An emerging technology hits the mainstream*. Experimental Hematology **30,** 503–512 (2002).

47. Goetz, R. M., Holtz, J. *Enhanced angiotensin-converting enzyme activity and impaired endothelium-dependent vasodilation in aortae from hypertensive rats: evidence for a causal link*. Clinical Science **97,** 165–174 (1999).

48. Gohla, A., Schultz, G., Offermanns, S. *Role for G12/G13 in agonist-induced vascular smooth muscle cell contraction*. Circulation Research **87,** 221–227 (2000).

49. Gorlach, A., Klappa, P., Kietzmann, T. *The Endoplasmic Reticulum: Folding, Calcium Homeostasis, Signaling, and Redox Control*. Antioxidants & redox signaling **8.** ISBN: 1523-0864, 1907–1939 (2006).

50. Goto, K., Kitazono, T. *Chloride Ions, Vascular Function and Hypertension*. Biomedicines **10,** 1–15 (2022).

51. Green, I. D., Liu, R., Wong, J. J. *The expanding role of alternative splicing in vascular smooth muscle cell plasticity.* International Journal of Molecular Sciences **22** (2021).

52. Gudi, S., Nolan, J. P., Frangos, J. A. *Modulation of GTPase activity of G proteins by fluid shear stress and phospholipid composition.* Proceedings of the National Academy of Sciences of the United States of America **95,** 2515–2519 (1998).

53. Guilluy, C. *et al. The Rho exchange factor Arhgef1 mediates the effects of angiotensin II on vascular tone and blood pressure.* Nature Medicine **16.** ISBN: 1546-170X (Electronic)\r1078-8956 (Linking), 183–190 (2010).

54. Gurevich, V. V., Gurevich, E. V. *GPCR signaling regulation: The role of GRKs and arrestins.* Frontiers in Pharmacology **10,** 1–11 (FEB 2019).

55. Haanes, K. A. *et al. New insights on pyrimidine signalling within the arterial vasculature - Different roles for P2Y2 and P2Y6 receptors in large and small coronary arteries of the mouse.* Journal of Molecular and Cellular Cardiology **93.** Publisher: Elsevier Ltd, 1–11 (2016).

56. Herring, N., Paterson, D. J. *Levick's Introduction to Cardiovascular Physiology* (2018).

57. Huang, J. *et al. Angiotensin-converting enzyme-induced activation of local angiotensin signaling is required for ascending aortic aneurysms in fibulin-4-deficient mice.* Science Translational Medicine **5,** 1–21 (2013).

58. Iwao, H. *Renin-Angiotensin System in Genetically Hypertensive Mice.* Chemical Pharmaceutical Bulletin, 2091 (1984).

59. Izzo, R. *et al. Enhanced GRK2 expression and desensitization of Ar vasodilatation in hypertensive patients.* Clinical and Translational Science **1,** 215–220 (2008).

60. Jablonskis, L. T., Howe, P. R. *Elevated plasma adrenaline in spontaneously hypertensive rats.* Blood Pressure **3,** 106–111 (1994).

61. Jackson, K. L., Head, G. A., *et al. Mechanisms responsible for genetic hypertension in schlager bph/2 mice.* Frontiers in Physiology **10** (OCT 2019).

62. Jackson, K. L., Marques, F. Z., *et al. A novel interaction between sympathetic overactivity and aberrant regulation of renin by miR-181a in BPH/2J genetically hypertensive mice.* Hypertension **62,** 775–781 (2013).

63. Jackson, W. F. *Ion channels and vascular tone.* Hypertension **35,** 173–178 (2000).

64. Jackson, W. F. *KV channels and the regulation of vascular smooth muscle tone.* Microcirculation **25,** 191–193 (2018).

65. Jama, H. A. *et al. Rodent models of hypertension.* British Journal of Pharmacology **179,** 918–937 (2022).

66. Jelinic, M. *et al. Endothelium-dependent relaxation is impaired in Schlager hypertensive (BPH/2J) mice by region-specific mechanisms in conductance and resistance arteries.* Life Sciences **320.** Publisher: Elsevier Inc., 121542 (March 2023).

67. Jensen, A. B. *et al. Variable Contribution of TMEM16A to Tone in Murine Arterial Vasculature.* Basic and Clinical Pharmacology and Toxicology **123,** 30–41 (2018).

68. Johns, D. G., Dorrance, A. M., Leite, R., Weber, D. S., Webb, R. C. *Novel signaling pathways contributing to vascular changes in hypertension.* Journal of Biomedical Science **7,** 431–443 (2000).

69. Kauffenstein, G. *et al. Central Role of P2Y 6 UDP Receptor in Arteriolar Myogenic Tone.* Arteriosclerosis, Thrombosis, and Vascular Biology **36,** 1598–1606 (2016).

70. Kim, E. C., Choi, S. K., Lim, M., Yeon, S. I., Lee, Y. H. *Role of endogenous ENaC and TRP channels in the myogenic response of rat posterior cerebral arteries.* PLoS ONE **8** (2013).

71. Kitazawa, T., Kitazawa, K. *Size-dependent heterogeneity of contractile Ca2+ sensitization in rat arterial smooth muscle.* Journal of Physiology **590,** 5401–5423 (2012).

72. Knot, H. J., Nelson, M. T. *Regulation of arterial diameter and wall [Ca2+] in cerebral arteries of rat by membrane potential and intravascular pressure*, 199–209 (1998).

73. Kolberg, L., Raudvere, U., Kuzmin, I., Vilo, J., Peterson, H. *gprofiler2 – an R package for gene list functional enrichment analysis and namespace conversion toolset g: Profiler.* F1000Research **9,** 1–27 (2020).

74. Kraehling, J. R., Sessa, W. C. *Contemporary approaches to modulating the nitric oxide-cGMP pathway in cardiovascular disease.* Circulation Research **120,** 1174–1182 (2017).

75. Krege, J. H., Hodgin, J. B., Hagaman, J. R., Smithies, O. *A noninvasive computerized tail-cuff system for measuring blood pressure in mice.* Hypertension **25,** 1111–1115 (1995).

76. Kügelgen, I. von. *Pharmacological profiles of cloned mammalian P2Y-receptor subtypes.* Pharmacology and Therapeutics **110,** 415–432 (2006).

77. Kuriakose, J., Montezano, A. C., Touyz, R. M. *ACE2/Ang-(1-7)/Mas1 axis and the vascular system: Vasoprotection to COVID-19-associated vascular disease.* Clinical Science **135,** 387–407 (2021).

78. Lamont, C., Vial, C., Evans, R. J., Wier, W. G. *P2X1 receptors mediate sympathetic postjunctional Ca 2+ transients in mesenteric small arteries.* American Journal of Physiology - Heart and Circulatory Physiology **291,** 3106–3113 (2006).

79. Lazarowski, E. R., Boucher, R. C. *UTP as an extracellular signaling molecule.* News in Physiological Sciences **16,** 1–5 (2001).

80. Levick, J. R. *An Introduction to Cardiovascular Physiology., Fourth ed.* (2003).

81. Lin, Q. *et al. IP3 receptors regulate vascular smooth muscle contractility and hypertension.* JCI Insight **1,** 1–12 (2016).

82. Linde, C. I. *et al. Increased arterial smooth muscle Ca 2+-signaling, vasoconstriction, and myogenic reactivity in milan hypertensive rats.* American Journal of Physiology - Heart and Circulatory Physiology **302** (2012).

83. Liu, D. *et al. Increased transient receptor potential canonical type 3 channels in vasculature from hypertensive rats.* Hypertension **53,** 70–76 (2009).

84. Liu, Z., Khalil, R. A. *Evolving mechanisms of vascular smooth muscle contraction highlight key targets in vascular disease.* Biochemical Pharmacology **153.** ISBN: 5426115657734 Publisher: Elsevier, 91–122 (December 2017 2018).

85. Livak, K. J., Schmittgen, T. D. *Analysis of relative gene expression data using real-time quantitative PCR and the 2-ΔΔCT method.* Methods **25,** 402–408 (2001).

86. Lorigo, M., Oliveira, N., Cairrao, E. *PDE-Mediated Cyclic Nucleotide Compartmentation in Vascular Smooth Muscle Cells: From Basic to a Clinical Perspective.* Journal of Cardiovascular Development and Disease **9** (2022).

87. Ma, J. *et al. Signaling pathways in vascular function and hypertension: molecular mechanisms and therapeutic interventions.* Signal transduction and targeted therapy **8.** Publisher: Springer US, 168 (2023).

88. Makarewich, C. A. *et al. A caveolae-targeted L-type Ca 2+ channel antagonist inhibits hypertrophic signaling without reducing cardiac contractility.* Circulation Research **110,** 669–674 (2012).

89. Martin-Aragon Baudel, M., Espinosa-Tanguma, R., Nieves-Cintron, M., Navedo, M. F. *Purinergic Signaling During Hyperglycemia in Vascular Smooth Muscle Cells.* Frontiers in Endocrinology **11,** 1–14 (May 2020).

90. Masuzawa, K., Matsuda, T., Asano, M. *Decreased arterial responsiveness to multiple cyclic AMP-generating receptor agonists in spontaneously hypertensive rats.* British Journal of Pharmacology **96,** 227–235 (1989).

91. Matchkov, V. V. *et al. A paradoxical increase of force development in saphenous and tail arteries from heterozygous ANO1 knockout mice.* Physiological Reports **8,** 1–17 (2020).

92. Matsumoto, T., Szasz, T., Tostes, R. C., Webb, R. C. *Impaired -adrenoceptor-induced relaxation in small mesenteric arteries from DOCA-salt hypertensive rats is due to reduced K Ca channel activity.* Pharmacological Research **65.** Publisher: Elsevier Ltd, 537–545 (2012).

93. Mayet, J., Hughes, A. *Cardiac and vascular pathophysiology in hypertension.* Heart **89,** 1104–1109 (2003).

94. Mcdonald, J. H. *Handbook of biological statistics*, 282 (2008).

95. Mehta, P. K., Griendling, K. K. *Angiotensin II cell signaling: Physiological and pathological effects in the cardiovascular system.* American Journal of Physiology - Cell Physiology **292,** 82–97 (2007).

96. Messerli, F. H., Williams, B., Ritz, E. *Essential hypertension.* Lancet **370,** 591–603 (2007).

97. Mhatre V. Ho, J.-A. L., Martin, K. C., Dien et al., 2. *Altered beta2 adrenergic receptor gene expression in human clinical hypertension.* Bone **23.** ISBN: 6176321972 _eprint: NIHMS150003, 1–7 (2008).

98. Mills, K. T., Stefanescu, A., He, J. *The global epidemiology of hypertension.* Nature Reviews Nephrology **16.** Publisher: Springer US (April 2020).

99. Moreno-Domínguez, A., Cidad, P., Miguel-Velado, E., López-López, J. R., Pérez-García, M. T. *De novo expression of Kv6.3 contributes to changes in vascular smooth muscle cell excitability in a hypertensive mice strain.* Journal of Physiology **587,** 625–640 (2009).

100. Morgado, M., Cairrão, E., Santos-Silva, A. J., Verde, I. *Cyclic nucleotide-dependent relaxation pathways in vascular smooth muscle.* Cellular and Molecular Life Sciences **69,** 247–266 (2012).

101. Müller, C. E., Namasivayam, V. *Recommended tool compounds and drugs for blocking P2X and P2Y receptors.* Purinergic Signalling **17.** ISBN: 0123456789 Publisher: Springer Netherlands, 633–648 (2021).

102. Mulvany, M. J., Halpern, W. *Contractile properties of small arterial resistance vessels in spontaneously hypertensive and normotensive rats.* Circulation Research **41,** 19–26 (1977).

103. Murphy, R. A., Rembold, C. M. *The latch-bridge hypothesis of smooth muscle contraction.* Canadian Journal of Physiology and Pharmacology **83,** 857–864 (2005).

104. Nabika, T., Ohara, H., Kato, N., Isomura, M. *The stroke-prone spontaneously hypertensive rat: Still a useful model for post-GWAS genetic studies?* Hypertension Research **35.** Publisher: Nature Publishing Group, 477–484 (2012).

105. Narayanan, J., Imig, M., Roman, R. J., Harder, D. R. *Pressurization of isolated renal arteries increases inositol trisphosphate and diacylglycerol.* American Journal of Physiology - Heart and Circulatory Physiology **266** (1994).

106. Nelson, M. T., Patlak, J. B., Worley, J. F., Standen, N. B. *Calcium channels, potassium channels, and voltage dependence of arterial smooth muscle tone.* American Journal of Physiology - Cell Physiology **259** (1990).

107. Nishida, M. *et al. P2Y6 receptor-G 12/13 signalling in cardiomyocytes triggers pressure overload-induced cardiac fibrosis.* EMBO Journal **27,** 3104–3115 (2008).

108. Nishimura, A., Sunggip, C., Oda, S., *et al. Purinergic P2Y receptors: Molecular diversity and implications for treatment of cardiovascular diseases.* Pharmacology and Therapeutics **180.** Publisher: The Author(s), 113–128 (2017).

109. Nishimura, A., Sunggip, C., Tozaki-saitoh, H., *et al. Purinergic P2Y 6 receptors heterodimerize with angiotensin AT1 receptors to promote angiotensin II – induced hypertension.* **9,** 1–13 (2016).

110. Noh, M. R., Jang, H. S., Kim, J., Padanilam, B. J. *Renal sympathetic nerve-derived signaling in acute and chronic kidney diseases.* International Journal of Molecular Sciences **21** (2020).

111. Nomura, Y., Asano, M. *Increased Ca2+ buffering function of sarcoplasmic reticulum in small mesenteric arteries from spontaneously hypertensive rats.* Hypertension Research **25,** 231–239 (2002).

112. Noorani, M. M., Noel, R. C., Marrelli, S. P. *Upregulated TRPC3 and downregulated TRPC1 channel expression during hypertension is associated with increased vascular contractility in rat.* Frontiers in Physiology **JUL,** 1–9 (July 2011).

113. Okuno, K. *et al. Angiotensin II Type 1A Receptor Expressed in Smooth Muscle Cells is Required for Hypertensive Vascular Remodeling in Mice Infused with Angiotensin II.* Hypertension **80,** 668–677 (2023).

114. Oparil, S. *et al. Hypertension.* Nature Reviews Disease Primers **4** (2018).

115. Palma-Rigo, K. *et al. Renin-angiotensin and sympathetic nervous system contribution to high blood pressure in Schlager mice.* Journal of Hypertension **29,** 2156–2166 (2011).

116. Patel, S. K. *et al. From gene to protein-experimental and clinical studies of ACE2 in blood pressure control and arterial hypertension.* Frontiers in Physiology **5 JUN,** 1–12 (June 2014).

117. Perez, D. M. *Current Developments on the Role of 1-Adrenergic Receptors in Cognition, Cardioprotection, and Metabolism.* Frontiers in Cell and Developmental Biology **9,** 1–23 (May 2021).

118. Pesic, A., Madden, J. A., Pesic, M., Rusch, N. J. *High blood pressure upregulates arterial L-type Ca2+ channels: is membrane depolarization the signal?* Circulation research **94** (2004).

119. Pfeifer, A. *et al. Defective smooth muscle regulation in cGMP kinase I-deficient mice.* EMBO Journal **17,** 3045–3051 (1998).

120. Phipson, B., Lee, S., Majewski, I. J., Alexander, W. S., Smyth, G. K. *Robust hyperparameter estimation protects against hypervariable genes and improves power to detect differential expression.* Annals of Applied Statistics **10.** _eprint: 1602.08678, 946–963 (2016).

121. Prada, M. P. *et al. AKAP5 complex facilitates purinergic modulation of vascular L-type Ca2+ channel CaV1.2.* Nature Communications **11.** Publisher: Springer US, 1–14 (2020).

122. Pratt, P. F., Bonnet, S., Ludwig, L. M., Bonnet, P., Rusch, N. J. *Upregulation of L-type Ca2+ channels in mesenteric and skeletal arteries of SHR.* Hypertension **40,** 214–219 (2002).

123. Quitterer, U. *et al. Beta-Arrestin1 Prevents Preeclampsia by Downregulation of Mechanosensitive AT1-B2 Receptor Heteromers.* Cell **176.** Publisher: Elsevier Inc., 318–333.e19 (2019).

124. Ralevic, V. *History of Geoff Burnstock's research on P2 receptors.* Biochemical Pharmacology **187,** 1–7 (October 2020 2021).

125. Raudvere, U. *et al. G:Profiler: A web server for functional enrichment analysis and conversions of gene lists (2019 update).* Nucleic Acids Research **47.** Publisher: Oxford University Press, W191–W198 (W1 2019).

126. Riegel, A.-k. *et al. Selective induction of endothelial P2Y 6 nucleotide receptor promotes vascular inflammation.* **117,** 2548–2555 (2011).

127. Ritchie, M. E. *et al. Limma powers differential expression analyses for RNA-sequencing and microarray studies.* Nucleic Acids Research **43,** e47 (2015).

128. Rukavina Mikusic, N. L., Silva, M. G., Pineda, A. M., Gironacci, M. M. *Angiotensin Receptors Heterodimerization and Trafficking: How Much Do They Influence Their Biological Function?* Frontiers in Pharmacology **11,** 1–20 (August 2020).

129. Sanders, K. M. *Signal Transduction in Smooth Muscle Invited Review: Mechanisms of calcium handling in smooth muscles.* Journal of Applied Physiology **90.** ISBN: 8750-7587 (Print)\r0161-7567 (Linking), 1593–1599 (2001).

130. Santana, L. F. *et al. Calcium sparklets in arterial smooth muscle.* Clin Exp Pharmacol Physiol. **159.** ISBN: 0000000000000, 1–26 (2008).

131. Schlager, G. *Selection for blood pressure levels in mice.* Genetics, 537–549 (1974).

132. Schroeder, B. C., Cheng, T., Jan, Y. N., Jan, L. Y. *Expression Cloning of TMEM16A as a Calcium-Activated Chloride Channel Subunit.* Cell **134,** 1019–1029 (2008).

133. Schubert, R., Mulvany, M. J. *The myogenic response: established facts and attractive hypotheses.* Clinical Science **96,** 313 (1999).

134. Scudieri, P., Sondo, E., Ferrera, L., Galietta, L. J. *The anoctamin family: TMEM16A and TMEM16B as calcium-activated chloride channels.* Experimental Physiology **97,** 177–183 (2012).

135. Seko, T. *et al. Activation of RhoA and inhibition of myosin phosphatase as important components in hypertension in vascular smooth muscle.* Circulation Research **92,** 411–418 (2003).

136. Sellers, M. M., Stallone, J. N. *Sympathy for the devil: The role of thromboxane in the regulation of vascular tone and blood pressure.* American Journal of Physiology - Heart and Circulatory Physiology **294,** 1978–1986 (2008).

137. Sengupta, P., Jovanovic-Talisman, T., Lippincott-Schwartz, J. *Quantifying spatial organization in point-localization superresolution images using pair correlation analysis.* Nature Protocols **8.** Publisher: Nature Publishing Group, 345–354 (2013).

138. Sengupta, P., Jovanovic-Talisman, T., Skoko, D., *et al. Probing protein heterogeneity in the plasma membrane using PALM and pair correlation analysis.* Nature Methods **8,** 969–975 (2011).

139. Silverthorn, D. U. *Human Physiology: An Integrated Approach* (2018).

140. Sim, M. K., Qiu, X. S. *Formation of des-asp-angiotensin i in the hypothalamic extract of normo- and hypertensive rats.* Blood Pressure **3,** 260–264 (1994).

141. Sobey, C. G. *Potassium channel function in vascular disease.* Arteriosclerosis, Thrombosis, and Vascular Biology **21,** 28–38 (2001).

142. Somlyo, A. P., Somlyo, A. V. *Ca2+ sensitivity of smooth muscle and non-muscle myosin II: Modulated by G proteins, kinases, and myosin phosphatase.* Physiological Reviews **83,** 1325–1358 (2003).

143. Søndergaard, A. M. *et al. Rat mesenteric small artery neurogenic dilatation is predominantly mediated by ß1-adrenoceptors in vivo.* Journal of Physiology **597,** 1819–1831 (2019).

144. Spiers, A., Padmanabhan, N. *A guide to wire myography.* Methods in molecular medicine **108,** 91–104 (2005).

145. Su, C., Xue, J., Ye, C., Chen, A. *Role of the central renin-angiotensin system in hypertension (Review).* International Journal of Molecular Medicine **47,** 1–16 (2021).

146. Sunggip, C. *et al. Purinergic P2Y6 receptors: A new therapeutic target of age-dependent hypertension.* Pharmacological Research **120.** Publisher: Elsevier Ltd, 51–59 (2017).

147. Supiano, M. A., Hogikyan, R. V., Sidani, M. A., Galecki, A. T., Krueger, J. L. *Sympathetic nervous system activity and -adrenergic responsiveness in older hypertensive humans.* American Journal of Physiology - Endocrinology and Metabolism **276** (1999).

148. Tajada, S., Cidad, P., Colinas, O., *et al. Down-regulation of CaV1.2 channels during hypertension: How fewer CaV1.2 channels allow more Ca2+ into hypertensive arterial smooth muscle.* Journal of Physiology **591,** 6175–6191 (2013).

149. Tajada, S., Cidad, P., Moreno-Domínguez, A., Pérez-García, M. T., López-López, J. R. *High blood pressure associates with the remodelling of inward rectifier K+ channels in mice mesenteric vascular smooth muscle cells.* Journal of Physiology **590,** 6075–6091 (2012).

150. Tan, S. C., Yiap, B. C. *DNA, RNA, and protein extraction: The past and the present.* Journal of Biomedicine and Biotechnology **2009** (2009).

151. Timmons, J. A., Szkop, K. J., Gallagher, I. J. *Multiple sources of bias confound functional enrichment analysis of global -omics data.* Genome Biology **16.** Publisher: Genome Biology, 15–17 (2015).

152. Turu, G., Balla, A., Hunyady, L. *The role of -arrestin proteins in organization of signaling and regulation of the AT1 angiotensin receptor.* Frontiers in Endocrinology **10,** 1–9 (August 2019).

153. Tykocki, N. R., Erika M. Boerman, William F. Jackson. *Smooth Muscle Ion Channels and Regulation of Vascular Tone in Resistance Arteries and Arterioles.* Physiology & behavior **176.** ISBN: 2065431091, 139–148 (2017).

154. Uddin, M., Harris-Nelson, N. *Renin activity and angiotensin I concentration in genetically selective inbred line of hypertensive mice.* Biochemical and Biophysical Research Communications **316.** ISBN: 1615327665, 842–844 (2004).

155. Valovič, P., Behuliak, M., Vaněčková, I., Zicha, J. *Impaired vascular -adrenergic relaxation in spontaneously hypertensive rats: The differences between conduit and resistance arteries.* European Journal of Pharmacology **958,** 176045 (April 2023).

156. Veatch, S. L. *et al. Correlation functions quantify super-resolution images and estimate apparent clustering due to over-counting.* PLoS ONE **7** (2012).

157. Versari, D., Daghini, E., Virdis, A., Ghiadoni, L., Taddei, S. *Endothelium-dependent contractions and endothelial dysfunction in human hypertension.* British Journal of Pharmacology **157,** 527–536 (2009).

158. Vial, C., Evans, R. J. *P2X1 receptor-deficient mice establish the native P2X receptor and a P2Y6-like receptor in arteries.* Molecular Pharmacology **62,** 1438–1445 (2002).

159. W. M. Bayliss. *On the local reactions of the arterial wall to changes of internal pressure.* Artery (1902).

160. Wang, B., Li, C., Huai, R., Qu, Z. *Overexpression of ANO1/TMEM16A, an arterial Ca2+-activated Cl- channel, contributes to spontaneous hypertension.* Journal of Molecular and Cellular Cardiology **82.** Publisher: Elsevier B.V., 22–32 (2015).

161. Wellman, G. C., Nelson, M. T. *Signaling between SR and plasmalemma in smooth muscle: Sparks and the activation of Ca2+-sensitive ion channels.* Cell Calcium **34,** 211–229 (2003).

162. Welsh, D. G., Morielli, A. D., Nelson, M. T., Brayden, J. E. *Transient receptor potential channels regulate myogenic tone of resistance arteries.* Circulation Research **90,** 248–250 (2002).

163. Wenceslau, C. F. *et al. Guidelines for the measurement of vascular function and structure in isolated arteries and veins.* American Journal of Physiology - Heart and Circulatory Physiology **321,** H77–H111 (2021).

164. Werstiuk, E. S., Lee, R. M. *Vascular -adrenoceptor function in hypertension and in ageing.* Canadian Journal of Physiology and Pharmacology **78,** 433–452 (2000).

165. Wilson, P. C. *et al. The arrestin-selective angiotensin AT1 receptor agonist [Sar1,Ile4,Ile8]-AngII negatively regulates bradykinin B2 receptor signaling via AT1-B2 receptor heterodimers.* Journal of Biological Chemistry **288,** 18872–18884 (2013).

166. Wirth, A. *et al. G12-G13-LARG-mediated signaling in vascular smooth muscle is required for salt-induced hypertension.* Nature Medicine **14.** ISBN: 1546-170X (Electronic), 64–68 (2008).

167. Wit, C. de, Boettcher, M., Schmidt, V. J. *Signaling across myoendothelial gap junctions - Fact or fiction?* Cell Communication and Adhesion **15,** 231–245 (2008).

168. Woll, K. A., Van Petegem, F. *Calcium-release channels: Structure and function of IP3 receptors and ryanodine receptors.* Physiological Reviews **102,** 209–268 (2022).

169. Woodsome, T. P., Polzin, A., Kitazawa, K., Eto, M., Kitazawa, T. *Agonist- and depolarization-induced signals for myosin light chain phosphorylation and force generation of cultured vascular smooth muscle cells.* Journal of Cell Science **119,** 1769–1780 (2006).

170. Wootten, D., Christopoulos, A., Marti-Solano, M., Babu, M. M., Sexton, P. M. *Mechanisms of signalling and biased agonism in G protein-coupled receptors.* Nature Reviews Molecular Cell Biology **19.** Publisher: Springer US, 638–653 (2018).

171. Yang, J. W. *et al. Acupuncture Attenuates Renal Sympathetic Activity and Blood Pressure via Beta-Adrenergic Receptors in Spontaneously Hypertensive Rats.* Neural Plasticity **2017** (2017).

172. Yang, Y. D. *et al. TMEM16A confers receptor-activated calcium-dependent chloride conductance.* Nature **455,** 1210–1215 (2008).

173. Yu, Z. *et al. Differences between human plasma and serum metabolite profiles.* PLoS ONE **6,** 1–6 (2011).

174. Zhang, J. *et al. Role of Cav1.2 L-type Ca2+ channels in vascular tone: Effects of nifedipine and Mg2+.* American Journal of Physiology - Heart and Circulatory Physiology **292,** 415–425 (2007).

175. Zulian, A. *et al. Upregulation of Na+/Ca2+ exchanger and TRPC6 contributes to abnormal Ca2+ homeostasis in arterial smooth muscle cells from Milan hypertensive rats.* American Journal of Physiology - Heart and Circulatory Physiology **299,** 624–633 (2010).

8 Appendix

Effect of removing the extracelular Cl^- (Cl_0) on membrane potential (V_M)

The Goldman-Hodgkin-Katz equation was used to estimate V_M:

$$V_m = \frac{R \cdot T}{F} \ln\left(\frac{P_k \cdot K_o + P_{Na} \cdot Na_o + P_{Cl} \cdot Cl_i}{P_k \cdot K_i + P_{Na} \cdot Na_i + P_{Cl} \cdot Cl_o}\right) \quad \text{(Eq. 8.1)}$$

Instantaneous change in membrane potential (ΔV_M) when Cl^- was removed from the extracellular medium ($Cl_o = 0$):

$$\Delta V_{m\,Cl_i}^{Cl_o=0} = V_{m\,Cl_i}^{Cl_o=0} - V_{m\,Cl_i}^{Cl_o} \quad \text{(Eq. 8.2)}$$

$$\Delta V_{m\,Cl_i}^{Cl_o=0} =$$

$$= \frac{R \cdot T}{F}\left[\ln\left(\frac{P_k \cdot K_o + P_{Na} \cdot Na_o + P_{Cl} \cdot Cl_i}{P_k \cdot K_i + P_{Na} \cdot Na_i}\right) - \quad (Continues)\right.$$

$$\left. \ln\left(\frac{P_k \cdot K_o + P_{Na} \cdot Na_o + P_{Cl} \cdot Cl_i}{P_k \cdot K_i + P_{Na} \cdot Na_i + P_{Cl} \cdot Cl_o}\right)\right]$$

$$= \frac{R \cdot T}{F} \ln\left(\frac{\dfrac{P_k \cdot K_o + P_{Na} \cdot Na_o + P_{Cl} \cdot Cl_i}{P_k \cdot K_i + P_{Na} \cdot Na_i}}{\dfrac{P_k \cdot K_o + P_{Na} \cdot Na_o + P_{Cl} \cdot Cl_i}{P_k \cdot K_i + P_{Na} \cdot Na_i + P_{Cl} \cdot Cl_o}}\right)$$

$$= \frac{R \cdot T}{F} \ln\left(\frac{P_k \cdot K_o + P_{Na} \cdot Na_o + P_{Cl} \cdot Cl_i}{P_k \cdot K_i + P_{Na} \cdot Na_i}\right)$$

$$\boxed{\Delta V_{m\,Cl_i}^{Cl_o=0} = \frac{R \cdot T}{F} \ln\left(1 + \frac{P_{Cl} \cdot Cl_o}{P_k \cdot K_i + P_{Na} \cdot Na_i}\right)} \quad \text{(Eq. 8.3)}$$

If we take into account that both P_{Na} and Na_i are smaller than P_k and K_i, we can assume that:

$$P_k \cdot K_i \gg P_{Na} \cdot Na_i \;\rightarrow\; P_k \cdot K_i + P_{Na} \cdot Na_i \simeq P_k \cdot K_i \qquad \text{(Eq. 8.4)}$$

And then

$$\Delta V_{m\,Cl_i}^{Cl_o=0} = \frac{R \cdot T}{F} \ln\left(1 + \frac{P_{Cl} \cdot Cl_o}{P_k \cdot K_i}\right) \qquad \text{(Eq. 8.5)}$$

If we substitute the absolute permeability by the relative permeability to K^+,

$$\alpha_i = \frac{P_i}{P_k} \qquad \text{(Eq. 8.6)}$$

$$\boxed{\Delta V_{m\,Cl_i}^{Cl_o=0} = \frac{R \cdot T}{F} \ln\left(1 + \alpha_{Cl} \frac{Cl_o}{K_i}\right)} \qquad \text{(Eq. 8.7)}$$

Equation Eq. 8.7 tell us that the sudden elimination of Cl_o produces a depolarization that is mainly determined by the relative Cl^- permeability (since the ratio Cl_o/K_i is close to 1).

Change in membrane potential in the steady-state (when Cl_o=0 and Cl_i=0):

$$\Delta V_{m\,Cl_i=0}^{Cl_o=0} = V_{m\,Cl_i=0}^{Cl_o=0} - V_{m\,Cl_i}^{Cl_o} \qquad \text{(Eq. 8.8)}$$

$$\Delta V_{m\,Cl_i=0}^{Cl_o=0} = \frac{R\cdot T}{F}\ln\left(\frac{P_k\cdot K_o + P_{Na}\cdot Na_o}{P_k\cdot K_i + P_{Na}\cdot Na_i}\right) - \qquad (Continues)$$

$$\frac{R\cdot T}{F}\ln\left(\frac{P_k\cdot K_o + P_{Na}\cdot Na_o + P_{Cl}\cdot Cl_i}{P_k\cdot K_i + P_{Na}\cdot Na_i + P_{Cl}\cdot Cl_o}\right)$$

$$= \frac{R\cdot T}{F}\ln\left(\frac{\dfrac{P_k\cdot K_o + P_{Na}\cdot Na_o}{P_k\cdot K_i + P_{Na}\cdot Na_i}}{\dfrac{P_k\cdot K_o + P_{Na}\cdot Na_o + P_{Cl}\cdot Cl_i}{P_k\cdot K_i + P_{Na}\cdot Na_i + P_{Cl}\cdot Cl_o}}\right)$$

$$= \frac{R\cdot T}{F}\ln\left(\frac{(P_k\cdot K_o + P_{Na}\cdot Na_o)\cdot(P_k\cdot K_i + P_{Na}\cdot Na_i + P_{Cl}\cdot Cl_o)}{(P_k\cdot K_i + P_{Na}\cdot Na_i)\cdot(P_k\cdot K_o + P_{Na}\cdot Na_o + P_{Cl}\cdot Cl_i)}\right)$$

Taking common factor and rearranging:

$$\Delta V_{mCl_i=0}^{Cl_o=0} = \frac{R\cdot T}{F}\cdot \qquad (Continues)$$

$$\ln\left(\frac{P_k\,K_o\,(P_k\,K_i + P_{Na}\,Na_i) + P_{Na}\,Na_o\,(P_k\,K_i + P_{Na}\,Na_i) + P_{Cl}\,Cl_o\,(P_k\,K_o\,P_{Na}\,Na_o)}{P_k\,K_o\,(P_k\,K_i + P_{Na}\,Na_i) + P_{Na}\,Na_o\,(P_k\,K_i + P_{Na}\,Na_i) + P_{Cl}\,Cl_i\,(P_k\,K_i\,P_{Na}\,Na_i)}\right) \qquad \text{(Eq. 8.9)}$$

Taking into account Eq. 8.4

$$\Delta V_{m\,Cl_i=0}^{Cl_o=0} = \frac{R\cdot T}{F}\ln\left(\frac{P_k\,K_o\,P_k\,K_i + P_{Na}\,Na_o\,P_k\,K_i + P_{Cl}\,Cl_o\,(P_k\,K_o\,P_{Na}\,Na_o)}{P_k\,K_o\,P_k\,K_i + P_{Na}\,Na_o\,P_k\,K_i + P_{Cl}\,Cl_i\,P_k\,K_i}\right) \qquad \text{(Eq. 8.10)}$$

And rearranging:

$$\Delta V_{m\,Cl_i=0}^{Cl_o=0} = \frac{R\cdot T}{F}\ln\left(\frac{P_k\,K_o\,P_k\,K_i + P_{Na}\,Na_o\,P_k\,K_i + P_{Cl}\,Cl_o\,(P_k\,K_o\,P_{Na}\,Na_o)}{P_k\,K_o\,P_k\,K_i + P_{Na}\,Na_o\,P_k\,K_i + P_{Cl}\,Cl_i\,P_k\,K_i}\right) \qquad \text{(Eq. 8.11)}$$

$$\Delta V_{m\,Cl_i=0}^{Cl_o=0} = \frac{R\cdot T}{F}\ln\left(\frac{P_k\,K_i\,(P_k\,K_o + P_{Na}\,Na_o) + P_{Cl}\,Cl_o\,(P_k\,K_o + P_{Na}\,Na_o)}{P_k\,K_i\,(P_k\,K_o + P_{Na}\,Na_o) + P_{Cl}\,Cl_i\,P_k\,K_i}\right) \qquad \text{(Eq. 8.12)}$$

$$\Delta V_{m\,Cl_i=0}^{Cl_o=0} = \frac{R \cdot T}{F} \ln \left(\frac{1 + \dfrac{P_{Cl}\, Cl_o}{P_k\, K_i}}{1 + \dfrac{P_{Cl}\, Cl_i}{(P_k\, K_o + P_{Na}\, Na_o)}} \right) \qquad \text{(Eq. 8.13)}$$

$$\Delta V_{m\,Cl_i=0}^{Cl_o=0} = \frac{R \cdot T}{F} \left[\ln \left(1 + \frac{P_{Cl}\, Cl_o}{P_k\, K_i} \right) - \ln \left(1 + \frac{P_{Cl}\, Cl_i}{P_k\, K_o + P_{Na}\, Na_o} \right) \right] \qquad \text{(Eq. 8.14)}$$

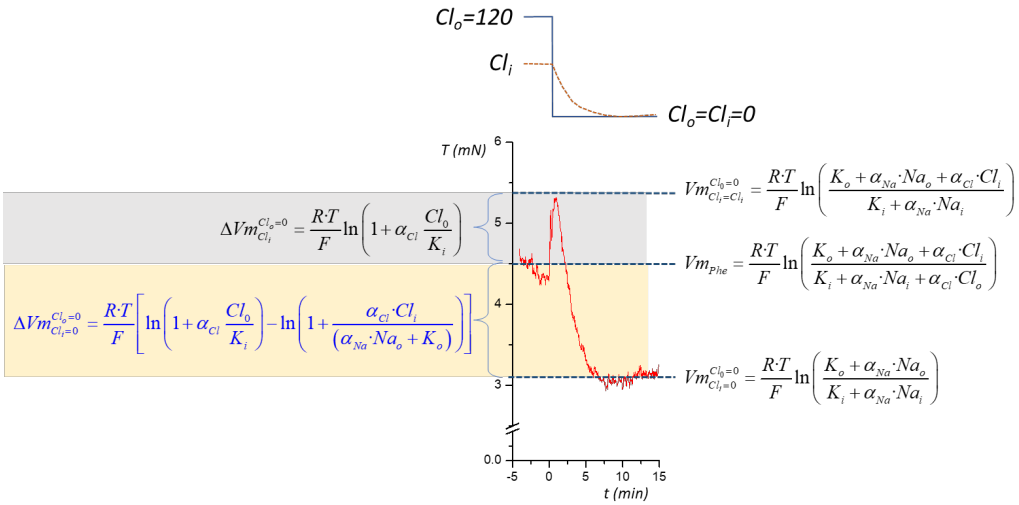

And finally expressing absolute permeabilities as relative permeabilties to K^+ (Eq. 8.6):

$$\Delta V_{m\,Cl_i=0}^{Cl_o=0} = \frac{R \cdot T}{F} \left[\ln \left(1 + \alpha_{Cl} \frac{Cl_o}{K_i} \right) - \ln \left(1 + \frac{\alpha_{Cl}\, Cl_i}{\alpha_{Na}\, Na_o} \right) \right] \qquad \text{(Eq. 8.15)}$$

Equation Eq. 8.15 tell us that after the initial depolarization, the membrane potential hyperpolarizes as intracellular Cl^- exit the cells to reach the steady-state (Cl_o=0 and Cl_i=0) and that the final membrane potential mainly depends of the relative permeability of Cl^-, of intracellular Cl^- concentration and the relative permeability to Na^+.

The equations are depicted in the figure besides a trace (red) illustrating a record of tension obtained in an artery precontracted with Phe with the protocol of removing Cl_o shown in the upper part of the figure.